SPACE TECHNOLOGY

Volume II SPACECRAFT MECHANICAL ENGINEERING

Adams

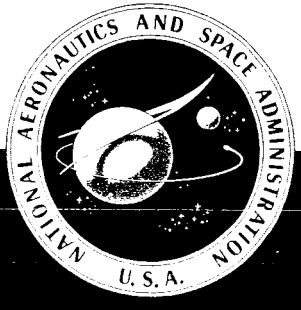

NATIONAL AERONAUTICS AND SPACE ADMINISTRATION

NASA SP-66

SPACE TECHNOLOGY

Volume II

SPACECRAFT MECHANICAL ENGINEERING

JAMES L. ADAMS

Jet Propulsion Laboratory

Scientific and Technical Information Division 1965
NATIONAL AERONAUTICS AND SPACE ADMINISTRATION
Washington, D.C.

FOR SALE BY THE SUPERINTENDENT OF DOCUMENTS, U.S. GOVERNMENT PRINTING OFFICE
WASHINGTON, D.C., 20402-PRICE 60 CENTS

Preface

THIS IS THE SECOND of a series of publications prepared as notes for a course in Space Technology, given by the California Institute of Technology (Caltech) in cooperation with the Jet Propulsion Laboratory (JPL) from June 19 to July 31, 1964. The program was sponsored by the National Aeronautics and Space Administration under Grant No. NsG–598 and was taught by engineers from industry, from Caltech, and from JPL. It is planned that the complete set will consist of

Volume I	*Space Systems* by L. H. ABRAHAM DOUGLAS AIRCRAFT CO., INC.
Volume II	*Spacecraft Mechanical Engineering* by JAMES L. ADAMS, JPL
Volume III	*Spacecraft Propulsion* by F. E. MARBLE, CALTECH
Volume IV	*Spacecraft Guidance and Control* by J. R. SCULL, JLP
Volume V	*Telecommunications* by J. J. STIFFLER, JPL

Contents

		page
	FOREWORD	*vii*
1	BASIC STRUCTURAL THEORY	1
2	MATERIALS	17
3	COMPUTERS AND TESTING	31
4	SPACECRAFT STRUCTURES	41
5	TEMPERATURE CONTROL THEORY	55
6	SPACECRAFT TEMPERATURE CONTROL THEORY AND TESTING	75
7	SPACECRAFT TEMPERATURE CONTROL	91
8	MECHANISM THEORY	101
9	BEARINGS AND LUBRICATION	117
10	SPACECRAFT MECHANISMS	127
11	ELECTRONIC PACKAGING	139
12	SPACECRAFT ELECTRONIC PACKAGING	153

Foreword

THIS VOLUME CONTAINS NOTES used during the mechanical engineering portion of a 6-week Institute on Space Technology taught at the California Institute of Technology during the summer of 1964. The course was attended by junior or senior students majoring in technical subjects. Only 20 percent were mechanical engineering students. The notes and the accompanying lectures were, therefore, necessarily directed at the technically trained student in general, rather than specifically at the mechanical engineering student. A junior-year level of mathematical competence and some knowledge of elementary mechanics were all that the course content assumed.

The course was not intended to produce polished spacecraft engineers, but rather to demonstrate some of the processes employed by the mechanical engineer who is involved in the design, development, fabrication, testing, and operation of spacecraft. An attempt was made to describe the technical environment in which the spacecraft engineer works, his manner of operation, and some of the results.

In many courses, the greatest emphasis is placed on theory, less on design technique and experimentation, and the least emphasis on application. This course was intended to present a more balanced picture of spacecraft mechanical engineering. An attempt was made to describe the tools available to the engineer and the limitations and peculiarities of these tools as applied to actual situations. The hardware was presented as well as the theory.

Because of the author's affiliation, course lectures and notes were heavily slanted toward the Jet Propulsion Laboratory (JPL) and unmanned payloads. This tendency, however, should not have proven detrimental to the course. Despite the relative youth of space exploration, JPL has had considerable experience in designing and building spacecraft. Although unmanned payloads do not involve life support, they suffer from a plenitude of space engineering problems.

Spacecraft mechanical engineering was presented in four parts: structures, temperature control, mechanisms, and electronic packaging. In each of these sections some basic theory was presented for

the sake of students unfamiliar with mechanical engineering. Applications of both theory and experiment relative to spacecraft were next examined, and actual examples of spacecraft hardware were discussed.

Since the lectures did not repeat the notes, this volume does not include all the material presented in the course. However, it is hoped that the information contained herein may prove useful to both students and engineers who are curious about the functions performed by mechanical engineers in the design and development of spacecraft.

CHAPTER 1

Basic Structural Theory

EFFICIENT STRUCTURES are extremely important in spacecraft. With present knowledge, a large amount of machinery is necessary to propel a payload into space and to protect it during flight. For example, in 1964 an Atlas-Agena B booster combination was required in order to send a 600-lb spacecraft on the Mars flyby. A typical weight breakdown for the 600 lb might have been:

	Weight, lb
Electronics and cables (not including structural chassis and brackets)	175
Propellant (fuel) and gas	30
Battery	25
Solar cells and wiring	35
Scientific instruments and electronics	70
Remainder	265
Total	600

The 265 lb remainder consists mainly of parts that are either structure or perform structural functions. It is easy to see that a very small change in structural efficiency in either the booster or the spacecraft can have an extremely large effect upon payload. If other factors are constant, a pound of spacecraft structure is "worth" a pound of payload. It is essential that structures in spacecraft and boosters be as light as possible, consistent with schedule, cost, and absolute confidence that they will not fail.

An efficient structure requires that the structural geometry utilize each member efficiently and that each member be designed to operate efficiently. Structures are designed by an iterative process which combines synthesis and experience with analysis and testing. The first step is the hypothesizing of a structure based upon experience and proven good practice. Loads in the various members are then found either analytically, experimentally, or by a combination of the two techniques. Geometries and materials are then adjusted so that the member stresses remain within the desired ultimate strengths, elastic limits, or whatever parameters may be critical. The result is then used as a stepping-off point for another iteration.

In this chapter, the concepts of loads, stresses, and strains as interrelated by the geometries of the structure and the physical properties of the materials will be discussed. Some examples will be given of the type of thinking used to find the relation between them. Statics and dynamics will be briefly mentioned as techniques of relating forces, displacements, and motions. The structural designer must obviously go far beyond the elementary examples which will be presented here. However, these simple examples will illustrate the manner in which the structural engineer builds theory and solves problems by using simple physical relationships, basic concepts of mechanics, and mathematical manipulation.

LOADS

Loads may arise either statically or dynamically. Static loads may be either steady or quasi-steady (varying slowly enough so that they can be assumed to be steady at any one value and not excite appreciable dynamic loading). Static loads may result from the weight of various parts of the spacecraft under Earth gravity or the quasi-steady acceleration of launch, pressures in tanks, aerodynamic inputs, prestressed members, and so on.

Dynamic loads are forces resulting from reactions due to excitation of spacecraft masses by dynamic inputs. These inputs may originate from aerodynamic loading, fuel sloshing, rocket motor burning, or guidance and control inputs to the vehicle. Such dynamic inputs vary either regularly or irregularly. The dividing line between static and dynamic loading depends upon the magnitude of accelerations and is frequently hazy. However, by using both static and dynamic analyses and experimental techniques, the designer is able to define structural loads with surprising accuracy.

STRESS

Structural loads cause stresses. Stresses are forces per unit area within the material of the structural members. Let us look at the general case of a two-dimensional body in order to gain more understanding of stress. If a small area is cut from a stressed two-dimensional body, it will appear as shown in figure 1.1.

Stresses s_x and s_y are called normal stresses and act to extend or compress the element. Stresses s_{xy} are termed shear stresses and act to deform the body from its rectangular shape. These stresses are usually expressed in force per unit area. Because of static considerations, it is apparent that the stresses in the x and y directions will be equal and opposite (no movement), and that the shearing stresses on the faces must be as shown (no rotation). Let us now

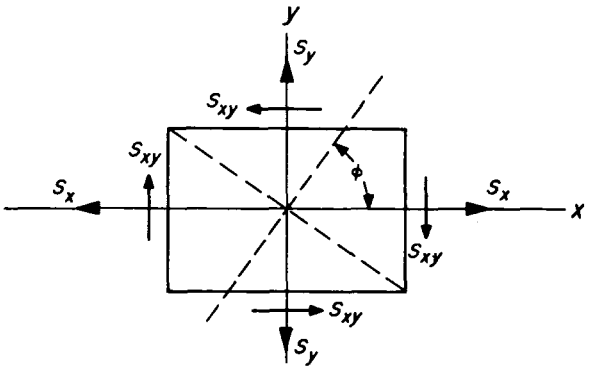

FIGURE 1.1—Area of stressed two-dimensional body.

find the variation of normal and shear stresses with direction in the body element.

Assume that the rectangular area is cut so that its diagonal is normal to the desired observation direction, which makes an angle ϕ with the x-axis. The stress relationship for one-half of the infinitesimal area is shown in figure 1.2.

It is possible to equate the forces upon the faces in order to obtain static equilibrium. The results are the expressions

$$s_n=\frac{s_x+s_y}{2}+\frac{s_x-s_y}{2}\cos 2\phi-s_{xy}\sin 2\phi \tag{1.1}$$

and

$$s_s=\frac{s_x-s_y}{2}\sin 2\phi+s_{xy}\cos 2\phi \tag{1.2}$$

By differentiating these expressions and setting the result equal to 0, the planes for maximum (or minimum) normal stress and shear are, respectively,

$$\tan 2\phi=-\frac{2s_{xy}}{s_x-s_y} \tag{1.3}$$

and

$$\tan 2\phi=\frac{s_x-s_y}{2s_{xy}} \tag{1.4}$$

From these expressions the following conclusions can be made:

(1) The maximum and minimum normal stresses occur on planes which are 90° apart
(2) The maximum and minimum shearing stresses occur on planes which are 90° apart
(3) The maximum and minimum normal stresses occur on the planes where the shearing stress is zero

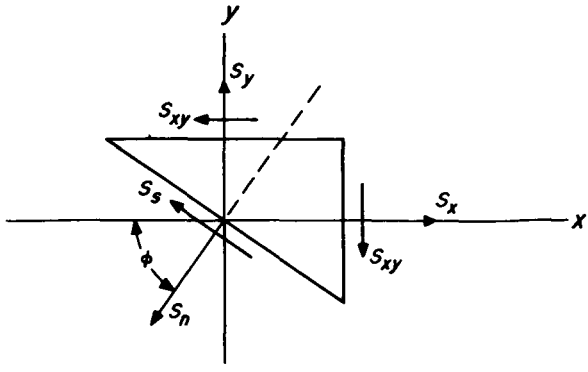

FIGURE 1.2—Portion of stressed two-dimensional body.

(4) The planes of maximum and minimum shearing stress make angles of 45° with the planes of maximum and minimum normal stresses

From the general expressions shown in equations (1.1) and (1.2), simple relations between stresses can be obtained by setting various terms equal to zero. For example, if a fine ribbon is in tension, a small section of the ribbon will appear similar to figure 1.1, except that s_{xy} and s_y will be zero. The expressions for normal and shearing stress are

$$s_n=\frac{s_x}{2}+\frac{s_x}{2}\cos 2\phi$$

and

$$s_s=\frac{s_x}{2}\sin 2\phi$$

Therefore, when ϕ equals 0, $s_n=s_x$ and $s_s=0$. When $\phi=90°$, $s_n=0$ and $s_s=0$. When $\phi=45°$, $s_n=s_x/2$ and $s_s=s_x/2$.

Another example would be a material in tension in one direction and in compression in the perpendicular direction. Let us assume that $s_{xy}=0$, $s_x=s$, and $s_y=-s$. The stress expressions then reduce to

$$s_n=s\cos 2\phi$$

$$s_s=s\sin 2\phi$$

If

$\phi=0$: $s_n=s$, $s_s=0$

$\phi=90°$: $s_n=-s$, $s_s=0$

$\phi=45°$: $s_n=0$, $s_s=s$

Equations (1.1) to (1.4) allow the normal and shearing stresses to be found in any direction in a plane body in which the normal and shear stresses are known in one direction. Similar reasoning can evolve expressions for a three-dimensional body.

STRAIN

Stress results in deformation in an elastic body; this deformation is called strain. If the body is indeed elastic, stress is directly proportional to strain. The constant of proportionality is called Young's modulus and is represented by E. This relationship (Hooke's law) is written as

$$E=\frac{\text{Stress}}{\text{Strain}}$$

Materials are generally elastic up to some value of stress. If this point (the elastic limit) is exceeded, the material deforms plastically and will not recover completely when the stress is removed.

STRESSES FROM LOADS

As an example of the type of thinking required to derive a set of stresses within a body from loads upon the body, the familiar cases of normal and shear stresses due to plane bending in a beam will be examined. These cases are covered in more detail in reference 1.

A beam supported in some manner and loaded so as to deflect in the plane of the loading will have at any point a shearing force tending to shear the beam (fig. 1.3) and a bending moment tending to bend the beam (fig. 1.4). These can be found by cutting the beam and

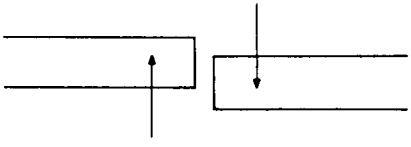

FIGURE 1.3—Shearing force in beam.

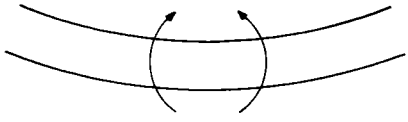

FIGURE 1.4—Bending moment in beam.

placing either end in equilibrium. For example, examine a simple beam pivoted at each end and loaded as shown in figure 1.5. Here R_1 must be 125 lb and R_2 must be 175 lb. As seen from figure 1.6, the moment in the center of the beam must be 150 ft-lb. The shearing force is 25 lb. Knowing the bending moment M and the shearing force V, the stresses in the beam due to plane bending can be found.

Normal Stresses in Bent Beam

Consider a beam in pure bending (neglect vertical shear) as shown in figure 1.7. Assume that lines *aa* and *bb* remain straight during

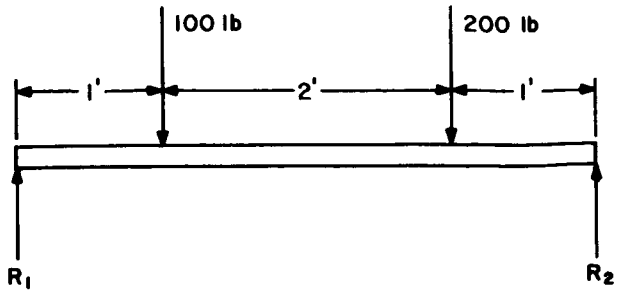

FIGURE 1.5—Simple beam.

bending (shown to be good), stress is proportional to strain, and there is no shearing stress between fibers of the beam.

The elongation of the fiber at distance y from the neutral axis is de. The strain e_x is

$$e_x=\frac{de}{fc}=\frac{ce}{\rho}=-\frac{y}{\rho}$$

from similar triangles. Since $s_x=Ee_x$, s_x in the fiber is $-Ey/\rho$ (negative sign gives positive value for s_x for tension). The forces distributed over the cross section of the beam must balance the applied bending moment M at any point in the beam. Since they must represent a pure moment, their sum must equal 0.

$$-\int_{\substack{\text{Cross}\\ \text{section}}}\frac{Ey}{\rho}\,dA=0$$

where dA is an element of area on the beam cross section a distance y from the neutral axis. An interesting relationship can be seen from this expression. If $\int y\,dA=0$ the neutral axis must pass through the centroid of the beam cross section.

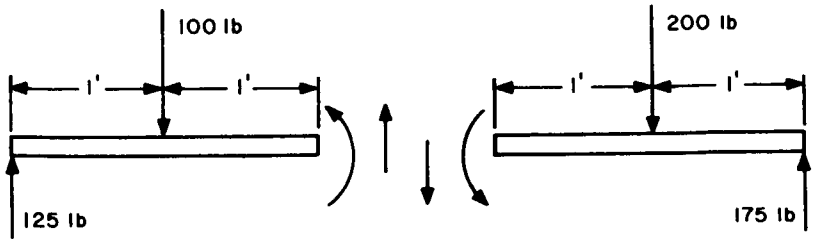

FIGURE 1.6—Equilibrium in simple beam.

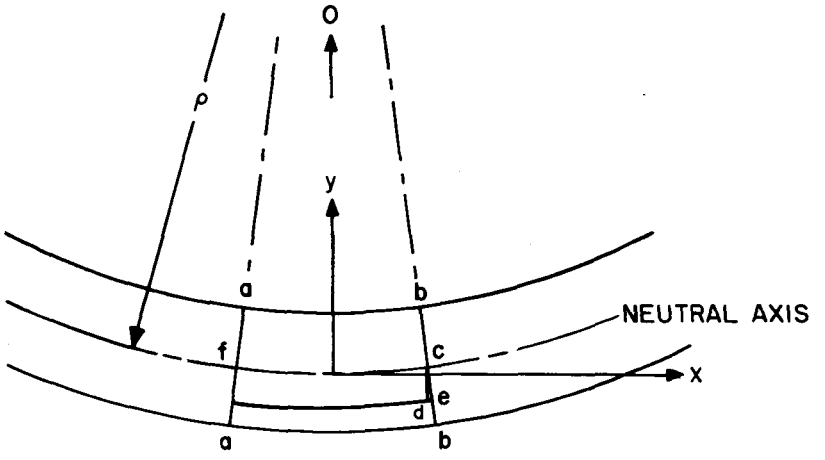

FIGURE 1.7—Portion of beam in pure bending.

Equating the moment of the distributed forces to the applied bending moment:

$$M=\int \frac{Ey}{\rho}\, y\, dA=\frac{E}{\rho}\int y^2\, dA=\frac{E}{\rho} I_z$$

$$\frac{1}{\rho}=\frac{M}{EI_z}$$

and since

$$s_x=-\frac{Ey}{\rho}$$

substitution yields

$$\frac{s_x}{Ey}=-\frac{M}{EI_z} \text{ and } s_x=-\frac{My}{I_z}$$

Since the maximum stress is at the outside fiber, this is usually written $s=Mc/I$, where c is the distance from the neutral axis to the outside fiber, and s is the absolute value of the stress.

Shearing Stresses in Bent Beam

Vertical shearing force V in the cross section of a beam is accompanied by shear stress in the direction of the fibers. This was seen in figure 1.1, where shear was required in two directions to prevent rotation. Intuitively it can be seen that shear forces will attempt to "split" a beam (fig. 1.8).

Consider the beam element *abed*, with no outside loads between *af* and *bg*, shown in figure 1.9. The forces in the x direction are the shearing stresses on side *de* and the normal stresses on sides *ad* and *be*.

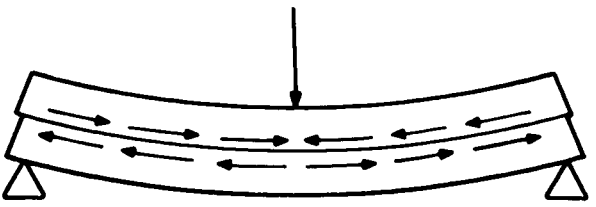

FIGURE 1.8—Shear in beam.

If bending is not pure (shear is present) M will vary along the beam. The force on side *ad* can then be written as

$$\int_{y_1}^{c} \frac{My}{I}\,dA$$

The force on side *be* is

$$\int_{y_1}^{c} \frac{M+dM}{I}\,y\,dA=\int_{y_1}^{c} \frac{My}{I}\,dA+\int_{y_1}^{c} \frac{dM}{I}\,y\,dA$$

and the force on side *de* is $s_s b\,dx$, where b is the beam width.

Equating forces gives

$$s_s b\,dx=\int_{y_1}^{c} \frac{dM}{I}\,y\,dA$$

and

$$s_s=\frac{dM}{dx}\,\frac{1}{Ib}\int_{y_1}^{c} y\,dA$$

However, by investigating a small section of beam with no outside loads acting on the section (fig. 1.10) we see that $V\,dx$ must equal dM and thus $dM/dx=V$.

The shear expression is, therefore,

$$s_s=\frac{V}{Ib}\,Q$$

where

$$Q=\int_{y_1}^{c} y\,dA$$

or the moment about the neutral axis of the cross-sectional area above the level where the shear stress value is desired

STATICS AND DYNAMICS

Simple static techniques have already been used in this section to find load and stress distributions. Static analyses take advantage of

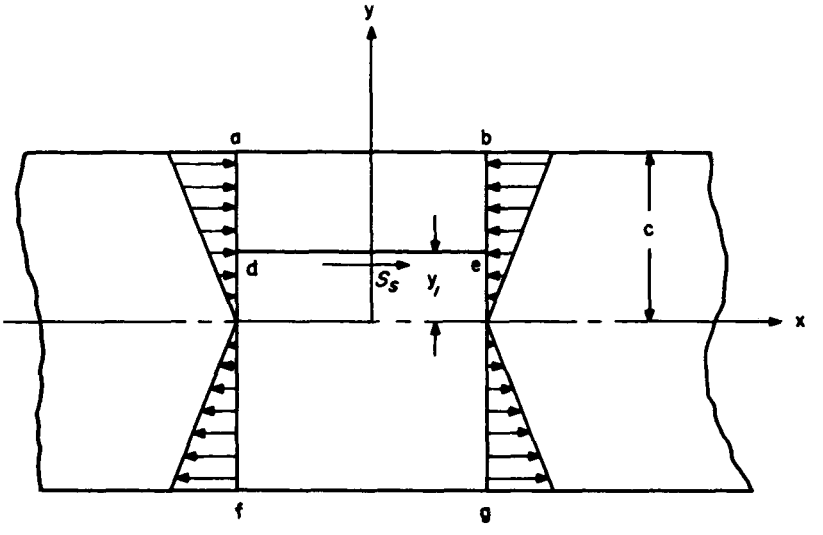

FIGURE 1.9—Section of beam.

the lack of accelerations in the situation being investigated. If there are no accelerations, there can be no differential forces or moments. By balancing moments and forces on elements and portions of elements it is therefore possible to find load and stress distributions. The principles of statics will not be reviewed in this section because the student is probably much more at ease with statics than with dynamics and because dynamic considerations are frequently the most important aerospace structural criteria. The most critical structural environment is the dynamic input to the structure during launch.

Three examples follow which represent the type of thinking in dynamic analysis. Dynamic problems are solved by application of Newton's laws of motion. The principles of dynamics are treated in references 2 and 3.

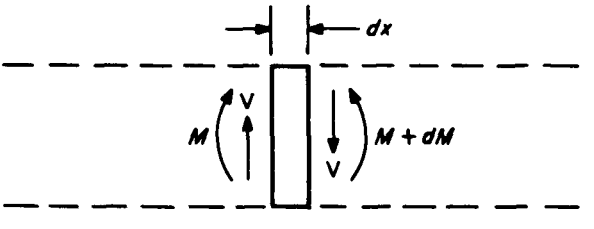

FIGURE 1.10—Shear-moment relationship.

Example 1: The spring-mass-dashpot system with a linear spring and viscous damping. In figure 1.11, if the mass is displaced a distance x from equilibrium and then released, it will move under a force kx from the spring (opposite to the displacement). This force will be

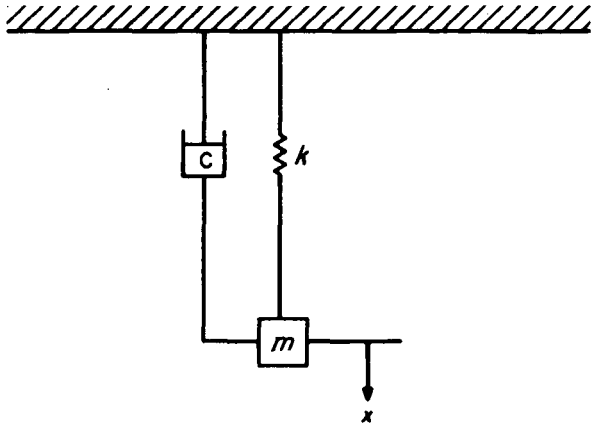

FIGURE 1.11—Spring–mass–dashpot.

resisted by the dashpot ($c\dot{x}$) and the acceleration of the mass ($m\ddot{x}$). The equation of motion is therefore

$$m\ddot{x}+c\dot{x}+kx=0$$

It is customary to introduce the notations $k/m=p^2$ and $c/m=2n$. The above expression then becomes

$$\ddot{x}+2n\dot{x}+p^2x=0$$

The general solution to this expression is

$$x=Ae^{r_1t}+Be^{r_2t}$$

where

$$r_1=-n+\sqrt{n^2-p^2}$$

$$r_2=-n-\sqrt{n^2-p^2}$$

Examination of this expression reveals the behavior of a spring-mass-dashpot system (an extremely useful model, as it qualitatively approximates the behavior of many elements of an elastic structure in free vibration).

(1) Assume no damping ($c=n=0$):

$$x=Ae^{ipt}+Be^{-ipt}=A\sin pt+B\cos pt$$

The constants A and B represent initial conditions. The solution represents the familiar simple harmonic motion with period

$$p=\sqrt{\frac{k}{m}} \text{ rad/sec or } \frac{1}{2\pi}\sqrt{\frac{k}{m}} \text{ cps}$$

(2) Assume a large damping coefficient and a small spring constant so that $n^2>p^2$. Then r_1 and r_2 have real values. Assume also initial conditions $x=x_o$ and $\dot{x}=0$ when $t=0$. The general solution then becomes

$$x=\frac{x_o}{r_1-r_2}(r_1e^{r_2t}-r_2e^{r_1t})$$

A plot of displacement x versus time is shown in figure 1.12. If $n=p$, this behavior reaches what is termed critical damping.

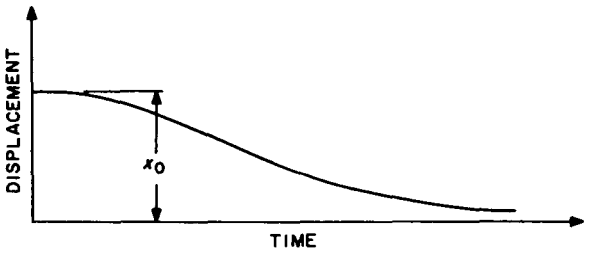

FIGURE 1.12—Overdamped system.

(3) Assume a large spring constant and a small damping coefficient, so that $n^2<p^2$. Then r_1 and r_2 are complex. The solution then becomes

$$x=Ae^{-nt}\cos(p_1t-\alpha)$$

where

$$p_1=\sqrt{p^2-n^2}$$

The resulting motion is a damped free vibration, such as that illustrated in figure 1.13.

Example 2: Resonance of a forced spring-mass system (linear spring, sinusoidal input). Figure 1.14 is a model of a forced vibration which is the type of vibration encountered by spacecraft during launch. The equation of motion is

$$m\ddot{x}+kx=kX\sin\omega t$$

Substituting

$$\frac{k}{m}=p^2 \text{ and } \frac{kX}{m}=X_o$$

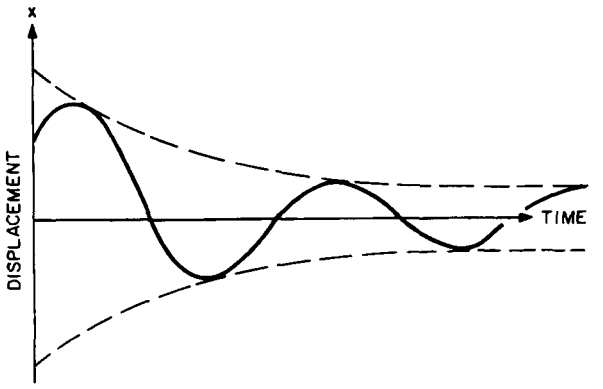

FIGURE 1.13—Damped free vibration.

gives

$$\ddot{x}+p^2x=X_o \sin \omega t$$

With initial conditions $x=0$ and $\dot{x}=0$ when $t=0$, the solution to this equation is

$$x=X \frac{1}{1-\frac{\omega^2}{p^2}} \sin \omega t$$

(Note that these initial conditions eliminate the transient portion of the solution.)

A plot of β versus ω/p appears in figure 1.15. In this figure

$$\beta=\frac{\text{Displacement (maximum)}}{\text{Static } X \text{ displacement}}$$

The curve goes to $+\infty$ when ω (frequency of input) is equal to p (natural frequency of the spring-mass system). This phenomenon is

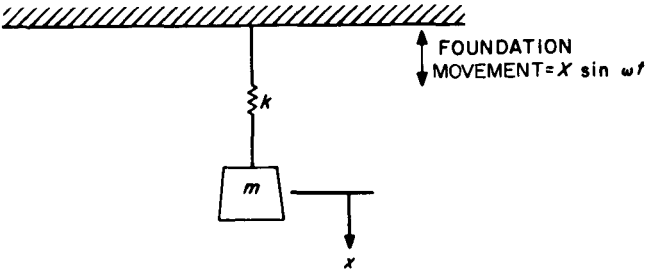

FIGURE 1.14—Forced vibration.

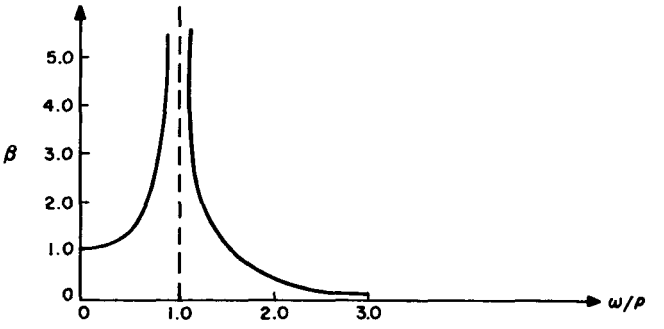

FIGURE 1.15—Variation of β with ω/p for forced undamped system.

called resonance. It should be noted that below resonance ($\omega < p$) the vibrations are in phase with the disturbing force, and above resonance ($\omega > p$) the vibrations are out of phase.

Actual resonating systems do not have infinite displacements, however, both because they would fail and because the presence of damping limits the displacements. A calculation similar to that above, but including the effects of viscous damping, will show the influence of damping. The calculation will not be done here, but it results in curves like those of figure 1.16. In this figure,

$$\gamma = \frac{2n}{p} = \frac{\text{Damping}}{\text{Spring force}}$$

and

$$\beta = \text{Magnification factor} = \frac{\text{Mass displacement (maximum)}}{\text{Displacement } X}$$

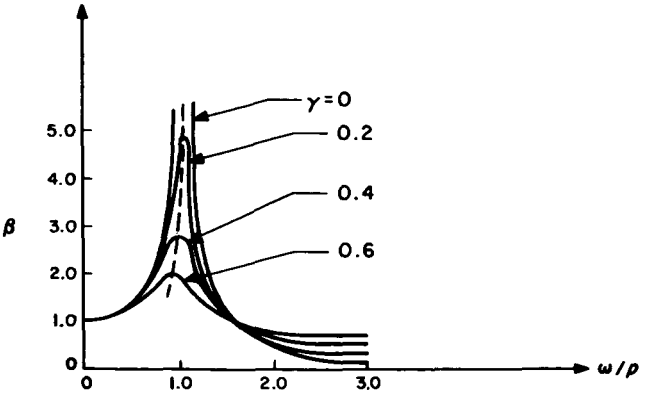

FIGURE 1.16—Variation of β with ω/p including damping.

Example 3: Vibration of an axially loaded column by the energy method. In a so-called conservative system, no energy is lost in friction or damping. Energy is merely transferred between its two identities, kinetic and potential. This behavior can be used to solve dynamic problems. Let us examine an axially loaded column in vibration as illustrated in figure 1.17.

The natural circular frequency of vibration of the system is p rad/sec. The position of any element at any location x will be $Y(x)$ sin pt. The maximum velocity of any element at any location x will be pY. The maximum kinetic energy of the beam plus the load will then be

$$\frac{1}{2}\frac{w_b}{g}p^2\int_0^l y^2\,dy+\frac{1}{2}\frac{W}{g}Y_l^2p^2$$

where w_b/g is mass per unit length of beam.

If an element of beam is bent through an angle $d\theta$, the stored energy in the element will be $(M/2)\,d\theta$, where $d\theta=dx/\rho$. As was observed when examining the simple bending of a beam, $M=EI/\rho$, so that the potential energy for a beam element becomes

$$\frac{1}{2}\frac{EI}{\rho}\frac{dx}{\rho}$$

If curves are small,

$$\frac{1}{\rho}=-\frac{d^2y}{dx^2}$$

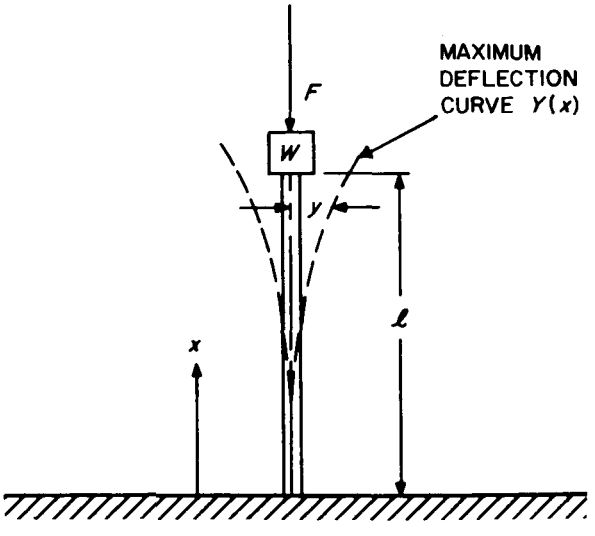

FIGURE 1.17—Axially loaded column in vibration.

and the bending potential energy of the beam is

$$\frac{1}{2} EI \int_0^l \left(\frac{d^2y}{dx^2}\right)^2 dx$$

The axial load also adds to the potential energy in the beam. The beam has an axial load $W+F$. The potential energy in a beam at any time due to axial load and elongation of the beam is

$$\left(T_a+\frac{1}{2} ke\right) e$$

where T_a is axial tension and e is the elongation,

$$e=\int_0^l (ds-dx)=\int_0^l \left(\sqrt{1+\left(\frac{dy}{dx}\right)^2}-1\right) dx$$

For small curvatures,

$$e \approx \frac{1}{2} \int_0^l \left(\frac{dy}{dx}\right)^2 dx$$

For this particular beam, $T_a=-(W+F)$. Therefore, assuming that $|W+F|>>|\frac{1}{2}ke^2|$ (large axial load, small deflections),

$$\text{P.E.}=-\frac{1}{2} (W+F) \int_0^l \left(\frac{dy}{dx}\right)^2 dx$$

Now setting maximum potential energy equal to maximum kinetic energy:

$$\frac{1}{2} \frac{w_b}{g} p^2 \int_0^l y^2 dx+\frac{1}{2} \frac{W}{g} p^2 Y_i^2=\frac{1}{2} EI \int_0^l \left(\frac{d^2y}{dx^2}\right)^2 dx-\frac{1}{2} (W+F) \int_0^l \left(\frac{dy}{dx}\right)^2 dx$$

or

$$p^2=\frac{EI \int_0^l \left(\frac{d^2y}{dx^2}\right)^2 dx-(W+F) \int_0^l \left(\frac{dy}{dx}\right)^2 dx}{\frac{w_b}{g} \int_0^l y^2 dx+\frac{W}{g} Y_i^2}$$

Assuming that the deflection curve of the loaded beam is

$$y=a\left(1-\cos \frac{\pi x}{2l}\right)$$

the solution is approximately:

$$p=34.4 \sqrt{\frac{EI-0.41 (W+F) l^2}{0.23 w_b l^4+W l^3}}$$

The following points should be noted:

(1) As F increases, p decreases; an axial compressive load tends to "soften" a beam (decreases the resonant frequency).

(2) When $(W+F)=EI/0.405l^2$, $p=0$. This is the critical Euler buckling load. At this load, if the beam is slightly displaced it will remain displaced. If the load is increased it will become unstable and fail.

(3) As F decreases, p increases; an axial tension "stiffens" a beam (increases the resonant frequency).

GENERAL

As stated earlier, the structural designer must go far beyond the elementary examples presented in this chapter. He must have models which take into consideration nonelastic behavior and complex and distributed geometries. He must have techniques of analytical bookkeeping to avoid being overwhelmed by long and involved analyses. Most of all he must have a feeling for the applicability of various models and the ability to make a shrewd guess if his models prove insufficient.

The ability to use structural theory well comes from experience with actual structures and from an understanding of the strengths and weaknesses of theory. All of structural theory evolves from a few basic concepts. The structural engineer does not have to have all aspects of the theory filed in his mind. However, he must understand the basic concepts, and he must also understand the methods of building theory from these concepts. If he is not familiar with derivations, he may apply the theory blindly. This will result in inefficiency, erroneous assumptions, and misleading results.

In addition to an ability to apply structural theory intelligently, the structural engineer must also have information on the properties of the materials with which he must work. This problem will be discussed in chapter 2. He must also understand fabrication processes and costs, which limit the geometries that he can use. The careful spacecraft structural engineer relies heavily on tests to check, refine, and orient his analysis. Chapter 3 discusses this aspect of structural design, and briefly discusses a typical structural computer application.

REFERENCES

1. TIMOSHENKO, S., and MACCULLOUGH, G. H.: *Elements of Strength of Materials.* D. Van Nostrand Co., Inc., 1958.
2. JACOBSEN, L. S., and AYRE, R. S.: *Engineering Vibrations.* McGraw-Hill Book Co., Inc., 1958.
3. TIMOSHENKO, S., and YOUNG, D. H.: *Advanced Dynamics.* McGraw-Hill Book Co., Inc., 1948.

CHAPTER 2

Materials

THE STRUCTURAL DESIGNER must choose member sizes and materials that will prevent failures. To do this, he must have both information about loads and the resulting stresses and information concerning the characteristics of various materials under various stress conditions. These characteristic properties are determined experimentally by subjecting materials to both standard and special tests. Although the designer usually sizes structural members so that elastic limits are not exceeded, he is interested in material behavior up to the ultimate strength. Structures are designed to working stresses, which are somewhat lower than critical stress values in order to allow for variations in materials, unpredictable stress concentrations, and other uncertainties. To achieve efficient and reliable structures, these working stresses must be established at realistic values. In order to obtain these realistic values, the engineer must understand material failure modes.

STATIC-LOAD FAILURE

Figure 2.1 illustrates a typical stress-strain curve for a ductile ferrous material in tension (curve *A*). Curve *B* shows the typical behavior of some nonferrous ductile materials, such as aluminum and magnesium. These materials do not have well-defined elastic limits and yield points. The yield stress is therefore defined as that corresponding to a strain of 0.002 in./in. (0.2 percent offset).

In an elastic structure, failure occurs if the elastic limit is exceeded, as the material will elongate plastically and will not return to its original size; i.e., permanent set will be induced. If plastic elongation can be tolerated, failure will occur at the ultimate strength of the material. This assumes a constant load, of course, since failure will not necessarily occur if the load is reduced as the material elongates. Failures of ductile materials in tension are accompanied by considerable "necking down" of the specimen, and are referred to as shear fractures, since the shear stress is usually the critical property. Ductile materials in compression fail either because the material yields in shear and "barrels," or because the member becomes unstable and buckles.

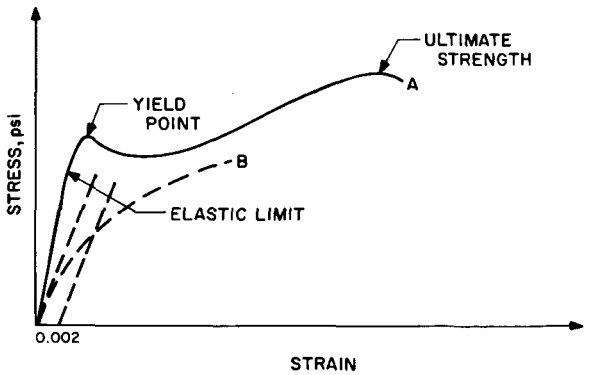

FIGURE 2.1—Stress-strain curves for ductile materials.

Brittle materials have much less capacity to deform plastically. These materials are generally stronger in compression than tension and have very low proportional limits. Tensile failures show little necking. Fractures of this class are called cohesive fractures, and they occur when the magnitude of the normal stress on one of the principal planes of the material reaches the critical value. Figure 2.2 shows a stress-strain curve for a brittle material.

Static-load failures occur because a poor choice of member material and/or size allows the stress to exceed the critical normal stress or shearing stress values, whether they be elastic or ultimate. Such failures may be caused by "stress concentrations," which are physical and/or metallurgical material discontinuities that allow local stress levels to exceed expected values. These stress concentrations have more of an effect upon materials which are lacking in toughness. In such materials local yielding around discontinuities does not take

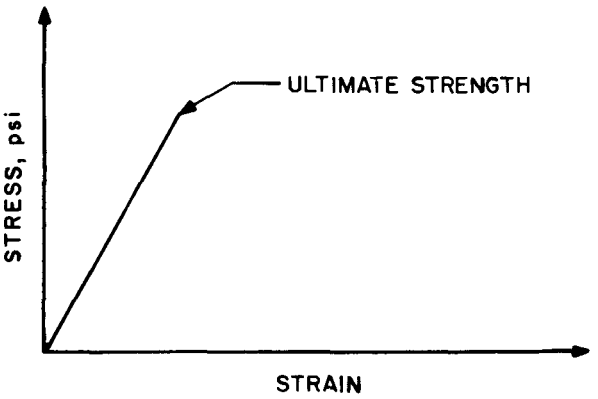

FIGURE 2.2—Stress-strain curve for brittle material.

place and failure occurs at a stress much lower than the predicted critical value. It should be noted that the properties of materials vary not only with tension and compression, but also with temperature, rate of loading, and in some materials (such as rolled beryllium sheet) with the direction of the stress in the material.

FATIGUE FAILURES

Structural members associated with motion may be loaded dynamically, with the result that stresses may be fluctuating instead of constant. Such fluctuating stresses can cause failure at levels below ultimate strength values. Failures of this class are called fatigue failures, and are extremely common whenever alternating stresses occur; for example, in loaded rotating shafts and in spacecraft components undergoing launch vibrations.

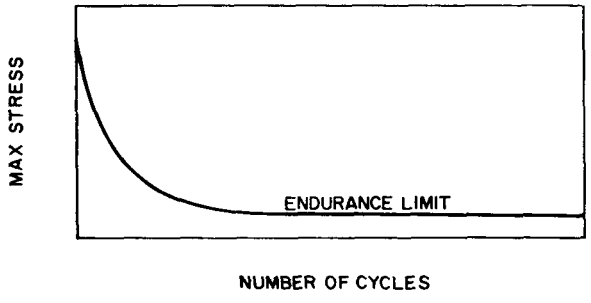

FIGURE 2.3—Endurance curve for a ferrous material.

Figure 2.3 shows a plot of maximum stress required to cause failure of a rotating steel shaft as a function of the number of cycles completed. The magnitude of the stress required to produce failure decreases as the number of cycles of stress increases. For nonferrous materials, such as aluminum, there is no definite endurance limit. A working endurance limit is defined as the maximum fracture stress at 500 million cycles. Failure occurs because an infinitesimal crack occurs within the material owing to a local defect or a stress concentration. The crack then spreads until the remaining cross-sectional area is so small that failure results. This type of fracture contains two regions, one rather smooth due to the gradual development of the crack, the other silky and fibrous due to the sudden brittle fracture. The appearance of the brittle portion causes this type of fracture to be incorrectly called "crystallization" by the layman.

IMPACT FAILURE

An impact load is one in which the time required for the force value to increase from zero to maximum is small compared with the natural

period of vibration of the member. Testing is performed by applying standard impacts to standard specimens. The failures range from brittle to ductile, depending upon the temperature and material of the specimen. Impact testing provides a good indication of the toughness (the ability to absorb energy during plastic deformation) of a material. Materials susceptible to brittle impact failure are dangerous for structural use, since fractures may occur at ambient temperature with no deformation or forewarning.

CREEP FAILURE

Materials deform plastically under a steady load over a period of time. Such deformation is called creep and is extremely temperature sensitive. In some materials, such as plastics and the lower melting-point metals, the creep can be pronounced at normal usage temperatures. If a creep test is performed within a temperature range in which work hardening will occur, the initial deformation will provide this work hardening and the specimen will deform until it can support the applied load. The curve of elongation versus time will then appear similar to curve *A*, figure 2.4. If the test is performed above the temperature range in which work hardening can occur, the initial

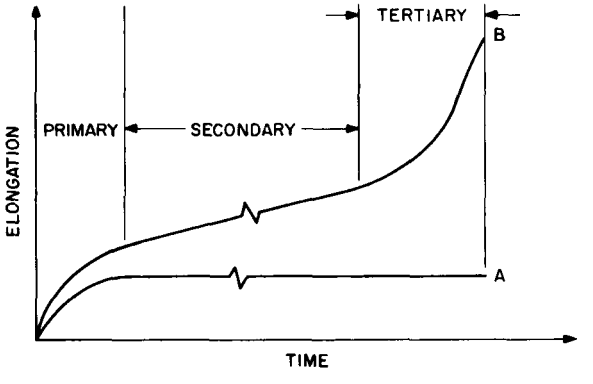

FIGURE 2.4—Typical creep curves.

rapid deformation will decrease to a steady rate of elongation (secondary creep) rather than to zero (see curve *B*). This nearly constant rate may persist for long periods of time. Eventually it will pass into a third stage of creep (tertiary creep) during which the specimen elongates at an increasing rate, and then necking-down and fracture will occur. Creep causes failure by plastically deforming critical structural members, thus relieving stresses in the creeping member and increasing stresses in others.

Creep tests are usually performed at various temperature levels for practical time periods and then extrapolated by designers who must consider creep in their structures. However, this is not too satisfactory as the curves cannot be extrapolated with a high degree of confidence. Tests of this nature generally establish the primary creep curve and part of the secondary creep region, but do not usually extend to the inflection point at the beginning of the tertiary creep region.

TECHNOLOGY DEVELOPMENT

At the present time, materials technology is expanding rapidly due to ever-increasing knowledge of the basic nature of materials. Although steel is not widely used in spacecraft, the history of the development of steel is a good example. Iron was one of the first metals used by man. However, it took man until the time of the swordmakers of Damascus to learn how to increase the ultimate strength of iron from 1500 lb/in^2 (a crystal of pure iron) to 150 000 lb/in^2 (the strength of the steel in some of the Damascus swords). The same slow rate of learning contined until comparatively recently. In this century, however, man has succeeded in alloying steels to improve various properties and in quantitizing heat treatment so as to be able to reproducibly manufacture steel products with various degrees of strength, hardnesses, and so forth. Early in this century it also became possible to predict the theoretical strengths of metals through a knowledge of interatomic forces. For iron, the computed value of strength was about 1.6 million lb/in^2, or approximately a factor of 1000 over the strength of a pure crystal of iron and a factor of 10 over the highest strength steels obtainable.

In the 1930's the dislocation theory was advanced to explain the disparity between theoretical and actual strength. Dislocations are discontinuities in the lattice of metal crystal structure which propagate rapidly and easily through the metal when stress is applied. These defects explain the weakness of real metals. The theory is also consistent with the known methods of increasing the strength of steel. These methods are:

(1) Adding carbon (carbon atoms in crystal structure immobilize dislocations)
(2) Decreasing grain size (dislocations cannot cross grain boundaries)
(3) Deforming the steel by cold working (deformation causes tangles of dislocations, which impede the progress of other dislocations)
(4) Precipitating hard particles in steel (particles trap dislocations)
(5) Quenching from high temperatures (carbon held in solution impedes dislocations)

Mild structural steels generally have an ultimate strength of about 60 000 lb/in^2. High-strength steels are generally heat treated to between 150 000 and 200 000 lb/in^2. Tool steels may occasionally reach strengths of 300 000 lb/in^2, but with corresponding losses in toughness and ductility. Until a few years ago such levels represented the best attainable steels.

Two recent developments in steels are perhaps typical of the current rate of progress. One is the development of Ausformed steel by the Ford Scientific Laboratory. This development was started in 1954 because of the discovery by two Dutch metallurgists, E. M. H. Lips and H. van Zuilen, that if steel is deformed in the austenitic form before it is quenched to martensite, the resulting properties are greatly improved. Alloys such at Type H–11 contain alloying ingredients which delay the breaking down of the austenite. Thus, properties can be quite closely controlled by varying the temperature at which the deforming takes place, the amount of deforming, and the alloying of the steels. One Ausformed steel (Vascojet MA) contains 0.55 percent carbon and a total of 12 percent of other alloying elements. This steel, when heated, deformed, quenched, and then tempered, has a yield strength of over 400 000 lb/in^2, an ultimate strength of over 475 000 lb/in^2, and ductility equal to or exceeding that of equivalent conventionally quenched and tempered steels.

The second development is that of Maraging (martensitic aging) steels by International Nickel. These steels contain essentially no carbon. A typical Maraging alloy may contain 15 percent nickel, 9 percent cobalt, 5 percent molybdenum, and 0.5 percent titanium. They are heat treated by first being heated to about 1500° F, and are then allowed to air cool to room temperature. The steel is then formed, as it is extremely soft and malleable in this temper. After forming, the steel is aged at about 900° F for several hours. After this aging process, the Maraging steels have ultimate strengths of about 300 000 lb/in^2, ductilities about twice those of conventional steels, and exceptional toughness.

PROPERTIES OF SPACECRAFT STRUCTURES

Most spacecraft structures consist of conventional aircraft materials. Special and exotic materials are currently used only for unusually critical components, such as those subjected to extremely high temperatures, those which must be transparent to radio frequencies, or those which must have extremely high thermal conductivities and capacities. It is of interest at this time to discuss briefly some of the most widely used spacecraft structural materials.

The properties of these materials are summarized in table 2.1. The values shown are for commercially available materials and do not represent values available in the laboratory.

Steels

Ordinary low- and medium-alloy carbon steels are rarely used in spacecraft. They are extremely magnetic, which will adversely affect any magnetic-field sensing experiments aboard the spacecraft. In addition, they oxidize and corrode rather rapidly and are extremely dense. They are used only in cases where high strength (either tensile, compressive, or shear or bearing) is essential; for instance, in springs, mechanism elements, and pins. The properties of an alloy steel are shown in table 2.1 for comparison with the other materials.

Stainless steels receive wider usage since they are resistant to corrosion and oxidation and are only very slightly magnetic. They are also employed when high strength is desired, as in nonmagnetic gears. Three stainless steels are shown in table 2.1. The 300-series steels, of which 301 is the lowest alloy member, are easily formed in the annealed condition. They are hardened by cold working and then stress relieved. Unfortunately, strain hardening tends to increase ferromagnetic properties. The high rate of strain hardening causes some problems, since once formed, these steels are difficult to re-form. They can be readily welded, however. The free-machining grade of the 300-series, Type 303 condition A, is frequently used for small gears and fittings.

The 17–4 PH stainless is an age-hardening steel, extremely stable and strong in its hardened state. Stainless A–286, which was initially developed for its resistance to high temperatures, is age hardenable, can be formed, machined, and joined similar to the other stainless steels, and is extremely nonmagnetic.

Aluminums

Aluminum alloys are only about one-third as dense as steels. However, as can be seen from table 2.1, the specific strengths (strength per pound) and the specific moduli of elasticity are quite similar. For uses which require only tensile strength or simple stiffness, there is little advantage in using aluminum instead of steel. However, a large amount of weight can be saved when aluminum is used in an actual structure. For one reason, many portions of a structure, such as end fittings, are geometrically constrained. A given amount of metal must be used to fabricate the component, even though the metal may carry extremely small loads. Obviously, the use of a lighter material for these fittings is advantageous. As another example of the advantage of lighter materials, let us examine the

The 5052 alloy is popular for use in extremely thin foils and sheets. It can withstand severe cold working without losing its formability.

The 6061–T6 alloy (solution heat treated and artificially aged) is widely used, even though it is not a very high-strength alloy. It has excellent formability, is extremely stable, and may be readily brazed and welded. It is the most weldable aluminum alloy listed in table 2.1.

The 7075–T6 is an extremely high-strength aluminum alloy. It is used in situations where high strength is desired even though some ductility, notch toughness, and formability must be sacrificed.

Magnesiums

Magnesium is only two-thirds as dense as aluminum. Applying the buckling example used in the previous section, the critical load which can be supported by a magnesium beam of equivalent weight is increased by a factor of 1.5 over that of the aluminum beam. This, in turn, represents a factor of 4 over the steel beam.

The AZ31B alloy is one of the most readily available in wrought forms. It has good formability and can be welded. Cold forming is possible only to a limited extent. This alloy cannot be heat treated and is strengthened only by cold working. Like all magnesium alloys, the machining characteristics are excellent, except, of course, in the annealed condition. Magnesium can even be machined on high-quality woodworking equipment.

The AZ80A–T5 alloy (artificially aged) is heat treatable and is one of the strongest forging alloys. However, it has poor notch sensitivity, is difficult to form, and has limited weldability.

The ZK60–T5 alloy has good strength and ductility with good notch toughness. The extrusion and forging properties of this alloy are excellent, but its weldability is poor.

Titanium

Titanium has high strength and good high-temperature qualities. It is used for such applications as fasteners and pressurized tanks. Because of its high hardness it is rather difficult to work with. The 6Al–4V alloy is heat treatable and many applications requiring intermediate strength levels are being found for its use. In the annealed conditions, it has superseded many of the non-heat-treatable alloys because of its good strength and stability up to 750° F. The impact strength and notch resistance of this alloy are also good at subzero temperatures. The alloy can be formed by special methods and has fair weldability. The machining characteristics are similar to those of the austenitic stainless steels.

Beryllium Copper

Beryllium copper is used for parts which require high strength and toughness, where carbon steels cannot be used for such reasons as magnetism. It is used for springs and high-strength electrical conductors. It is easily formed in the annealed (A) condition after which it is heat treated to a high strength (AT condition) using a low-temperature aging cycle.

Beryllium

Beryllium is a very interesting structural material. As can be seen in table 2.1, it has extremely high strength-to-weight and stiffness-to-weight ratios. If the buckling-designed column were made from beryllium, it would be able to support a critical load 28.5 times that of the steel column. Since many spacecraft members are designed for stiffness in order to minimize deflections under the vibration environment, beryllium is highly attractive. In addition beryllium has high thermal capacity and conductivity. Unfortunately, it is extremely brittle and difficult to form. It cannot be successfully cast and must be produced by a combination of powder metallurgy and extrusion. If beryllium is formed by rolling, the product exhibits serious directionality in mechanical properties. Many of the deficiencies which occur in present beryllium, however, are attributed to impurities in the metal. Because of the large inherent advantages of beryllium, considerable research is currently being undertaken in an attempt to minimize these problems. As a point of interest, beryllium has a theoretical strength of 2.6 million lb/in^2, as opposed to 1.6 million for iron alloys, 0.6 million for aluminum, and 0.4 million for magnesium. Beryllium is obviously a material of very high potential.

Fiber Glass

Fiber glass is used where radio-frequency transparency, electrical or thermal resistivity, or extreme formability is required. The fiber-glass laminate listed in table 2.1 is the familiar fiber-glass-epoxy mixture containing equivalent quantities of glass fibers in both the warp (length) and fill (width) directions.

Unidirectional fiber glass may be manufactured by orienting the fibers in one direction. The qualities are increasingly good in that direction and correspondingly poorer in the normal direction. In table 2.1 properties in the strong direction are given for unidirectional glass made from epoxy and S-glass, a product of the Minnesota Mining and Manufacturing Company. The S-glass fibers are extruded and covered with a thin layer of epoxy, a process which minimizes notch formation. Since notch formation is a major source of weakness in

glass, the strength is thereby improved over that of uncoated glass fibers.

Lexan

The properties of Lexan, a thermoplastic resin material, are shown merely to provide a typical example of a nonmetallic structural material. Lexan is an extremely tough polycarbonate. It is easily formed and quite strong. However, it has the disadvantage of extreme susceptibility to certain chlorinated solvents.

Miscellaneous

A good example of the use of ingenuity and efficient materials to fill a need is the titanium roll-welded sandwich structure developed jointly by Battelle Memorial Institute and Douglas Aircraft Company. The sandwich structure, which is exceedingly useful for such applications as tank skin, where both strength and buckling are problems, is produced in the following manner:

(1) The skins and core forms are fabricated by conventional sheet-metal techniques. The core may typically be a corrugation.
(2) The skins and cores are laid up with mild-steel members in the openings in the sandwich.
(3) Mild-steel plates are placed on both sides and around the edges of the lay-up.
(4) The cover plates are welded together.
(5) The entire assembly is then rolled as if it were a slab of solid steel. The rolling operation bonds the titanium to the titanium and to the steel. The original dimensions were chosen so that after rolling the titanium members of the sandwich are of the desired dimensions. In general, the titanium sheet becomes thinner and the sandwich becomes wider and thinner.
(6) The plate is then formed to the desired shape for the sandwich by conventional forming methods. During this forming the titanium members cannot buckle, since they are supported by the steel. Because of this factor, the sandwich can be formed into very complex and doubly curved shapes.
(7) The steel is etched away by a reagent which does not affect the titanium (such as nitric acid). The resulting sandwich has acquired the desired form at an economical price. (Production cost is estimated to be approximately twice that of the titanium material.)

MANUFACTURING OF SPACECRAFT STRUCTURES

The manufacture of spacecraft structures is influenced by the importance of meeting delivery schedules, the extreme emphasis on

reliability, and the small number of items required. Planetary spacecraft must be fired on schedule, since with present booster capabilities the planets become accessible only periodically (approximately every 2 years for Mars and Venus). Lunar shots, earth orbiters, and deep-space probes may be launched more often, but the processes involved in developing and launching spacecraft are so complex that schedules must be maintained throughout the program to prevent intolerable inefficiency.

Because of the need for meeting schedules with complex and critical parts, conventional fabrication techniques are used whenever possible. The procurement of parts manufactured by exotic forming and joining techniques frequently results in lengthy and costly development programs on the process itself. As in most phases of spacecraft engineering, the tried and proven is desirable if it will do the job.

Because of the emphasis on reliability, spacecraft engineers seek to prevent the occurrence of unknown problems by designing parts as closely as possible to the desired nominal dimensions. Therefore, tolerances on spacecraft components tend to be somewhat tighter than those found in conventional manufacturing. Since engineering and development costs far outweigh manufacturing costs, tighter tolerances do not cause intolerable expenditures. On the other hand, the necessity for meeting fabrication schedules and the obvious senselessness of overly tight tolerances prevent the engineer from working to impractically small limits.

The most noticeable influence in spacecraft fabrication is the small quantity produced. For example, castings and stampings are scarce. Castings are avoided partly because of the difficulty of insuring homogeneity and lack of porosity. However, in most cases it is at least as economical to machine a part from solid stock as to pay for the necessary molds, dies, and fixtures to cast, stamp, or weld the job. Figure 2.5 is the back view of the radiometer reflector that scanned Venus during the 1962 Mariner flyby. It was machined from a solid block of material. The result was more predictable from a metallurgical standpoint, and involved no more expense than a casting or a weldment.

Spacecraft structures are assembled by conventional techniques. Riveted construction is preferred to welded construction in most structural usages because of ease of inspection, ability to hold very tight tolerances, greater structural damping, and the avoidance of unwanted heat treating and stress concentrations arising from welding. Screws must be used in conjunction with hard inserts in soft metals such as aluminum and magnesium. Screws, nuts, and bolts are frequently made of titanium because of its light weight and low

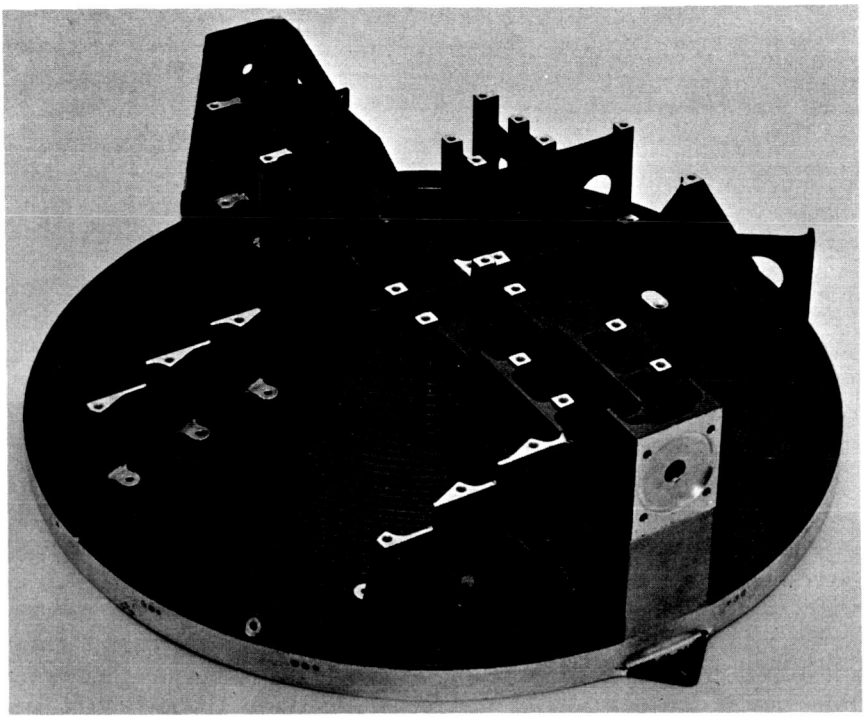

FIGURE 2.5—Mariner Venus 1962 planetary radiometer dish. (JPL photograph.)

magnetism. Locking screws and nuts are generally used whenever possible. Great care is taken during structural assembly to install fasteners to optimum torque and load values because of the critical and highly stressed nature of spacecraft structural components.

BIBLIOGRAPHY

1. Timoshenko, S.: *Strength of Materials.* Part II. D. Van Nostrand Co., Inc., 1956.
2. Aeronautical Systems Division, Air Force Systems Command: *Aerospace Structural Metals Handbook.* Vols. I and II. Syracuse Univ. Press, 1963.
3. Armed Forces Supply Support Center (Washington, D.C.): *Strength of Metal Aircraft Elements.* Military Handbook MIL–HDBK–5, 1961.

CHAPTER 3

Computers and Testing

STRUCTURAL USE OF COMPUTERS

THE ANALYSIS OF STRUCTURES requires a large amount of iterative and repetitive application of basic relationships. To speed up this process, structural engineers use shorthand notation whenever possible and make use of computers to perform laborious repetitive calculations. Using a computer for such calculations allows the structural engineer to extend his analyses to much greater detail than when he was limited by the necessity of performing manual calculations. However, unless well understood, the computer can also be a misleading and confusing influence. Mathematical trends and physical meaning can be masked by the quantity of numbers which the computer produces. It is also a great temptation for the engineer to argue that "the computer program says the part will not fail," even though the computer is operating solely upon the assumptions, constraints, and simplifications of the engineer. Jet Propulsion Laboratory (JPL) has a stiffness program which enables the structural designer to make systematic structural analyses rapidly and efficiently by use of a computer. An examination of this rather typical program may help clarify the use of a computer in the performance of structural calculations. A more thorough discussion of this program may be found in reference 1.

The JPL stiffness program has several forms. Its most widely used form assumes negligible structural damping. Another form has just been completed which can handle appreciable amounts of distributed and point damping. The program has the capability of analyzing the following types of structures:

(1) Three-dimensional structures with pinned joints
(2) Three-dimensional structures with rigid joints and circular member cross sections
(3) Planar structures with rigid joints, loaded in plane
(4) Planar grid structures with rigid joints, loaded normally to the structural plane

In addition, it must be assumed that the structure consists of uniform weightless members with all loads and inertias lumped at the joints.

In order to describe the structure, the following quantities must be fed into the program:

(1) The coordinates of the joints
(2) The locations of restraints
(3) The properties (geometric, elastic) of the members
(4) The inertias at the joints

To describe the loading, the following properties are fed into the program:

(1) The static loads at the joints
(2) The acceleration of a joint during free vibration in a normal mode

The program will then perform the necessary computations to find:

(1) Deflections and member stresses for static loading
(2) Frequencies, mode shapes, and member stresses during free vibration in normal modes

The program can handle structures of up to 130 degrees of freedom (computation time for 130 degrees of freedom on an IBM 7090 computer is approximately 20 minutes). As an example of overall times involved, a typical spacecraft structural run (90 degrees of freedom, statically indeterminate to the 48th degree) required, after idealization, 2 hours to write the input, 20 minutes to punch the cards, and 10 minutes of computer time.

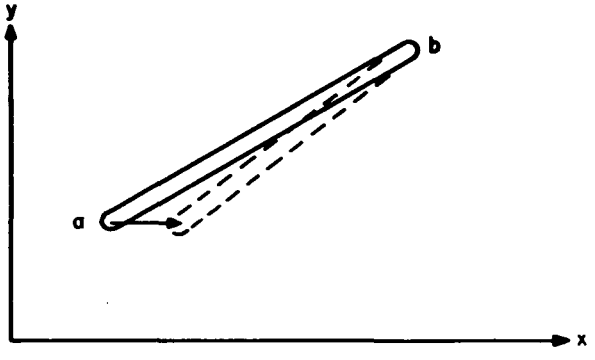

FIGURE 3.1—Truss member.

Matrix notation is commonly used in the analysis of structures because it serves as a convenient method of shorthand notation and because matrix algebra enables the sense of mathematical operations to be seen without being obscured by a massive amount of detail. Matrix algebra and matrix notation allow large numbers of linear relationships to be solved in an elegant, lucid, and compact manner. The JPL stiffness program makes use of matrices both in the engineer's

work and the computer's work. A brief examination of the method involved follows.

In a linear structure, member stresses are proportional to deflections. The constant of proportionality k is called the stiffness. The expression of equilibrium between a force applied to an n-degree-of-freedom system and the system may be written as

$$f_i=\sum_{j=1}^{n} k_{ij}u_j \qquad (i=1, 2, \ldots n)$$

where f_i is a component of force and u_j is a component of deflection. This relation can be written in matrix notation as

$$F=KU$$

If a joint in the structure undergoes free vibration in a normal mode m, the component deflections of the joint will be of the form

$$u_i=|u_{im}| \sin \omega_m t$$

The inertia load acting in the direction of the component of vibration will then be

$$f_i=-m_i\ddot{u}_i=m_i|u_{im}|\omega_m{}^2 \sin \omega_m t$$

This load can be substituted back into the expression for force equilibrium:

$$m_i|u_{im}|\omega_m{}^2=\sum_{j=1}^{n} k_{ij}u_{jm} \qquad (i=1, 2, \ldots n)$$

and this expression can be written in matrix notation as

$$MU_m\omega_m{}^2=KU_m$$

Knowing the set of loads F and finding the stiffness matrix K from the description of the structure, the computer can solve for the set of displacements U. Knowing the set of inertias M for the structure, the computer can solve for the normal mode shapes and frequencies (eigenvectors and eigenvalues). The computer can then find member stresses by using displacements from the static forces and the free-vibration mode shapes.

The computer generates the stiffness matrix K in the manner shown in figure 3.1. In this figure member ab has a length L and direction cosines θ_1 and θ_2, which can be computed from the coordinates of a and b. The area and elasticity of the member are known. By successively deflecting each end in the x and then the y direction by a small amount, simultaneously holding the other end

fixed, equilibrium relations lead to expressions such as the following.

If a is deflected through u_{ax},

$$f_{ax}=\frac{AE}{L}\theta_1^2 u_{ax}$$

$$f_{ay}=\frac{AE}{L}\theta_1\theta_2 u_{ax}$$

$$f_{bx}=\frac{AE}{L}(-\theta_1^2)u_{ax}$$

$$f_{by}=\frac{AE}{L}(-\theta_1\theta_2)u_{ax}$$

Since linear assumptions are used, the total components of force can be found by superposition of component forces resulting from discrete displacements:

$$f_{ax}=\frac{AE}{L}\theta_1^2 u_{ax}+\frac{AE}{L}\theta_1\theta_2 u_{ay}-\frac{AE}{L}\theta_1^2 u_{bx}-\frac{AE}{L}\theta_1\theta_2 u_{by}$$

The expression $F=KU$ then appears as

$$\begin{Bmatrix} f_{ax} \\ f_{ay} \\ f_{bx} \\ f_{by} \end{Bmatrix} = \frac{AE}{L} \left[\begin{array}{cc:cc} \theta_1^2 & \theta_1\theta_2 & -\theta_1^2 & -\theta_1\theta_2 \\ \theta_1\theta_2 & \theta_2^2 & -\theta_1\theta_2 & -\theta_2^2 \\ \hdashline -\theta_1^2 & -\theta_1\theta_2 & \theta_1^2 & \theta_1\theta_2 \\ -\theta_1\theta_2 & -\theta_2^2 & \theta_1\theta_2 & \theta_2^2 \end{array}\right] \begin{Bmatrix} u_{ax} \\ u_{ay} \\ u_{bx} \\ u_{by} \end{Bmatrix}$$

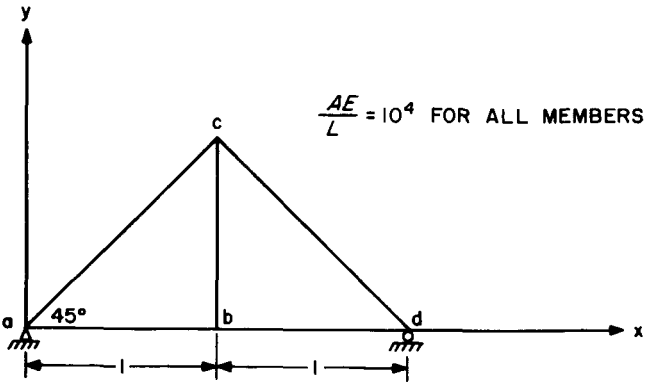

FIGURE 3.2—Simple truss.

which may be written as

$$\begin{Bmatrix} f_a \\ f_b \end{Bmatrix} = \begin{vmatrix} K_{aa} & K_{ab} \\ K_{ba} & K_{bb} \end{vmatrix} \begin{Bmatrix} u_a \\ u_b \end{Bmatrix}$$

Superposition can be used to build up matrices for any structure. For instance, by applying these principles to the simple structure shown in figure 3.2, the following matrix expression can be built up:

$$\begin{Bmatrix} f_a \\ f_b \\ f_c \\ f_d \end{Bmatrix} = 10^4 \left[\begin{array}{cc|cc|cc|cc} 1.5 & 0.5 & -1 & 0 & -0.5 & -0.5 & 0 & 0 \\ 0.5 & 0.5 & 0 & 0 & -0.5 & -0.5 & 0 & 0 \\ \hline -1.0 & 0 & 2 & 0 & 0 & 0 & -1 & 0 \\ 0 & 0 & 0 & 1 & 0 & -1 & 0 & 0 \\ \hline -0.5 & -0.5 & 0 & 0 & 1 & 0 & -0.5 & 0.5 \\ -0.5 & -0.5 & 0 & -1 & 0 & 2 & 0.5 & -0.5 \\ \hline 0 & 0 & -1 & 0 & -0.5 & 0.5 & 1.5 & 0.5 \\ 0 & 0 & 0 & 0 & 0.5 & -0.5 & 0.5 & 0.5 \end{array}\right] \begin{Bmatrix} u_a \\ u_b \\ u_c \\ u_d \end{Bmatrix}$$

Since $u_{ax}=u_{ay}=u_{dy}=0$, and because f_{ax}, f_{ay}, and f_{dy} are reactions which may be statically determined, the expression for the deflections may be simplified to

$$\begin{Bmatrix} f_{bx} \\ f_{by} \\ f_{cx} \\ f_{cy} \\ f_{dx} \end{Bmatrix} = 10^4 \begin{vmatrix} 2 & 0 & 0 & 0 & -1 \\ 0 & 1 & 0 & -1 & 0 \\ 0 & 0 & 1 & 0 & -0.5 \\ 0 & -1 & 0 & 2 & 0.5 \\ -1 & 0 & -0.5 & 0.5 & 1.5 \end{vmatrix} \begin{Bmatrix} u_{bx} \\ u_{by} \\ u_{cx} \\ u_{cy} \\ u_{dx} \end{Bmatrix}$$

The computer can easily solve such matrix relations (using matrix algebra techniques such as Gaussian elimination) for the deflection values. Solution of the dynamic equation requires more manipulation of the matrices, but once again the manipulation can be easily accomplished with a computer.

STRUCTURAL TESTING

Structural testing is an extremely important aspect of spacecraft engineering. Testing may be either destructive, to evaluate design

margins and physical properties, or nondestructive, to evaluate structural parameters and assure that structures have no invisible defects. It is essentially impossible ever to attain exact mathematical models for real structures. Therefore, testing is necessary to compensate for the limitations of analysis and to check the validity of the assumptions which go into analysis. Structural testing begins with tests on mockups of preliminary design ideas and extends through flight acceptance testing of completed flight hardware.

Structural testing may be either static or dynamic. In static testing, loads or pressures are applied to various portions of the structure and the deflections and failure modes are recorded. The equipment involved may include lead weights, pressurized fluids, centrifuges, sand, bags of shot, dial indicators, strain gages, fish scales, and any other apparatus suited to the job and available to the engineer. Static tests are usually quite straightforward and are done as needed to ascertain the elastic and plastic behavior of the structure under constant stresses.

In dynamic testing, the structure is subjected to a dynamic input. The testing may be either modal or environmental. Modal testing is used to determine natural mode shapes and natural frequencies (see ref. 2). Small vibration exciters (shakers) are applied to various portions of the structure in order to allow the engineer to understand more clearly the dynamic responses. The shakers are usually controlled-force machines. This type of testing is predominately a design tool.

Environmental testing is predominately used to prove designs and hardware. The shakers used are displacement controlled and are powerful enough so that they consider the test specimen as a black box; that is, the specimen does not influence the input. The shakers used below 20–50 cps are usually hydraulically operated, while those used above 50 cps are electromagnetically operated. Figure 3.3 is a diagram of an electromagnetic shaker.

The environmental dynamic structural input is intended to represent the flight input or some percentage of it. Unfortunately, the flight dynamic environment is neither simple nor absolutely predictable. Intuitively, the major portion of the input energy should be at the natural vibrational frequencies of the booster-spacecraft combination. Unfortunately, these frequencies change as fuel is consumed. Unpredictable inputs from aerodynamic forces and guidance inputs add another complication. As a result, an upper level of input can be determined; however, it is presently not possible to guarantee that inputs will be restricted to discrete frequency bands.

Composite dynamic inputs are, therefore, used for design and test. These inputs are conservative and are the result of a compilation of

flight data. They are quite severe, as they allow the majority of spacecraft components to reach full dynamic resonance in at least one natural mode. Table 3.1 shows the test levels used by JPL for testing the 1964 Mariner Mars spacecraft. These levels were applied to the spacecraft at the mounting interface with the Agena. Test levels for isolated components were, of course, increased to compensate for structural magnifications. The test acceptance levels are more severe than the expected worst-case flight levels and are for the purpose of proving the design. The flight acceptance levels represent the expected worst-case flight levels and are for proving hardware which is to be flown.

Shock tests and acoustic tests are also performed on spacecraft hardware. For conventional spacecraft missions (no high-impact

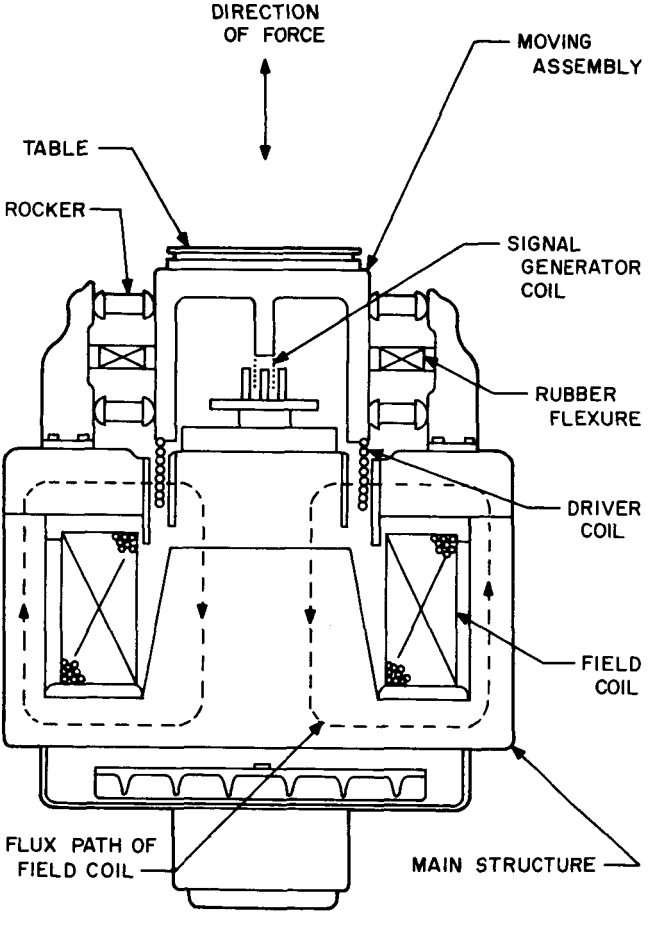

FIGURE 3.3—A typical electromechanical vibration exciter.

TABLE 3.1—Testing levels for 1964 Mariner Mars spacecraft.

Frequency	Amplitude	Time
Test acceptance		
1–4.4 cps	±1.5 in.	3 min
4.4–15 cps	3g peak value	3 min
Noise	14g rms	6 sec
Noise + 15–40 cps 40–250 cps 250–2000 cps	5g rms + 2g rms 9g rms 4.5g rms	600 sec
Noise	14g rms	18 sec
Flight acceptance		
Noise	9g rms	6 sec
Noise + 15–40 cps 40–250 cps 250–2000 cps	3g rms + 1.5g rms 6.0g rms 3.0g rms	200 sec
Noise	9g rms	6 sec

entries or landings) the most extreme shocks encountered are from handling. Equipment and handling fixtures and cases must be designed and tested to survive accidental jarring and dropping. Acoustic tests are used to simulate the acoustic input to the spacecraft. This input is transmitted to the spacecraft from the shroud through the gas between the shroud wall and the spacecraft. It is noisy in character since it is caused by aerodynamic phenomena in flight. Large, flimsy objects can be damaged by this acoustic input. Testing is usually done by subjecting portions of the structure to acoustic energy generated by various acoustical sources, such as loudspeakers and air-driven horns.

An interesting example of a test involving the structure as well as other portions of the spacecraft system is the Simulated Midcourse Interaction Test (SMIT) which is performed on JPL spacecraft. This test is done to prove that the spacecraft has no dynamic problems which would impair the successful performance of the midcourse correction maneuver. During the firing of the midcourse correction

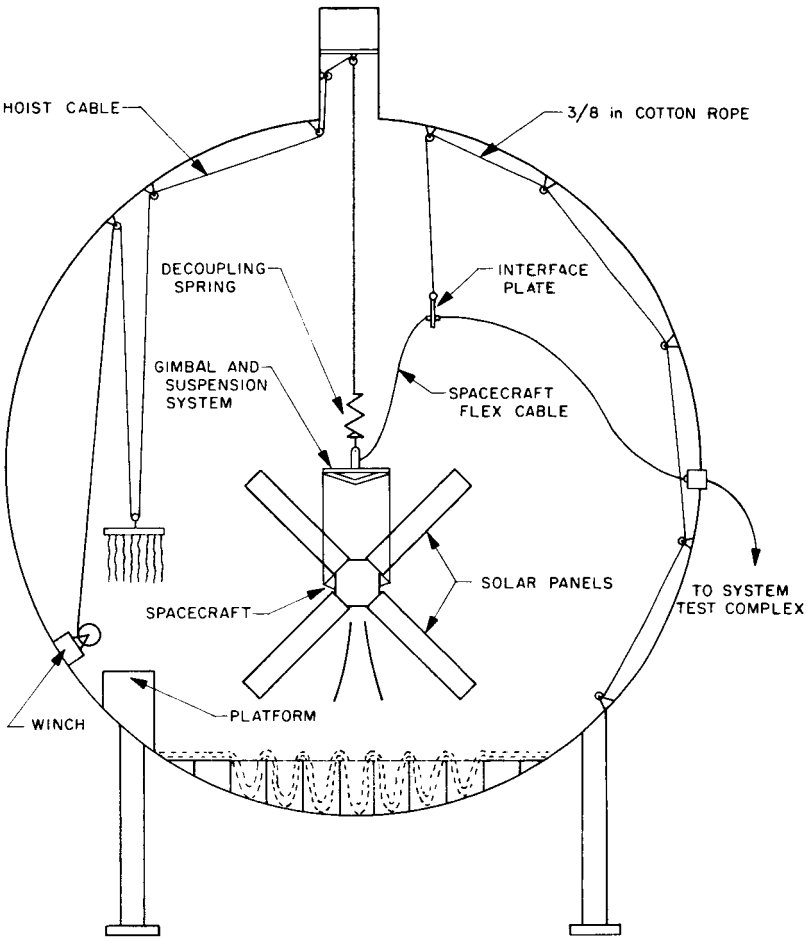

FIGURE 3.4—Setup for Simulated Midcourse Interaction Test.

motor, it is necessary to insure that the direction of the thrust vector is controlled. This may be done by using a firing duration which is very short compared with the natural period of the vehicle, by spinning the vehicle during firing, by using an extremely powerful attitude-control system, by gimballing the motor, or by using thrust deflectors in the rocket exhaust. The last system is used in the Mariner class spacecraft. These thrust deflectors are controlled by an autopilot which uses gyros for position and rate inputs.

Spacecraft attitude is also controlled during the midcourse maneuver by means of gyros. Unfortunately, the sensing gyros are located some distance from the attitude-control jets and from the thrust deflectors. Therefore, the elastic behavior of the structure enters into

the dynamics of the control loop. In missiles, this problem is sometimes referred to as the aeroservoelastic problem. Missile guidance systems use sensors to determine attitude errors. These errors then cause changes in the direction of the thrust vector. If the missile is not infinitely rigid, the direction change will excite normal vibration modes. Since the sensor will "see" the local slope of the missile structure, the shape and frequency of the vibration modes will directly affect stability.

Because of the inertia of the spacecraft and the relatively small thrust of the engine, the autopilot must be sensitive to low frequencies. Because of spacecraft weight limitations, structures tend to be flimsy and to have low resonant frequencies. If large structural resonances occur in the sensitive region of the autopilot, they will adversely affect the ability of the autopilot to perform its job.

After the design of Mariner Mars had been completed, the spacecraft was tested during a simulated midcourse firing in order to determine experimentally the effect of the dynamic spacecraft properties on the autopilot behavior. Figure 3.4 is a schematic of the test apparatus. The spacecraft was free to roll, pitch, yaw, and travel in a vertical direction. The test was run in a vacuum chamber to insure realistic rocket behavior and to avoid air-damping. A number of tests were made with various combinations of spacecraft and autopilot parameters. The tests confirmed that no serious dynamic interactions existed between the autopilot and the spacecraft structure. As is usual in the case of tests, much other information was also acquired concerning correlation between actual and predicted behavior.

REFERENCES

1. Batchelder, R. R., and Wada, B. K.: *Stiffness Matrix Structural Analysis.* Technical Memorandum 33–75, Jet Propulsion Lab., Feb. 1962.
2. Gayman, W. H.: *Some Facets of Model Vibration Testing.* Paper presented at 17th Annual Conference of Instrument Society of America, Oct. 1962.

CHAPTER 4

Spacecraft Structures

THIS CHAPTER contains illustrations of spacecraft equipment with pertinent description of structural detail. The examples shown, though too few in number to constitute a survey of structural approaches, do illustrate several spacecraft structural concepts.

Figure 4.1 shows the NASA–RCA Relay communications satellite. The satellite weighs 68 lb, is 27 in. in diameter at the base, and is 51 in. high overall. It radiates 10 watts of power and is capable of relaying 1 TV channel one way, 300 voice channels one way, or 12 voice channels two ways. The first Relay was launched on December 13, 1962, and the second on January 21, 1964. These satellites operate in an orbit with a 3000-mile apogee and an 800-mile perigee. They are spin stabilized with a spin rate of 150 rpm.

Figure 4.2 shows the Relay structure, which is made from formed and riveted 2024–T3 sheet aluminum and machined end fittings. The longitudinal resonance of the structure when loaded with the spacecraft components is approximately 100 cps. The total weight of the primary structure is 19.5 lb. The solar cells are bonded to epoxy-bonded aluminum honeycomb panels, each with three longitudinal stiffeners, 0.005-in. outer skins, and 0.003-in. inner skins. The vertical panel load is transferred to the primary structure at the upper hoop. At the lower end, the panels are mounted with reeds which are stiff only in the radial and the tangential directions. The panels are therefore isolated from column loading during launch. The set of 8 panels with cells, covers, wiring, and attachments weighs 32 lb.

Figure 4.3 shows the Bell Telephone Laboratories Telstar communication satellite. The satellite weighed 175 lb, was spin stabilized, and was the first commercially built satellite launched by the United States. Telstar I was launched on July 10, 1962, and Telstar II on May 7, 1963.

The electronic equipment in Telstar was contained in a hermetically sealed, foam-filled, $\frac{1}{16}$-inch 1100-series aluminum can. The sealed unit, complete with electrical system, weighed 85 lb and was extremely rigid. This container was suspended inside the structure with nylon lacings which were pretensioned so as to allow the package to have a first resonance at 40 cps in the axial (launch) direction and 15 cps in

771-733 O-65-4

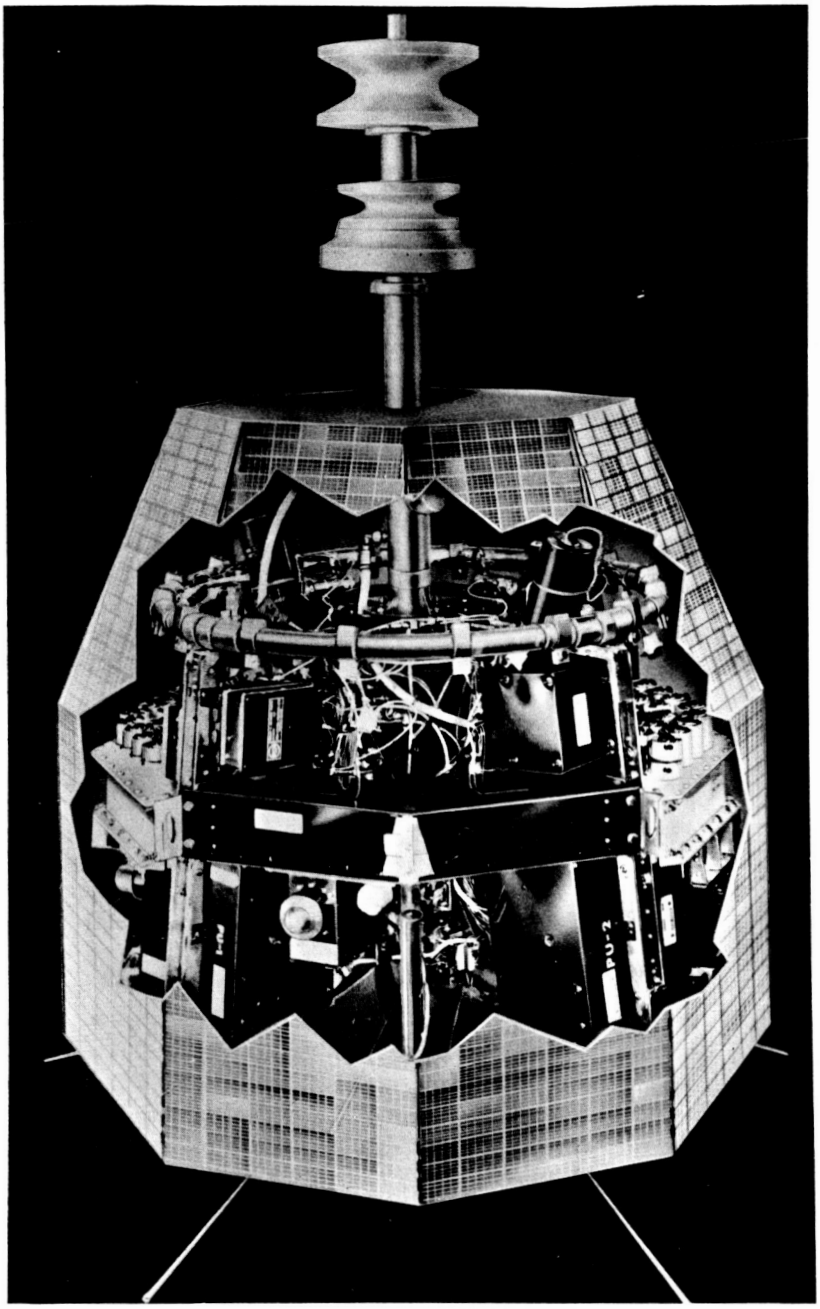

FIGURE 4.1—NASA–RCA Relay communications satellite. (RCA photograph.)

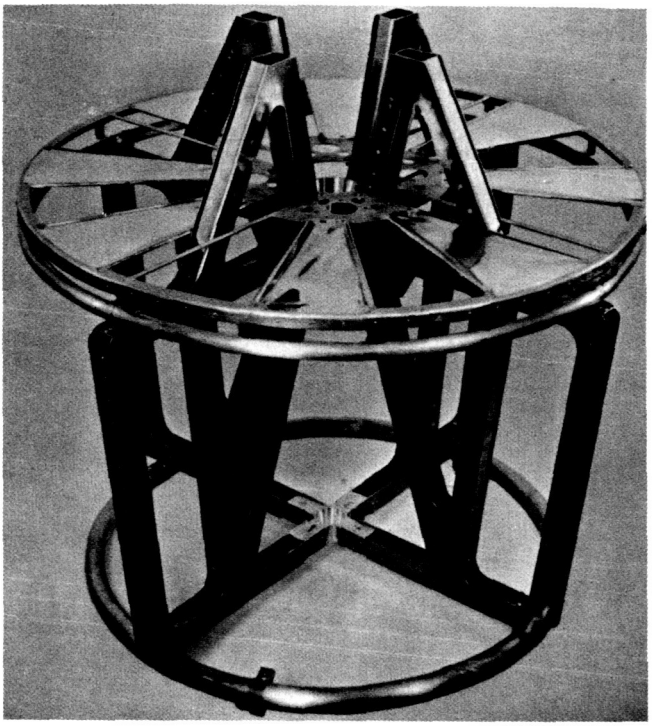

FIGURE 4.2—Relay satellite structure. (RCA photograph.)

the lateral direction. The lacings were intended both to isolate the package thermally from the outer skin and to attenuate any vibration inputs above the frequency of the first resonances.

The outer frame was the basic load-carrying portion of the satellite and weighed about 22 lb. The nominal diameter of the outside ball was 35 in. The frame was welded from ¾-in.-square ZK21A magnesium tubing with a wall thickness of 0.025 in. The sections of the structure were 30° trusses, which fitted together to form the ball. The structure was made in two halves, with a cylindrical cage attached to one half to support the electronics package. The facets of the structure trusses provided mounting surfaces for the solar-cell modules. The most critical loading was during launch, when the outer frame supported both the acceleration loading due to the thrust of the launch vehicle and the vibrational loading due to the first resonance of the electronic package.

The two halves of the Telstar structure were electrically isolated from each other to minimize eddy-current paths which would have been detrimental to the spin stabilization. The solar-cell panels,

which covered the facets of the structural framework, were fabricated from 6061–T6 aluminum alloy. They consisted of a cover sheet with hat sections brazed on the inside. The cells were attached to the panels with beryllium copper frames by twisting tabs through mounting slots in the cover sheet. The first resonance of the panels with the cells attached was approximately 200 cps.

Figure 4.4 shows the structure of the 1962 Mariner II Venus spacecraft made by JPL. The basic structure was hexagonal and consisted of six machined magnesium legs; upper and lower rings; shear ties; tubing intercostals between the feet; and brackets for objects such as the midcourse propulsion unit, the attitude-control gas bottles, the antenna drive mechanism, and various sensors and instruments. The electronics were in six boxes mounted on the six bays of the basic structure. The basic hexagonal structure is very similar to the basic Ranger structure. The weight, including fasteners and clamps, was about 40 lb. This structure, with the electronics attached, was extremely rigid dynamically. The upper structure, which acted as support for the science instruments and the omnidirectional antenna, was

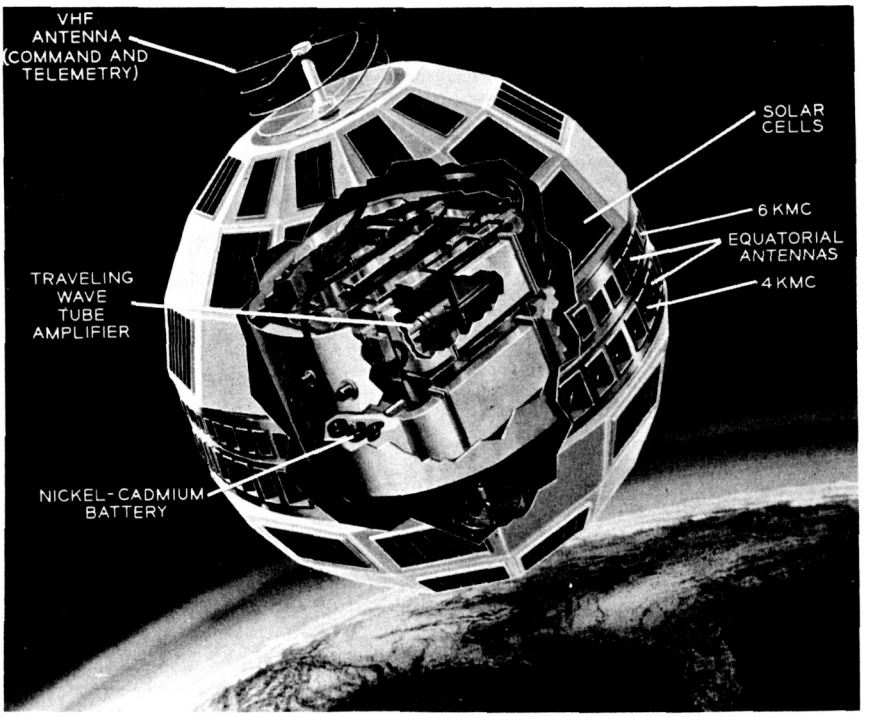

FIGURE 4.3—The Telstar satellite. (BTL photograph.)

made of 6061–T6 aluminum tubing riveted to end fittings. The weight of the upper structure was about 10 lb.

The magnesium boxes containing the electronics weighed a total of 23 lb. Other structural members, such as the yoke which supported the directional antenna, brought the total weight of the structure up to about 80 lb. Features of interest in figure 4.4, besides the structure, are the midcourse system inside the basic hex (a 50-lb-thrust liquid

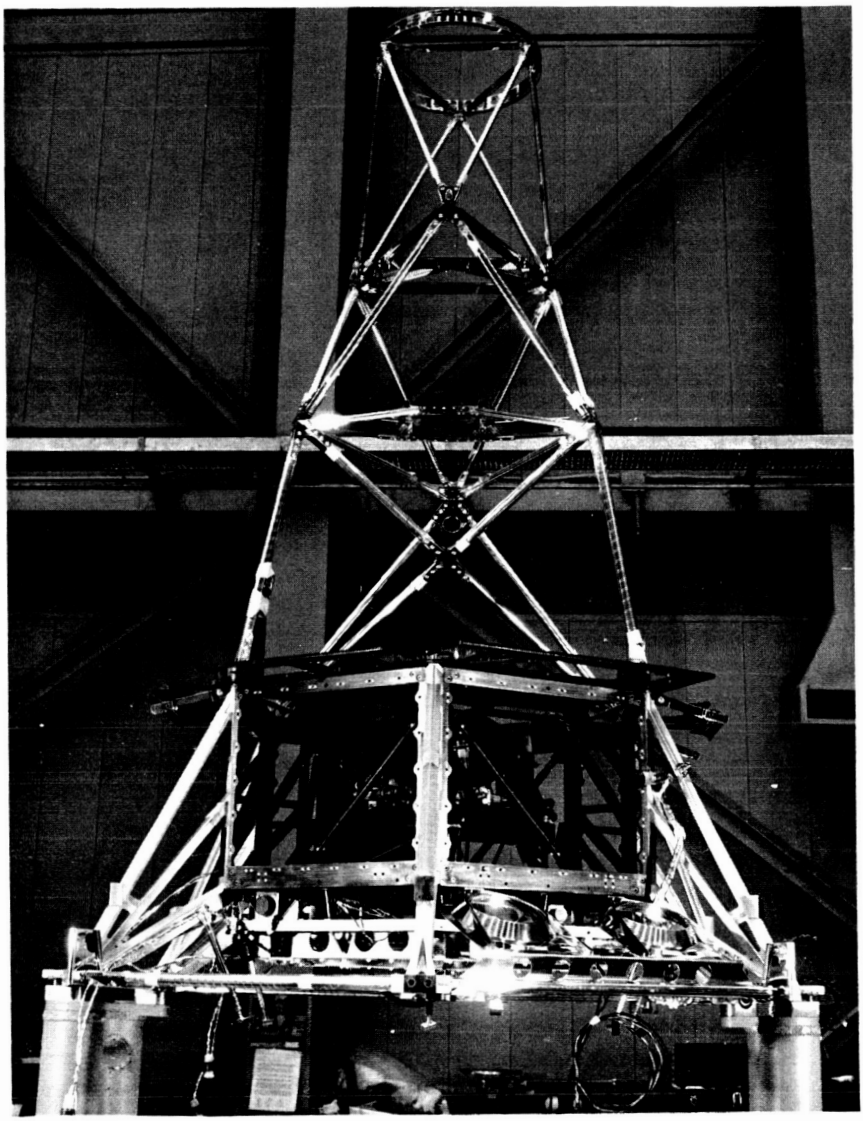

FIGURE 4.4—Mariner II structure. (JPL photograph.)

monopropellant system with an overall weight of 32 lb), the mounting plate into which the spherical nitrogen bottles are strapped (a mounting technique which eliminates the necessity of placing mounting bosses on the pressure tanks), and the honeycomb support for the multilayer aluminized Mylar upper thermal shield.

Figure 4.5 shows a structural mockup of the spacecraft on the shake table. The high-gain antenna (4-ft diameter; 10 lb including feed and drive) is beneath the basic hex within the adapter. The solar panels (26 lb including cells and wiring; 12.2 ft^2 each) are shown hinged at the feet of the legs and fastened to the upper structure by means of pyrotechnic pinpullers. The planetary scanning instruments (radiometer and infrared detector, about 25 lb including actuator) can be

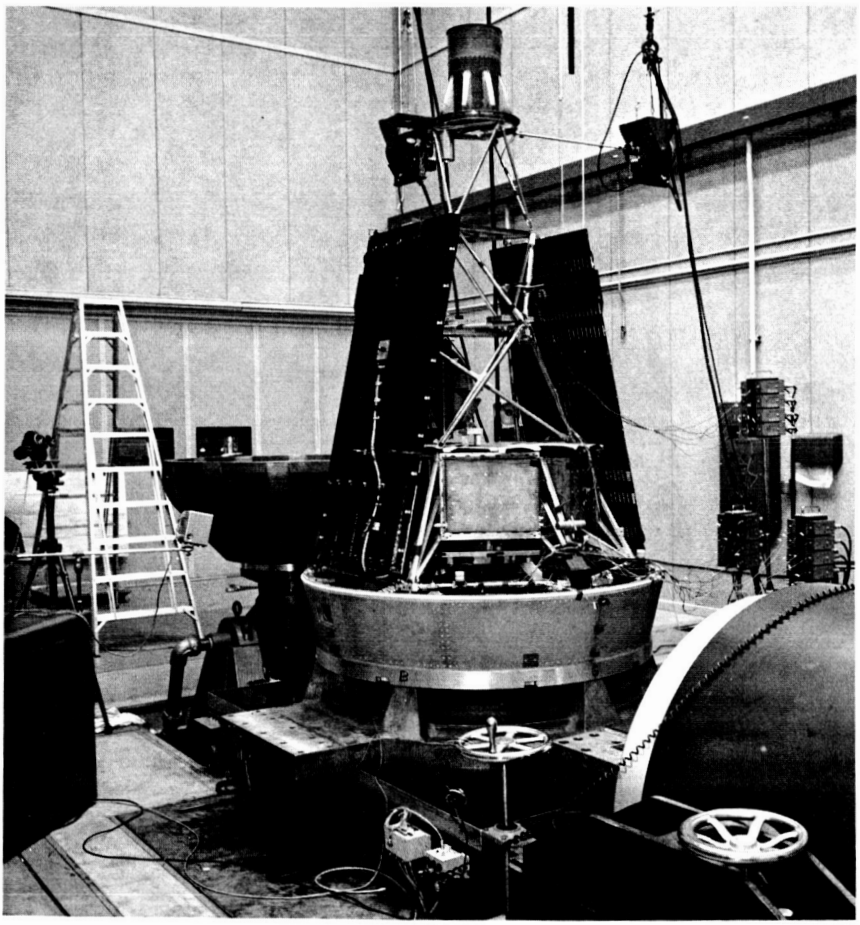

FIGURE 4.5—Mariner II structural mockup on shake table. (JPL photograph.)

seen behind the superstructure. The omnidirectional antenna (4 lb) is shown mounted on the upper structure.

The dynamic behavior of a structure as complex as this one is not simple to describe. In brief, the structural designer attempts to "detune" the various structural components so that they will not resonate at the same frequency. He attempts to stiffen any components which are deflection sensitive. The most harmful structural resonances generally occur below about 120–150 cps. Above this frequency, displacements are quite small. However, many sensitive instruments and sensors are harmed by higher frequencies and must be treated accordingly. Fortunately, the present emphasis on light weight forces the designer toward structures which resonate at lower frequencies. The structure therefore acts as a filter at the higher frequencies.

The first bending modes in both the spacecraft structure (on the adapter) and the solar panels of Mariner II were between 35 and 40 cps. The second bending mode of the structure in one direction was about 45 cps and in the other about 75 cps. Other important solar-panel bending modes took place at 60 cps and at 55 cps. The first local resonance of the high-gain antenna was at about 20 cps. Attitude-control jets and separation connectors resonated at about 70 to 80 cps. In general, all first resonances occurred below 100 cps and were detuned sufficiently to prevent overly severe excursions. Amplitude ratios for first resonances were ordinarily 10 or less, although ratios as high as 50 occurred for higher resonances.

Figure 4.6 shows the basic 1964 Mariner Mars structure, which differs from the Mariner II Venus structure in many respects. It is stiffer and more of a semimonocoque structure. The shear panels shown covering some of the bays of the octagon are replaced by the electronics chassis. The support in the middle is for the planetary scan platform. The midcourse unit is mounted in one of the octagon bays. Attitude-control gas tanks and cable troughs are also mounted on the secondary central structure. The octagonal structure as shown in figure 4.6 weighs about 30 lb. The upper truss shown weighs an additional 3 lb. The octagonal portion of the structure is made from magnesium and the upper truss is made of aluminum.

Figure 4.7 shows the basic Mariner Mars structure with the midcourse unit and electronic chassis mounted, the cable trough in position, and the high-gain antenna mounted. The structure is mounted on a mockup of the adapter to the Agena booster. Due to the trajectory used in the 1964 Mars mission, it was possible to use a fixed high-gain antenna in conjunction with a fixed omnidirectional antenna to obtain complete coverage. Viewed from the spacecraft, the Earth and the Sun hold practically the same relative position for 6 of the

9 months of the flight. The antenna has an elliptical area in order to obtain a beam broad enough in the direction of the ecliptic plane to compensate for the relative movement which does take place.

The antenna itself is a rather interesting structure. The 0.5-in.-thick dish core is made of 0.25-in.-cell honeycomb with walls 0.0007 in. thick. The skins are vacuum-formed from 0.004-in. aluminum and are bonded to the core with a 0.001-in. film of nylon-filled epoxy. The dish is supported by a horsecollar-shaped ring of sandwich construction. The core of the ring is composed of 0.25-in. cells with 0.0007-in. walls and is machined to shape with the cells running roughly perpendicular to the dish. The structural skins are 0.016-in. aluminum on the front and the back. Covers 0.004 in. thick are placed on the other surfaces and the ring is bonded to the back of the dish.

The reflector weighs approximately 2 lb, or 0.0025 lb/ft^2. The feed support truss, made of unidirectional fiber-glass tubing and Lexan

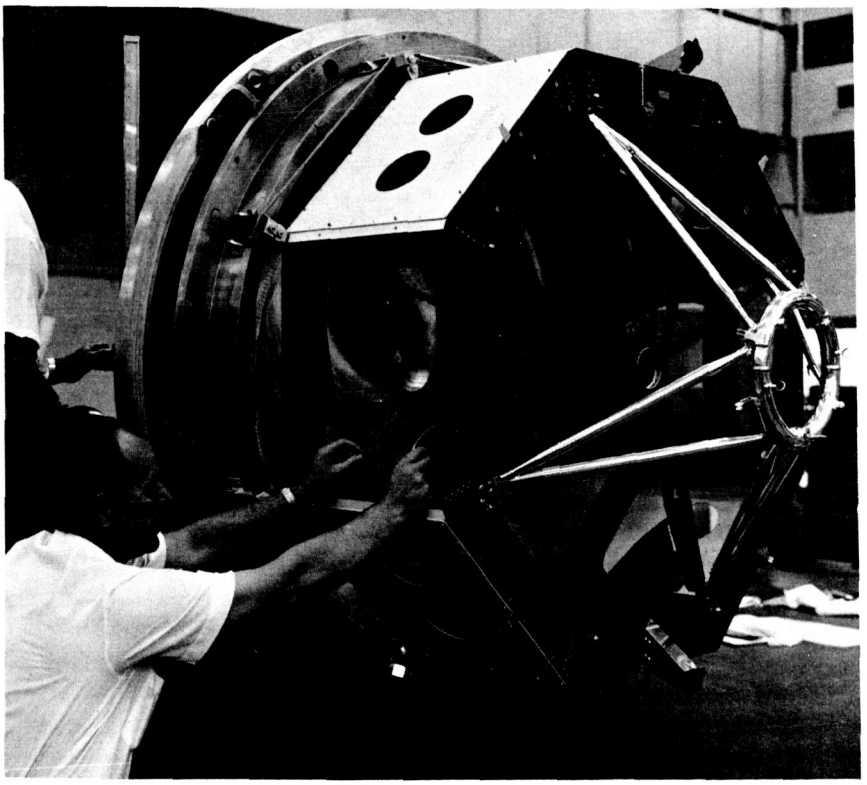

FIGURE 4.6—Mariner Mars basic structure. (JPL photograph.)

end fittings, weighs 0.3 lb. The coaxial lead to the phased dipole feed array weighs 0.2 lb. The complete antenna, including feed and attachments, weighs about 4.5 lb. The lowest vibration mode of the dish occurs at 120 cps. The feed is rigid to above 200 cps.

The Mariner Mars low-gain antenna is shown in figure 4.8. This

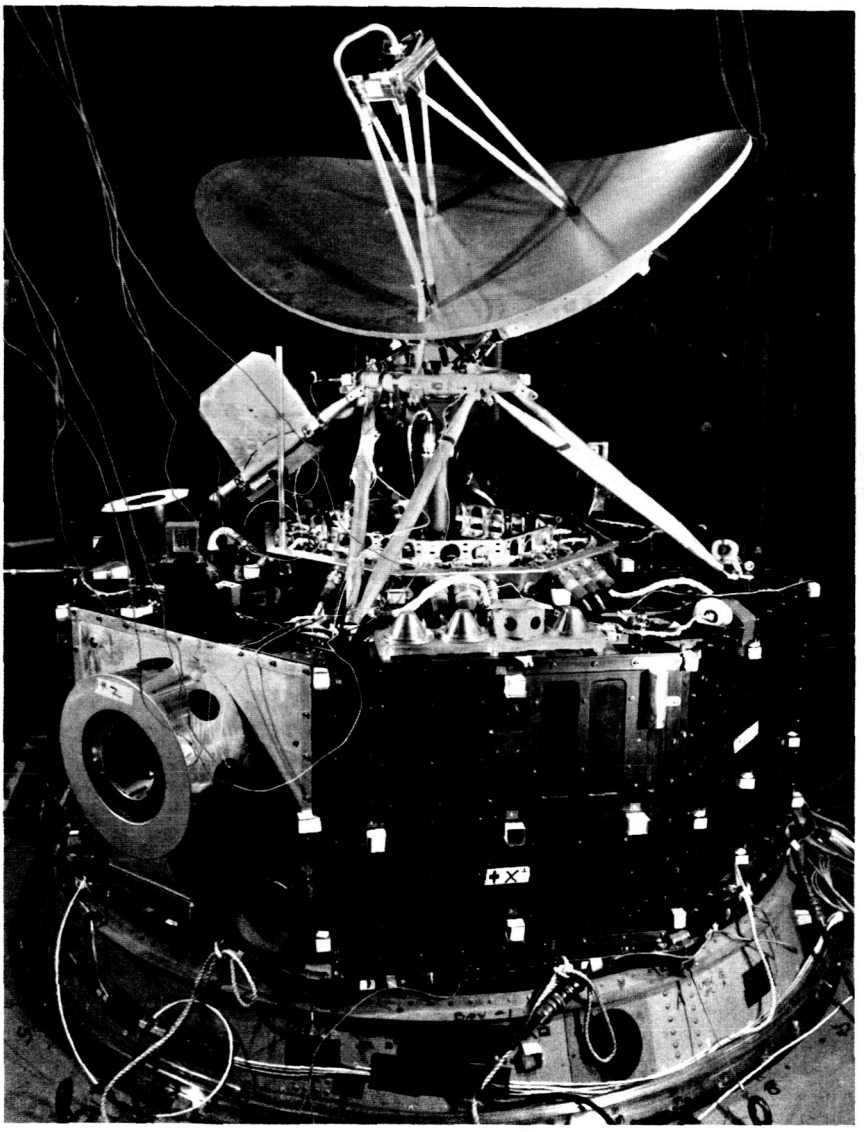

FIGURE 4.7—Basic Mariner Mars structure with midcourse unit and electronic chassis mounted, cable trough in position, and high-gain antenna mounted. (JPL photograph.)

antenna gives 6 db of gain with a $\pm 140°$ coverage. It is intended to provide two-way communications with the spacecraft for the first 80 days of flight. The antenna is basically a circular waveguide with the end crimped to provide a circularly polarized cross-dipole array. The tube is made of 6061–T6 aluminum drawn to a 0.025-in. wall thickness, and has a nominal diameter of about 4 in. The tube is 88 in. long and weighs 3.5 lb including the ground plane and attachments for the scientific instruments. These instruments are a mag-

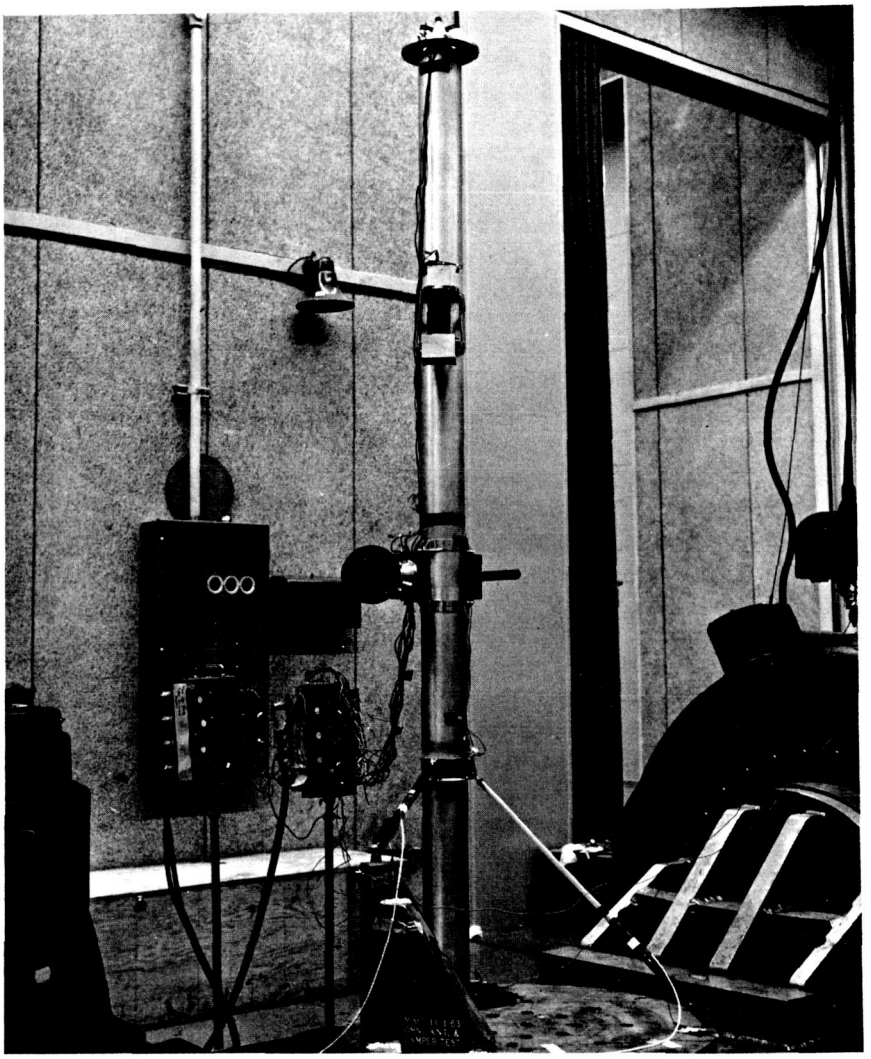

FIGURE 4.8—Mariner Mars low-gain antenna. (JPL photograph.)

netometer (1 lb, shown mocked-up toward the top of the tube) and an ion chamber (2.6 lb, located farther down). The tube is supported by two spring-centered dampers, which damp out the first bending mode of the tube (about 20 cps) and attenuate the higher modes. The tube is pivoted at the bottom with a hinge in one direction and a torsion bar in the orthogonal direction. The antenna is fed at the

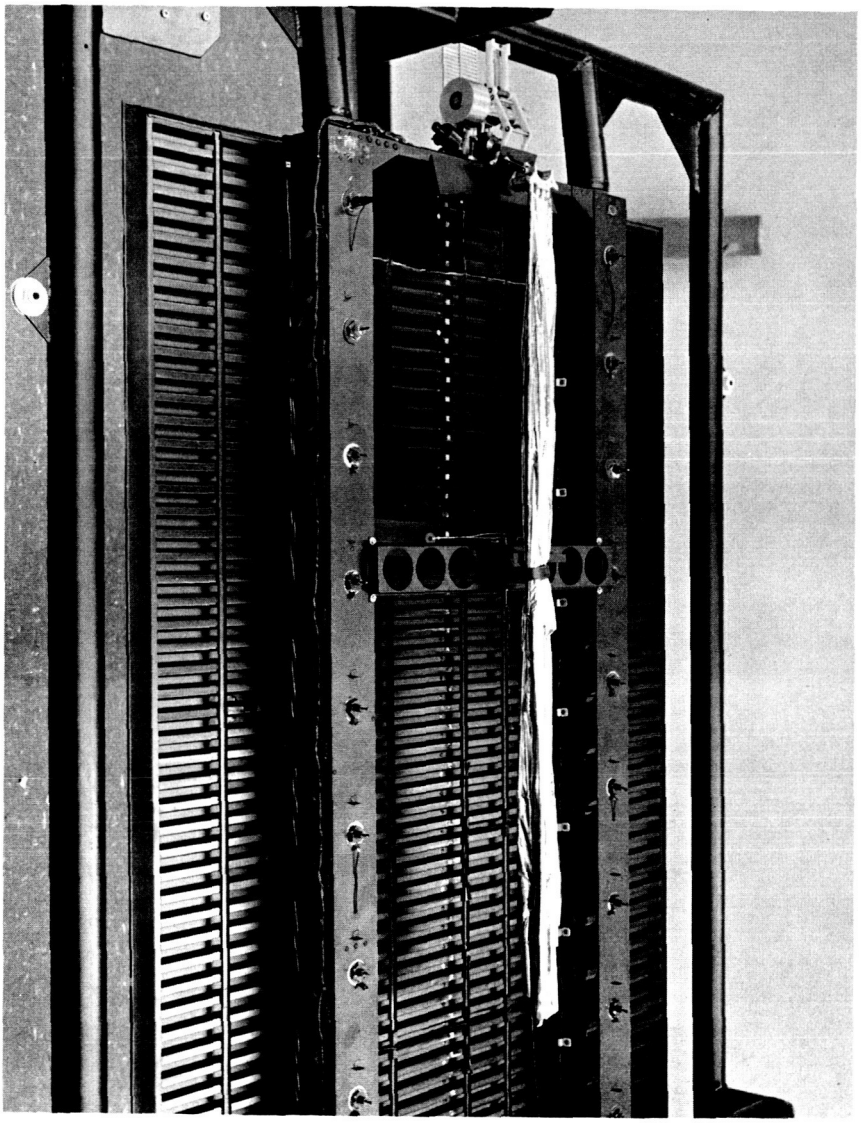

FIGURE 4.9—Mariner Mars solar panel. (JPL photograph.)

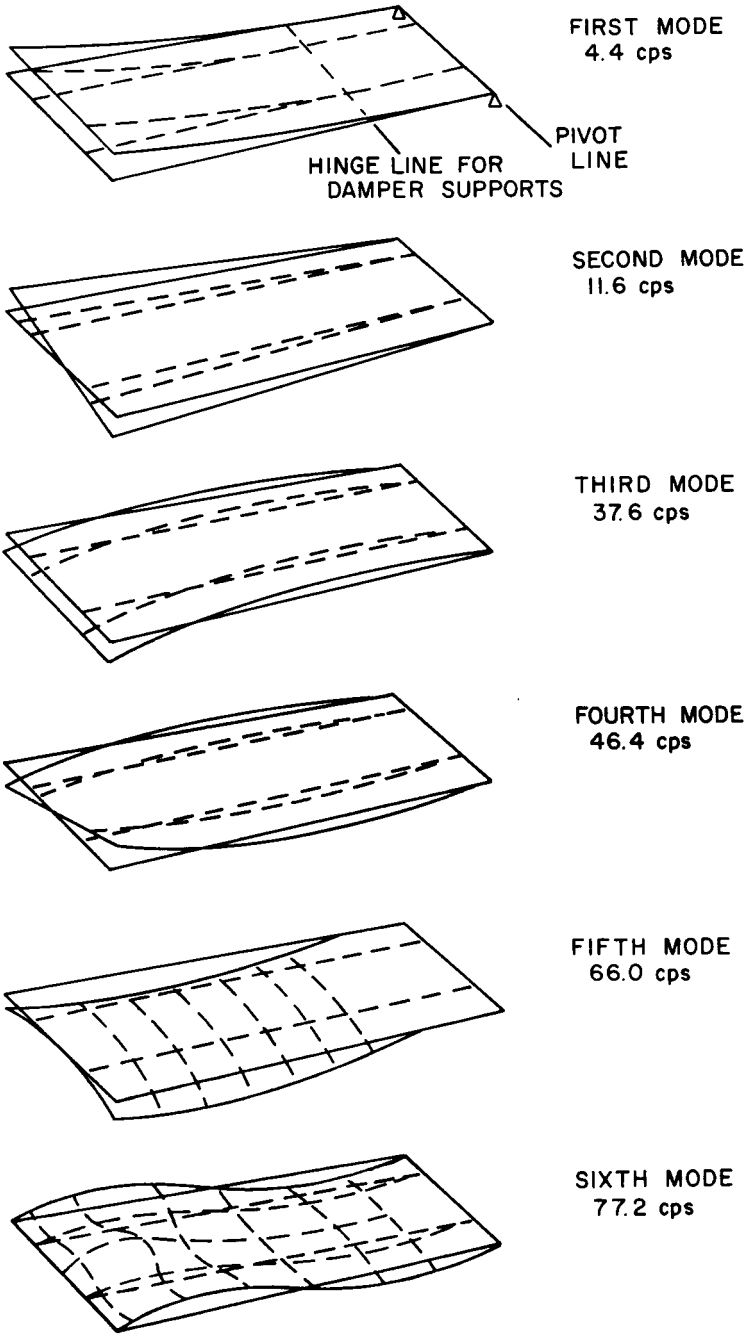

FIGURE 4.10—Vibration modes of Mariner Mars solar panel.

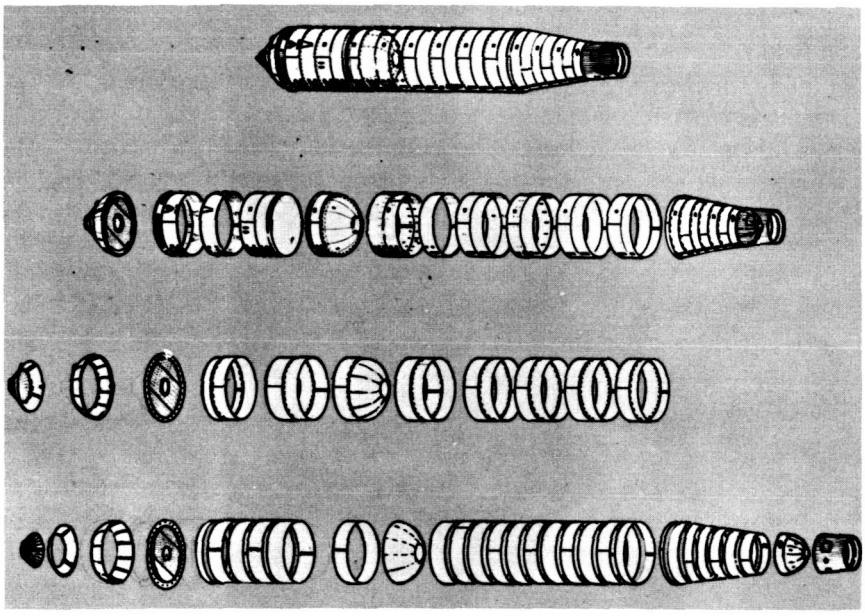

FIGURE 4.11—Tank section of Atlas booster. (Courtesy of General Dynamics Astronautics.)

bottom of the waveguide by a wide-band log-periodic emitter, which is merely a wire wrapped spirally upon a fiber-glass cone. The two spring-centered dampers, including struts and end fittings, weigh 0.5 lb.

Figure 4.9 shows a section of the Mariner Mars solar-panel structure. These panels are approximately 6 ft long and 3 ft wide. The structure weighs 10 lb. With cells, wiring, and attitude-control jets, the panels weigh 20 lb apiece. The front panel skins are 0.005-in. 5050–H38 aluminum. The corrugations are 0.004-in. material. The spars are built up from 6061–T6 aluminum. The spar webs are 0.020 in. and the caps are 0.032 in. The thickness of the caps was dictated by heat dissipation from the Zener overload diodes which are attached to the caps. The panels are pivoted to the spacecraft at the base and held in launch configuration by two spring-centered damped struts which are fastened to the panel approximately 2 ft from the bottom by pyrotechnic pinpullers. The panels are deployed with spring actuators. The deployment rate is controlled by a set of dampers which also damp the panel in the cruise mode during firing of the midcourse motor.

Figure 4.10 shows some of the vibration modes for a solar panel. These are typical of the many modes encountered with a complex structure.

Figure 4.11 shows a structure of a completely different type—the airframe structure for the Atlas booster. The section shown is about 60 ft long and 10 ft in diameter. It is of monocoque construction and is made up of thin-gage stainless steel. The forward part of the tank section is the oxidizer tank. This tank has a capacity of 18 600 gallons of oxidizer, plus space for tank pressurization. The aft portion of the tank section contains the fuel and has a capacity of 11 455 gallons plus space for tank pressurization. The tank is nonrigid and cannot support itself unless pressurized. To maintain structural rigidity of the bulkhead between the tanks, a minimum pressure differential of 0.65 lb/in^2 must be maintained between the tanks at all times. The thrust of the vernier engines is transmitted by the aft bulkhead of the fuel tank. A thrust ring welded to the aft end of the fuel tank receives the thrust from the booster engines.

CHAPTER 5

Temperature Control Theory

THIS CHAPTER and the two following chapters are concerned with the temperature control of the various parts of the spacecraft. A brief discussion of pertinent heat-transfer theory will first be presented, followed by a discussion of theory as applied to spacecraft temperature control. The problems of testing will then be mentioned, and finally a few examples of actual spacecraft temperature-control problems will be presented. The reader should not be misled by the fact that temperature control is treated independently in these notes. Spacecraft temperatures are dependent upon spacecraft geometries, materials, articulations, and power distribution. The spacecraft temperature-control engineer must therefore work extremely closely with engineers involved in the design and development of the spacecraft structure, mechanisms, and electronic packaging schemes.

There are three distinct mechanisms of heat transfer. In all cases, a temperature difference is the impetus for the movement of energy. The energy in motion is called heat. Heat is frequently transmitted by a combination of two or three mechanisms, with one quantitatively predominating. The familiar steam "radiator," for instance, transmits heat by convection as well as by radiation. For the purpose of examining heat transfer, it is convenient to separate the mechanisms. The three mechanisms can be defined as follows.

Conduction is a mechanism by which heat is transferred with no appreciable molecular displacement. The temperature of a particle of matter is defined by the average kinetic energy of the molecules within the particle. If the temperature of one portion of a material is raised, the molecules in that portion will acquire more kinetic energy. Part of this energy will then be transmitted to the molecules of the adjacent portion of material. This process is called conduction. It is hypothesized that the transfer takes place by elastic impact in fluids and by diffusion of faster moving electrons in solids. Conduction is the only mechanism of heat flow in opaque solids. In nonopaque solids and in fluids, conduction is often combined with radiation and convection.

Convection is the mechanism of transferring heat by fluid mixing. It is the chief means of transferring heat from a solid surface to a

fluid. The fluid will be in motion because of density differences resulting from differences in temperature (natural convection) and/or because of outside mechanical agitation (forced convection). The convection process is closely accompanied by conduction from the solid surface to the adjacent particles of fluid and between the fluid molecules. With transparent fluids, radiation will also be present.

Radiation. All bodies emit radiant energy. When this energy strikes another body, some of it will be absorbed and transformed into internal energy. The amount of energy emitted depends upon the temperature of the radiating body and the nature of its surface. The amount of energy absorbed depends upon the nature of the surface of the absorbing body, the nature of the incoming radiation, and the geometrical configuration of the two-body system.

CONVECTION

Within the atmosphere, convection is an extremely widespread and powerful heat-transfer mechanism. In space, it tends to be less important because of the general absence of gases. Convection is important in operations which take place within the atmosphere, such as prelaunch system testing and the launch and reentry portions of the mission. Convection must also be considered in portions of the spacecraft which are in contact with a fluid. Fluids are found in spacecraft either in conjunction with the propulsion system, as a reaction medium for control systems, as a necessary ingredient of life-support systems, or expressly for the purpose of augmenting heat transfer.

Expressions for the rate of heat transfer due to convection are deceptively simple. One form of the convection equation is

$$q = A\bar{h}_c(T_s - T_\infty) \tag{5.1}$$

where

- q rate of heat flow, Btu/hr
- A area through which the heat flows, taken normal to the flow direction, ft^2
- $\bar{h}_c$ average unit thermal convective conductance, Btu/hr-ft^2-°R
- T_s surface temperature, °R
- T_∞ a reference temperature in the fluid, °R

Unfortunately, $\bar{h}_c$ depends upon the geometry of the surface, the physical properties of the fluid, the velocity of the fluid, the temperature difference, whether or not the fluid is changing phase, and a large number of other factors. Equation (5.1) is actually only a definition of $\bar{h}_c$. The problem in solving convective heat-transfer problems is in evaluating $\bar{h}_c$. For instance, table 5.1, taken from reference 1, shows various ranges for $\bar{h}_c$.

Values of $\bar{h}_c$ are found by using principles of fluid flow, experimental data, various classical analogies, assumptions, approximations, and hard work. Heat-transfer rates are then evaluated. The form of equation (5.1) simplifies the task of combining convection with conduction and radiation. The thermal conductance for convective heat transfer is $\bar{h}_c A$ and the thermal resistance is $1/\bar{h}_c A$. These quantities are extremely consistent with methods of solving combined heat-transfer mechanism problems.

TABLE 5.1—Approximate range of values ordinarily encountered for $\bar{h}_c$

[From ref. 1]

Fluid	$\bar{h}_c$, Btu/hr-ft²-°R
Air, heating or cooling	0. 2–10
Steam, superheating	5. 0–20
Oils, heating or cooling	10–300
Water, heating	50–3000
Organic vapors, condensing	200–400
Water, boiling	300–9000
Steam, film-type condensation	1000–3000
Steam, dropwise condensation	5000–20 000

It should be emphasized that the solution of the spacecraft temperature-control problem requires heat transfer between heat sources and heat sinks and between the spacecraft and the environment. In most cases, the more powerful the heat-transfer mechanisms are, the better. Designers of unmanned spacecraft have nonetheless tended to avoid using a fluid specifically to augment heat transfer. This is because of the operational problems associated with sealing and pressurizing and the necessity of worrying about micrometeorite punctures. Since the temperature control problems in deep space without convection are more in keeping with the content of this book, since the absence of convection creates many severe problems, and since convection is so enmeshed with fluid theory that it becomes too involved to discuss briefly, convection will be discussed no further. Excellent discussions of convection can be found in references 1 and 2.

CONDUCTION

Conduction is a much more straightforward mechanism of heat transfer than convection. The basic relation, first proposed by Fourier, is

$$q_k = -kA\frac{dT}{dx} \tag{5.2}$$

TABLE 5.2—Thermal conductivity of materials.

[Most of these values were taken from ref. 3]

Material	k, Btu/hr-ft-°R	Temp., °F
Copper	224	Room
Gold	169	"
Beryllium oxide	130	200
Aluminum	117	Room
Beryllium	109	"
Magnesium	92	"
Molten sodium	42	700
Mild steel	26	Room
Molten potassium	26	300
Titanium	9.9	Room
18–8 stainless steel	9	"
Concrete	1.05	"
Glass	.59	200
Water	.343	32
Methyl alcohol	.124	Room
Fiber-glass-epoxy laminate	.15	"
Silicone grease	.11	"
Epoxy resin	.10	"
White pine	.078	"
Asbestos wool	.058	212
Corrugated cardboard	.037	Room
Styrofoam	.021	"
Steam	.0171	300
Nitrogen	.0140	32
Air	.0140	32

where

q_k rate of heat flow, Btu/hr

k thermal conductivity of the material, Btu/hr-ft-°R

A cross-sectional area through which the heat flows, taken normal to the direction of the heat flow, ft²

dT/dx temperature gradient at cross section A along x-axis, °R/ft

Table 5.2 shows typical values of k for various engineering materials. These values are shown for a particular temperature because k is, in general, temperature sensitive. Table 5.3 shows the variation of k with temperature for a few metals.

The conduction equation can be generalized to find the temperature distribution in three dimensions by considering a small element of volume, applying the Fourier relation to three mutually perpendicular directions, and then requiring that the net heat inflow (inflow minus

outflow) plus the heat generated inside the volume be equal to the increase in internal energy (energy balance). The resulting general equation is

$$\frac{\partial^2 T}{\partial x^2}+\frac{\partial^2 T}{\partial y^2}+\frac{\partial^2 T}{\partial z^2}+\frac{\dot{q}}{k}=\frac{1}{a}\frac{\partial T}{\partial \theta} \tag{5.3}$$

where

a thermal diffusivity, k/c_p
θ time
$\dot{q}$ rate of creation of internal energy per unit volume

If $\dot{q}=0$, equation (5.3) reduces to

$$\frac{\partial^2 T}{\partial x^2}+\frac{\partial^2 T}{\partial y^2}+\frac{\partial^2 T}{\partial z^2}=\frac{1}{a}\frac{\partial T}{\partial \theta} \tag{5.4}$$

This relationship is the Fourier equation.

If the system is in steady state, equation (5.3) reduces to the Laplace equation:

$$\frac{\partial^2 T}{\partial x^2}+\frac{\partial^2 T}{\partial y^2}+\frac{\partial^2 T}{\partial z^2}=0 \tag{5.5}$$

Equation (5.3) in cylindrical coordinates is

$$\frac{\partial^2 T}{\partial r^2}+\frac{1}{r}\frac{\partial T}{\partial r}+\frac{1}{r^2}\frac{\partial^2 T}{\partial \phi^2}+\frac{\partial^2 T}{\partial z^2}+\frac{\dot{q}}{k}=\frac{1}{a}\frac{\partial T}{\partial \theta} \tag{5.6}$$

Equation (5.3) in spherical coordinates is

$$\frac{1}{r}\frac{\partial^2 (rT)}{\partial r^2}+\frac{1}{r^2 \sin\phi}\frac{\partial}{\partial \phi}\left(\sin\phi\frac{\partial T}{\partial \phi}\right)+\frac{1}{r^2 \sin^2\phi}\frac{\partial^2 T}{\partial \psi^2}+\frac{\dot{q}}{k}=\frac{1}{a}\frac{\partial T}{\partial \theta}$$

TABLE 5.3—Thermal conductivity at various temperatures.

[From ref. 1]

Material	k, Btu/hr-ft-°R, at—						
	32° F	212° F	392° F	572° F	752° F	932° F	1112° F
Aluminum	177	119	124	133	144	155	----
Brass	56	60	63	66	67	---	----
Copper	294	218	215	212	210	207	204
Graphite	97	87	76	66	58	53	48
Nickel	36	34	33	32	---	---	----
Mild steel	--	26	26	25	23	22	21

These equations can be solved in several ways. Solutions of the equations in conjunction with boundary conditions and the Fourier equation enable conduction problems to be solved. Let us examine a few examples of conduction problems and methods of solution.

Example 1: Steady flow of heat through a plane wall of uniform temperature T_1 *on the hot side and* T_2 *on the cold side (see fig. 5.1).*

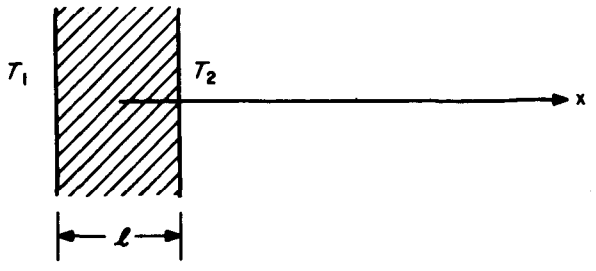

FIGURE 5.1—Conduction through plane wall.

To find the temperature distribution, apply equation (5.3). Since

$$\frac{\partial^2 T}{\partial y^2}=\frac{\partial^2 T}{\partial z^2}=\dot{q}=\frac{\partial T}{\partial \theta}=0$$

equation (5.3) reduces to $\partial^2 T/\partial x^2=0$, which integrates to

$$T=Ax+B$$

Applying boundary conditions $T=T_1$ when $x=0$ and T_2 when $x=l$, then

$$T=T_1-\frac{(T_1-T_2)}{l}x$$

so that the temperature distribution is linear through the wall. To find the heat flow, apply the Fourier relation:

$$q=-kA\frac{\mathrm{d}T}{\mathrm{d}x}=\frac{kA(T_1-T_2)}{l}$$

Example 2: Steady flow of heat through long concentric cylinders of different values of k. To apply the Fourier expression to a cylinder, choose a hollow cylindrical volume element dr thick and of radius r (see fig. 5.2).

$$q=-kA\frac{\mathrm{d}T}{\mathrm{d}r}$$

$$A=2\pi rl$$

so that

$$q=-2\pi rlk\frac{dT}{dr}$$

Separating variables and integrating gives

$$T_i-T_o=\frac{q}{2\pi kl}\ln\frac{r_o}{r_i}$$

so that

$$q=\frac{2\pi kl(T_i-T_o)}{\ln\frac{r_o}{r_i}}$$

If contact resistances are ignored, the heat flow through each cylinder must equal the heat flow through the others:

$$q=q_1=\frac{2\pi k_1 l}{\ln\frac{r_2}{r_1}}(T_1-T_2)=q_2=\frac{2\pi k_2 l}{\ln\frac{r_3}{r_2}}(T_2-T_3)=q_3=\frac{2\pi k_3 l}{\ln\frac{r_4}{r_3}}(T_3-T_4)$$

To eliminate the intermediate temperatures:

$$q=\frac{2\pi k_1 l}{\ln\frac{r_2}{r_1}}(T_1-T_2)$$

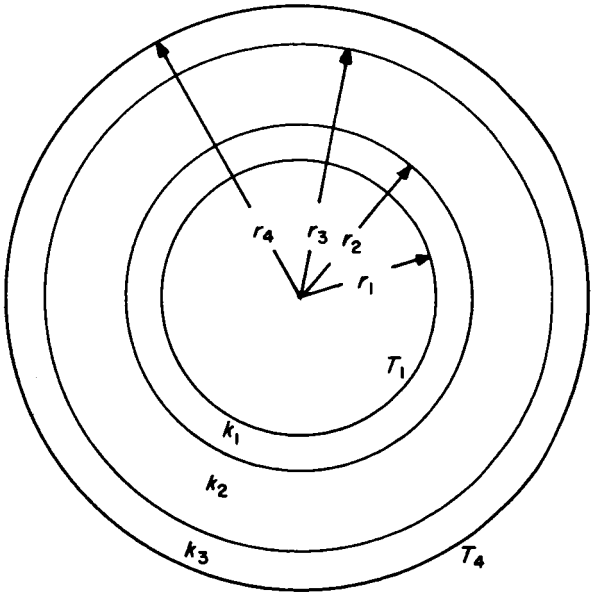

FIGURE 5.2—Conduction through concentric cylinders.

$$\frac{\ln \frac{r_3}{r_2}}{\ln \frac{r_2}{r_1}} \frac{k_1}{k_2} q = \frac{2\pi k_1 l}{\ln \frac{r_2}{r_1}} (T_2 - T_3)$$

Adding:

$$q \left(1 + \frac{k_1}{k_2} \frac{\ln \frac{r_3}{r_2}}{\ln \frac{r_2}{r_1}} \right) = (T_1 - T_3) \frac{2\pi k_1 l}{\ln \frac{r_2}{r_1}}$$

Similarly:

$$q \left(\frac{\ln \frac{r_4}{r_3}}{\ln \frac{r_2}{r_1}} \frac{k_1}{k_3} \right) = (T_3 - T_4) \frac{2\pi k_1 l}{\ln \frac{r_2}{r_1}}$$

Adding:

$$q \left(1 + \frac{k_1}{k_2} \frac{\ln \frac{r_3}{r_2}}{\ln \frac{r_2}{r_1}} + \frac{k_1}{k_3} \frac{\ln \frac{r_4}{r_3}}{\ln \frac{r_2}{r_1}} \right) = (T_1 - T_4) \frac{2\pi k_1 l}{\ln \frac{r_2}{r_1}}$$

or

$$q = \frac{T_1 - T_4}{\frac{\ln \frac{r_2}{r_1}}{2\pi k_1 l} + \frac{\ln \frac{r_3}{r_2}}{2\pi k_2 l} + \frac{\ln \frac{r_4}{r_3}}{2\pi k_3 l}}$$

Example 3: To find the temperature distribution in a long cylinder of radius r_o *with internal heat generation and outside temperature* T_o. Apply equation (5.6). Since

$$\frac{\partial^2 T}{\partial \phi^2} = \frac{\partial^2 T}{\partial z^2} = \frac{\partial T}{\partial \theta} = 0$$

equation (5.6) reduces to

$$\frac{d^2 T}{dr^2} + \frac{1}{r} \frac{dT}{dr} + \frac{\dot{q}}{k} = 0$$

By rewriting as

$$k \left(r \frac{d^2 T}{dr^2} + \frac{dT}{dr} \right) = -r\dot{q}$$

and noticing that

$$\frac{d}{dr} \left(r \frac{dT}{dr} \right) = r \frac{d^2 T}{dr^2} + \frac{dT}{dr}$$

this relation may be integrated to

$$kr\frac{dT}{dr}=-\frac{\dot{q}r^2}{2}+C_1$$

Since $dT/dr=0$ when $r=0$, $C_1=0$. Another integration yields

$$T=\frac{-\dot{q}r^2}{4k}+C_2$$

But $T=T_o$ when $r=r_o$, so that

$$C_2=T_o+\frac{\dot{q}r_o^2}{4k}$$

and

$$T=\frac{\dot{q}}{4k}(r_o^2-r^2)+T_o$$

Conduction problems obviously become more complex than these simple examples. Two- or three-dimensional steady-state heat conduction with no heat generation is described by the Laplace equation. This equation also describes "potential" fields in electromagnetism and in fluid mechanics. Various methods have been devised to solve the equation. In some instances it can be solved exactly by a separation-of-variables technique. Since the Laplace equation describes an electrical field, with voltage corresponding to temperature and current corresponding to heat flux, conduction problems can also be solved by use of an electrical analog. Special papers (Teledeltos paper, for example) have a high but constant surface resistivity. By applying highly conductive paint to edges which represent constant temperature boundaries and by leaving "insulator" edges untreated, very effective analog solutions can be obtained by using only a power supply and a voltmeter.

The Laplace equation can also be solved by applying numerical techniques. A very powerful method, especially in the hands of an experienced practitioner, is the relaxation method, which makes use of a cut-and-try approach. An approximate network of numbers is methodically iterated until the size of so-called "residual" values indicates that the network is sufficiently close to the solution throughout the net.

There are obviously transient conduction problems as well as steady-state conduction problems. Problems such as the heat treatment of metals, resistance heating, air conditioning, and the maneuvering of spacecraft require time-dependent considerations. Transient problems require consideration of the thermal capacity of the objects as well as the thermal conductivity. As an example of the type of thinking involved in transient conduction, let us examine transient

heating in a simple slab of thickness $2L$. Previous to time 0, the slab has a uniform temperature T_o. The slab is brought into contact with a fluid at temperature T_∞ at time 0 ($T_\infty > T_o$). Applying equation (5.3),

$$\frac{\partial^2 T}{\partial y^2} = \frac{\partial^2 T}{\partial z^2} = \dot{q} = 0$$

The expression therefore simplifies to

$$\frac{\partial^2 T}{\partial x^2} = \frac{1}{a} \frac{\partial T}{\partial \theta}$$

This is a rather simple partial differential equation which can be solved by assuming that there is a solution consisting of the product of two functions, one a function of time only and one a function of distance only. The general solution is

$$T = e^{-a\lambda^2\theta}(A \cos \lambda x + B \sin \lambda x)$$

where λ is a constant which must be evaluated along with A and B.

Applying the boundary condition $\partial T/\partial x = 0$ at $x = 0$ (no gradient at center of slab) and $B = 0$, yields the solution

$$T = Ae^{-a\lambda^2\theta} \cos \lambda x$$

In order to proceed further, it is necessary to equate heat flow from the fluid to the slab as well as through the slab. Convection is involved and the mathematics becomes somewhat tedious, so we shall not complete the solution here. The interested reader may refer to chapter 4 of reference 2. The final solution is in the form of an infinite series.

Figure 5.3 is a plot showing the temperature difference between a point in the slab and the fluid temperature normalized with the difference between the original temperature and the fluid temperature. The normalized temperature difference is plotted against position within the slab, with a time function $a\theta/L^2$ as a curve parameter. Four sets of curves are shown, representing different values of $k_s/\sqrt{h}L$, a parameter which represents the ratio of conduction to convection. For high values of this parameter, temperatures are quite uniform throughout the slab. For low values, large gradients occur.

RADIATION

Radiative heat transfer is inseparable from electromagnetic theory. To understand radiation heat-transfer problems, it is first necessary

to understand radiation. A good discussion of radiation is found in reference 4. Figure 5.4 shows the electromagnetic spectrum. The radiation of interest in heat transfer extends between 0.1 and 100 microns in wavelength. The mechanism of radiation has not yet been completely defined. Some phenomena can best be described by means of the wave theory, and other phenomena by means of the quantum theory.

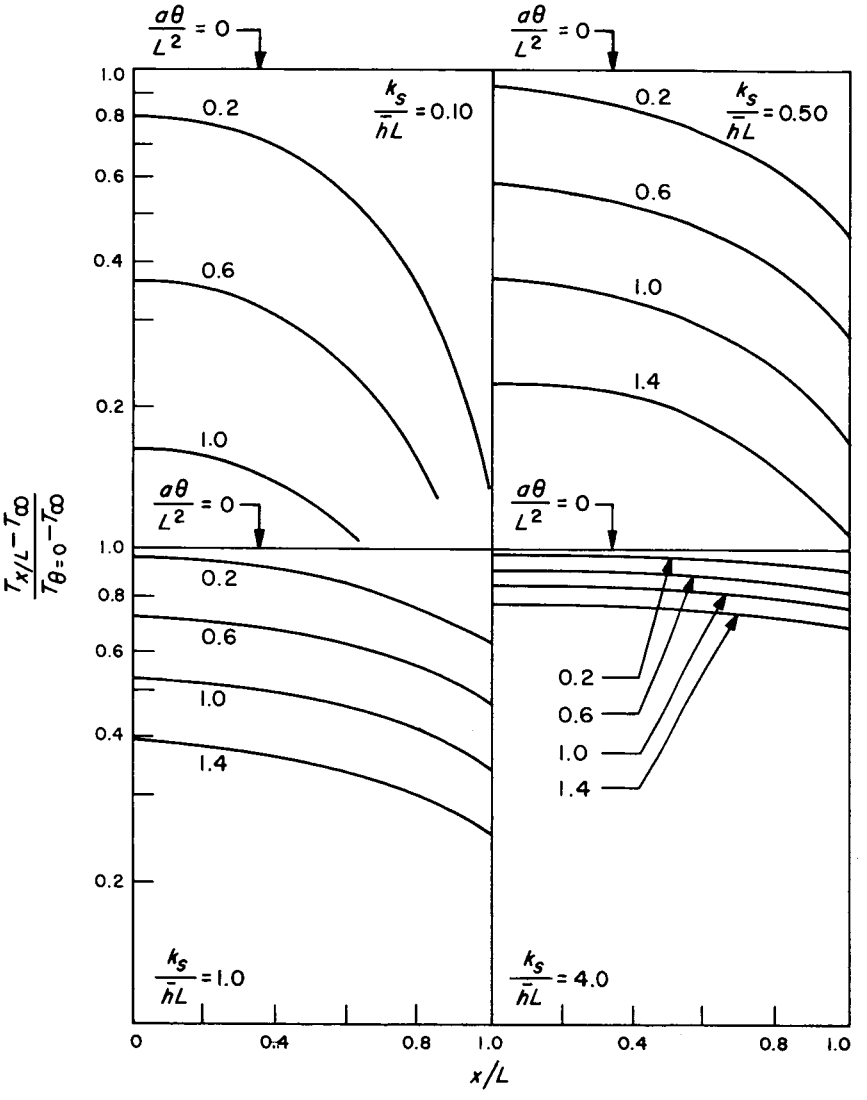

FIGURE 5.3—Dimensionless temperature distribution in one half of a slab of thickness $2L$ subjected to a sudden change in environmental temperature. (From ref. 2.)

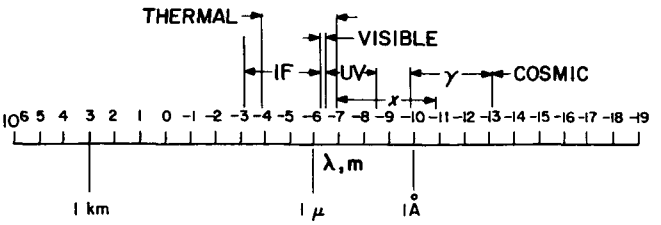

FIGURE 5.4—The electromagnetic radiation spectrum. (From ref. 2.)

Radiation travels at the speed of light and does not require intervening matter for propagation along its path. The amount and nature of radiation emitted from a body depends upon the nature of the surface and the temperature of the body. Figure 5.5 shows emission from an ideal radiator at various temperatures. The ideal radiator, or "blackbody," is used as a standard in radiation. A surface element of blackbody radiates diffusely, or uniformly in all directions. The total rate of emission per unit time per unit area of blackbody is given by

$$E=\sigma T^4$$

where

σ Stefan-Boltzmann constant, 0.1714×10^{-8} Btu/ft²-°R⁴
T temperature, °R

For a "gray body," the curve of emission as a function of wavelength is the same shape as for a blackbody. However, the magnitude of the curve is reduced at all wavelengths by a factor ϵ. This "gray body" concept is used in many engineering calculations, even though most materials do not actually fulfill the assumption. The total emission from a gray body is

$$E=\epsilon\sigma T^4$$

where ϵ is the emittance, which is not dependent on wavelength for a gray body.

For a real body, the emittance is not a constant with respect to wavelength. However, for use in engineering calculations it is possible to calculate or measure an average emittance value for use over a specific range of interest. For instance, for a given temperature the calculated value is equal to

$$\epsilon=\frac{\int_0^\infty \epsilon_\lambda E_\lambda \, d\lambda}{\int_0^\infty E_\lambda \, d\lambda}=\frac{\int_0^\infty \epsilon_\lambda E_\lambda \, d\lambda}{\sigma T^4}$$

where

ϵ_λ monochromatic emittance
E_λ blackbody monochromatic emission
λ wavelength

When a body radiates, it loses internal energy and its temperature decreases. When a body absorbs radiation, it gains internal energy and its temperature increases. When radiation strikes a body, some is absorbed, some is reflected, and some is transmitted. Opaque bodies do not transmit energy, so that all impinging radiation is either absorbed or reflected. For an opaque body, absorptance plus reflectance equals 1. For other bodies, absorptance plus reflectance plus transmittance equals 1. The values of absorptance, reflectance, and transmittance depend not only upon the surface of the absorbing body, but also upon the nature of the incoming radiation. As an example, a parachute made of 100-lb tensile strength Dacron is discussed in reference 5. When this parachute receives radiation from a blackbody

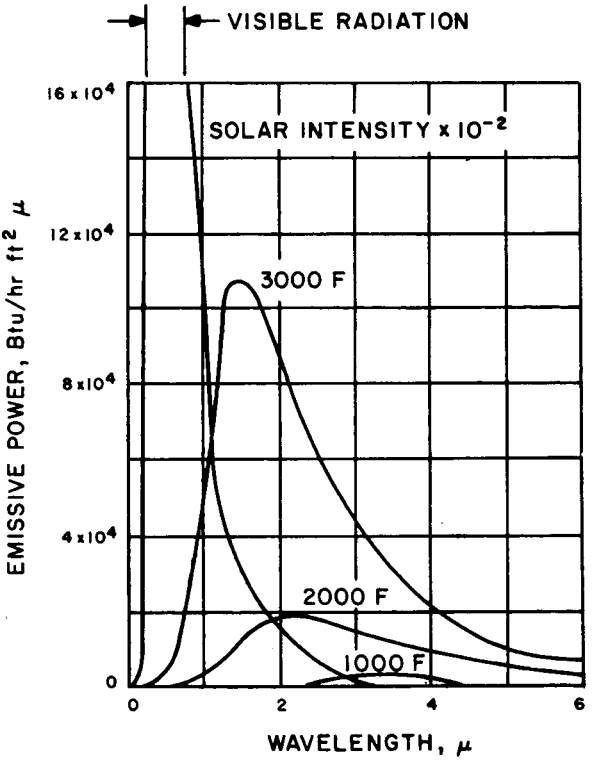

FIGURE 5.5—Radiation from a blackbody at various temperatures. (From ref. 2.)

source at 350 °F, it absorbs 75 percent of the incident radiation, transmits 17 percent, and reflects 8 percent. In sunlight, the parachute absorbs only 5 percent, transmits 60 percent, and reflects 35 percent.

For a blackbody, emittance and absorptance are equal to unity. Reflectance and transmittance are equal to zero. For gray bodies, absorptance is equal to emittance. For real bodies, the absorptance and emittance are equal *only for a given wavelength.* Absorptance and emittance vary with wavelength. Figure 5.6 shows the monochromatic absorptance (emittance) for polished aluminum and white paint. Average absorptance values for given incident radiation spectra can be measured or calculated similarly to average emittance values:

$$\alpha = \frac{\int_0^\infty \alpha_\lambda G_\lambda \, d\lambda}{\int_0^\infty G_\lambda \, d\lambda}$$

where

α_λ monochromatic absorptance
G_λ monochromatic incident emission

Radiations reflected from real surfaces may be either diffuse or spectral. Diffuse reflections are obtained from unpolished surfaces and, like diffuse emissions, are uniform in all directions. Spectral reflections are obtained from highly polished surfaces. The reflected radiation leaves at an angle equal and opposite to the angle of the incoming radiation. For most engineering calculations, reflections are assumed to be diffuse. The resulting calculations are much simpler than those required for spectral reflections. This is because the

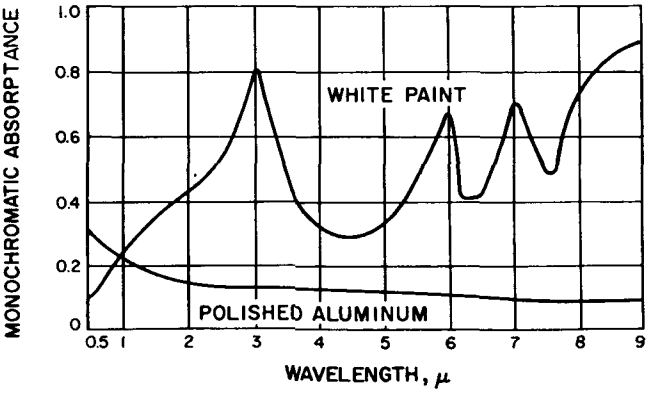

FIGURE 5.6—Variation of absorptance with wavelength for aluminum and white paint.

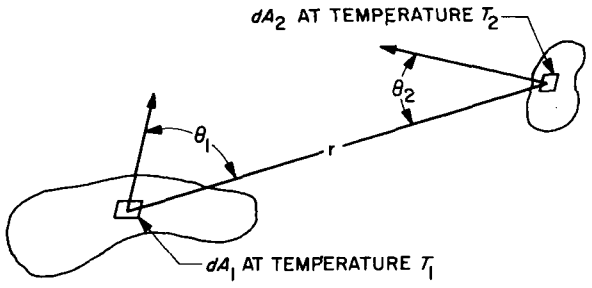

FIGURE 5.7—Blackbody radiation exchange.

radiation intercepted by a given area on a hemisphere placed over a diffusely reflecting body depends only upon the apparent size of the reflecting body and the amount of radiation being reflected. If spectral reflections are present, the intercepted radiation also depends upon the location, size, and shape of the area on the hemisphere and the nature of the radiation being reflected. Engineering materials usually approximate diffuse surfaces. Unfortunately, spacecraft have a high percentage of polished surfaces. Most calculations are made under the assumption that surfaces are diffuse, and the error is considered when the answers are interpreted.

Let us now examine the situation of two blackbodies exchanging energy by radiation (see fig. 5.7). Radiant heat transfer between two surfaces depends upon the emitting and absorbing characteristics of the two surfaces and upon the view the surfaces present to each other.

Radiation intensity I is defined as the energy radiated within a unit solid angle by a unit surface element projected upon a plane normal to the radiation direction. The rate of energy received from dA_1 by dA_2 in figure 5.7 is therefore

$$(I_1)(\text{Projection of } dA_1)(\text{Solid angle of } dA_2)$$

or

$$I_1(dA_1 \cos \theta_1) \frac{dA_2 \cos \theta_2}{r^2}$$

For a diffuse surface, I is constant. Total emission E from a unit of surface dA_1 is equal to

$$\int_0^{2\pi} \int_0^{\pi/2} I_1 \cos \theta_1 \frac{(r \sin \theta_1 d\phi) r \, d\theta_1}{r^2} = \int_0^{2\pi} \int_0^{\pi/2} I_1 \, d\phi \sin \theta \cos \theta \, d\theta$$

which integrates to πI_1. For a unit area of blackbody, $E = \sigma T_1^4$, so that $E_1 = \sigma T_1^4 = \pi I_1$. The above expression for energy becomes

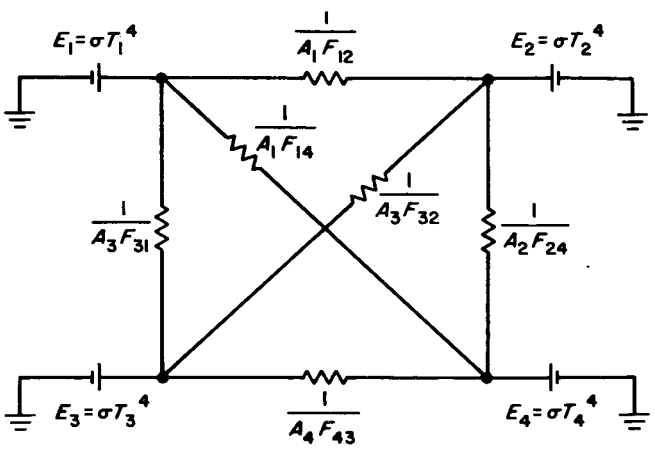

FIGURE 5.8—Network analog for four radiating blackbodies.

$$\sigma T_1^4 \, dA_1 \, \frac{\cos\theta_1 \cos\theta_2 \, dA_2}{\pi r^2}$$

Similarly, the energy rate from dA_2 to dA_1 is

$$\sigma T_2^4 \, dA_2 \, \frac{\cos\theta_1 \cos\theta_2 \, dA_1}{\pi r^2}$$

The net rate of radiation between the two surfaces is the integral of the difference, or

$$\sigma(T_1^4 - T_2^4) \int_{A_1} \int_{A_2} \frac{\cos\theta_1 \cos\theta_2 \, dA_1 \, dA_2}{\pi r^2}$$

It is customary to write the double integral either as A_1F_{1-2} or as A_2F_{2-1}, where F_{1-2} and F_{2-1} are called shape factors (also called view factors and form factors). They represent the fraction of the total radiant energy leaving one body which impinges upon the other body.

The net rate of blackbody heat transfer can be written merely as $\sigma A_1F_{12}(T_1^4 - T_2^4)$ or as $\sigma A_2F_{21}(T_1^4 - T_2^4)$. These shape factors may be determined by pseudographical techniques or experimental methods, or they may be calculated from geometrical considerations (the calculation is sometimes tedious). Many commonly used shape factors appear in the literature.

Similar thinking for two gray bodies results in the relations

$$A_1F_{12}(J_1 - J_2) \quad \text{or} \quad A_2F_{21}(J_1 - J_2)$$

where J is the radiosity, or total radiation from a unit area of surface,

and is equal to the emitted radiation plus the reflected radiation. This relationship can generally be written in the form

$$q_{12}=A_1\mathcal{J}(E_1-E_2)=\sigma A_1\mathcal{J}_{12}(T_1^4-T_2^4)$$

where $\mathcal{J}$, called a gray body shape factor, takes account of the various reflected radiation intensities. The factor $\mathcal{J}$ depends only upon system geometries and emittances.

The expressions $A_1F_{12}(E_1-E_2)$ and $A_1F_{12}(J_1-J_2)$ are identical in form with the Ohm's law expression $(1/R)(V_1-V_2)$. Radiation problems can therefore be symbolized as electrical networks. For instance, a network for four blackbodies at radiating "potentials" E_1, E_2, E_3, and E_4 is shown in figure 5.8. Solving for "currents" gives the heat transfer rates.

Bodies in radiation problems may be "floating" in that they are isolated from thermal inputs from outside the radiation system and reflect and emit radiation at the same rate at which they receive it. Figure 5.9 shows a "floating" body exchanging radiation with two sources or sinks.

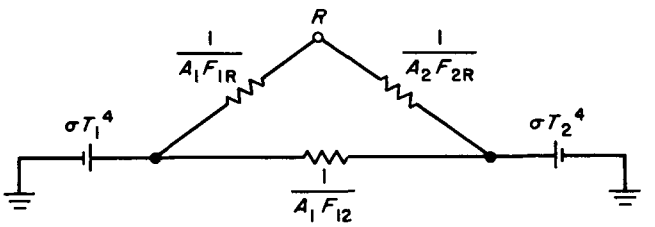

FIGURE 5.9—A "floating" body exchanging radiation with two sources or sinks.

The network method may also be used for gray surfaces. The radiosity J is equal to the emitted radiation ϵE plus the reflected radiation $(1-\epsilon)G$, where G is the incident radiation. The net rate of radiation loss per unit area of surface for a gray diffuse surface is

$$\frac{dq_{net}}{dA}=J-G$$

and

$$G=\frac{J-\epsilon E}{1-\epsilon}$$

so that

$$\frac{dq_{net}}{dA}=J-\frac{J-\epsilon E}{1-\epsilon}=\frac{J-\epsilon J-J+\epsilon E}{1-\epsilon}=\frac{\epsilon}{1-\epsilon}(E-J)$$

If temperature and irradiation are constant over area A,

$$q_{net}=\frac{A\epsilon}{1-\epsilon}(E-J)$$

This is the rate of heat flow between potentials E and J through resistance $(1-\epsilon)/A\epsilon$. Therefore, the equivalent network is similar to blackbody networks, except for an additional resistance $(1-\epsilon)/A\epsilon$ between the blackbody node point E, and the gray body node point J.

Figure 5.10 shows the network for two gray bodies exchanging radiation. The solution of this case is

$$q_{12}=\frac{1}{\frac{1-\epsilon_1}{A_1\epsilon_1}+\frac{1}{A_1F_{12}}+\frac{1-\epsilon_2}{A_2\epsilon_2}}(\sigma T_1^4-\sigma T_2^4)$$

The factor

$$\frac{1}{\frac{1-\epsilon_1}{A_1\epsilon_1}+\frac{1}{A_1F_{12}}+\frac{1-\epsilon_2}{A_2\epsilon_2}}$$

is called $A_1\mathcal{F}_{12}$. For a unit area of two large parallel plates (neglecting end effects),

$$A_1\mathcal{F}_{12}=\frac{1}{\frac{1-\epsilon_1}{A_1\epsilon_1}+\frac{1}{A_1}+\frac{1-\epsilon_2}{A_1\epsilon_2}}=\frac{A}{\frac{1}{\epsilon_1}+\frac{1}{\epsilon_2}-1}$$

so that

$$\mathcal{F}_{12}=\frac{1}{\frac{1}{\epsilon_1}+\frac{1}{\epsilon_2}-1}$$

As a point of interest, heat-transfer problems with combined heat-transfer mechanisms are frequently handled by equivalent circuits. The expressions for conduction and convection

$$q_{12}=kA(T_1-T_2)$$

$$q_{12}=\bar{h}_cA(T_s-T_\infty)$$

are also of the form $I=(1/R)(V_1-V_2)$. The radiation interchange expression

$$q_{12}=\sigma A_1F_{12}(T_1^4-T_2^4)$$

can be written as

$$q_{12}=\bar{h}_rA(T_1-T_2)$$

where

$$\bar{h}_r=F_{12}\frac{\sigma(T_1^4-T_2^4)}{T_1-T_2}$$

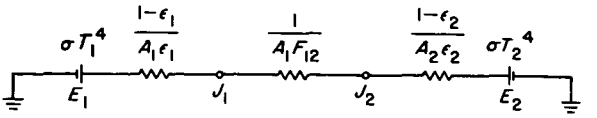

FIGURE 5.10—Radiation exchange between two gray bodies.

Tables of the quantity

$$\sigma \frac{T_1^4 - T_2^4}{T_1 - T_2}$$

called the temperature factor, as a function of the radiating surface temperatures, are available in the literature. Networks can be drawn with temperatures as driving potentials and resistances corresponding to the various heat-transfer mechanisms. In the case of the radiation links, if heat-transfer rates are desired and temperatures known, the temperature factor can be used directly. If either T_1 or T_2 are floating or unknown, it is necessary to assume values, evaluate the energy balance, and trim the assumed temperatures until the energy balance requirement is met.

REFERENCES

1. McAdams, W. H.: *Heat Transmission.* McGraw-Hill Book Co., Inc., 1954.
2. Kreith, F.: *Principles of Heat Transfer.* International Textbook Co. (Scranton, Pa.), 1958.
3. *Mark's Mechanical Engineering Handbook.* McGraw-Hill Book Co., Inc., 1958.
4. Kreith, F.: *Radiation Heat Transfer.* International Textbook Co. (Scranton, Pa.), 1962.
5. Harnett, Eckert, and Birkebak: "The Emissivity and Absorptivity of Parachute Fabrics," *Journal of Heat Transfer,* 81, 1959.

771-733 O-65-6

CHAPTER 6

Spacecraft Temperature Control Theory and Testing

MOST PEOPLE ASSOCIATED with the space effort occasionally must answer the question "What is the temperature of space?" The answer, of course, is that space has no temperature. Temperature is a measure of the internal energy of matter. Since space itself is the absence of matter, it can have no temperature. However, objects in space do have temperatures, and these temperatures will depend upon the nature of the objects themselves as well as the nature and proximity of other objects in space. A thin gold plate in deep space (beyond the thermal influence of any object other than the Sun) with its surface normal to the direction of the solar radiation, at 1 astronomical unit (the mean radius of the Earth's orbit) from the Sun, will reach a temperature of 405° F. If the plate is painted white, its temperature will drop to −18° F.

Objects in space acquire heat either by radiation from other objects or by converting stored energy, such as chemical fuel, into heat. They lose heat either by radiating to other objects or by radiating to "black" space. Other sources of heat, such as collisions with particles, can be neglected. By performing an energy balance (net heat input equals increase in internal energy) between the spacecraft or parts of the spacecraft, black space, and other objects of thermal interest, it is possible to solve for temperatures in the various parts of the spacecraft. These temperatures are the quantities of interest to spacecraft engineers because of the temperature sensitivity of various components of the spacecraft.

Like people, most components function best at approximately room temperature. Various components have various temperature requirements. Figure 6.1 presents curves of the efficiency of a solar cell at various temperatures. It is obvious that panels should be maintained at as low a temperature as possible. On the other hand, batteries must be maintained above 40° F., or they lose electrical capacity. If batteries become too hot (above 140°, in the case of the Mariner Mars silver-zinc battery), internal pressures become dangerously high. Most electronic equipment must be maintained below approximately 160° during operation. The cooler the equipment, the better, with the exception that if the temperature range

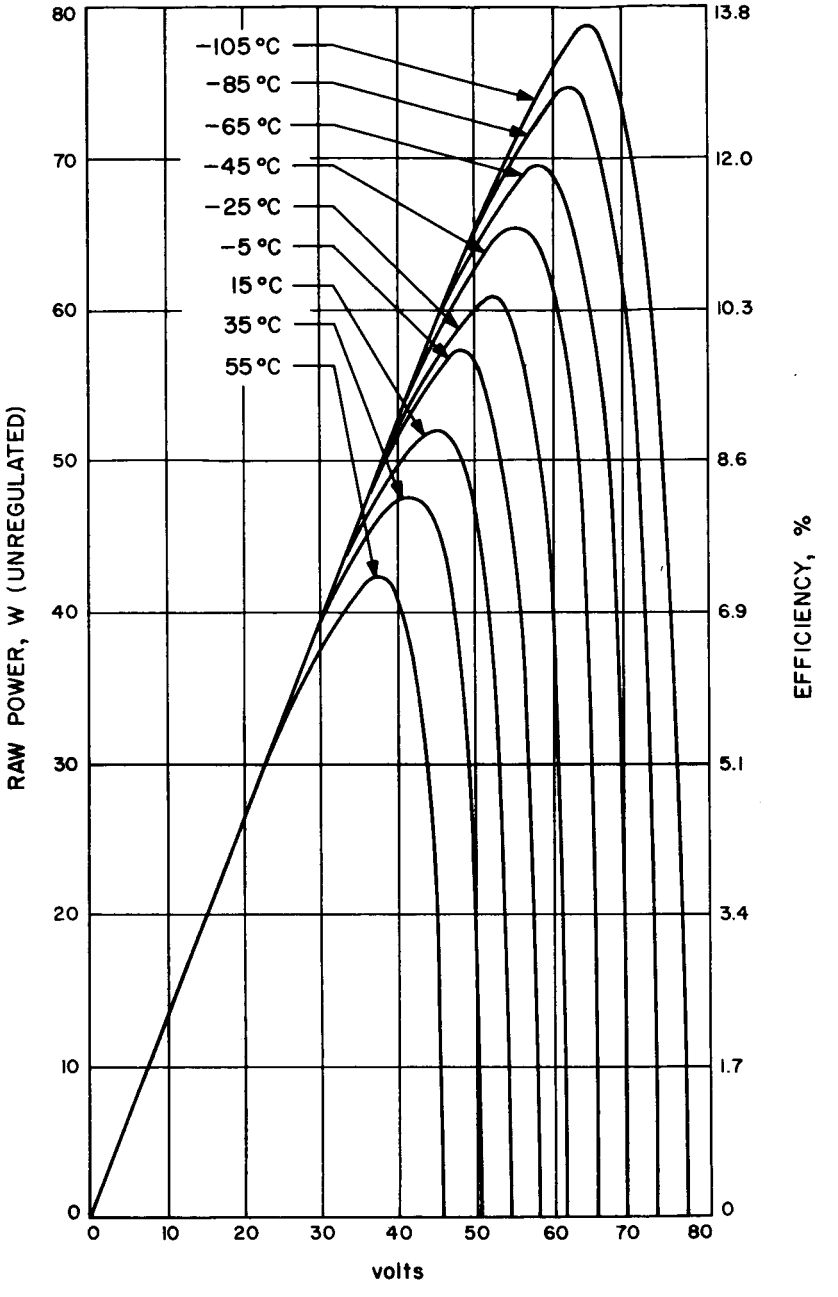

FIGURE 6.1—Maximum power as a function of voltage for a 4.3-ft² section of Mariner Mars solar panel. Earth solar constant. (JPL data.)

becomes too wide, temperature compensation in circuitry becomes difficult. The present practical lower temperature limit is about 15° F. Midcourse-correction motor fuel must be maintained between 40° F and 120° F so that it will neither freeze nor burn unpredictably. Gyro drift rate is generally a function of temperature. Some spacecraft usages require that gyro temperatures be controlled to within ±1° F. Other usages require that the temperature be controlled to within reasonable operating limits (50° F to 120° F) and predicted at the time of gyro use.

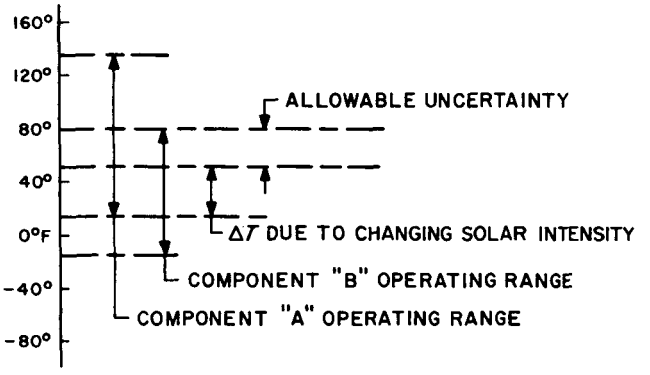

FIGURE 6.2—Spacecraft temperature-control problem.

The difficulty of the temperature control problem is schematically shown in figure 6.2. As different components are combined into assemblies, the allowable operating temperature range for the assembly decreases because component temperature requirements do not exactly coincide. After unavoidable variations such as temperature change due to solar intensity change and transient operation are subtracted, the allowable uncertainty becomes extremely small. Even though the spacecraft components may have operating limits spanning 50° to 150° F, the temperature-control engineer must control temperatures to within 10° or 20° F throughout the system.

In at least the near future, space exploration will be limited to the vicinity of our galaxy. The objects having the most thermal effect on spacecraft in space are the Sun, the planets, and other large bodies such as moons and asteroids which may at times be in proximity to the spacecraft.

The Sun is, perhaps, the most important object in space as it can never be ignored in temperature control problems within the solar system. The Sun has a diameter of 0.88 million miles, a mass of approximately 2.18×10^{27} tons, a mean density 1.41 times that of water, a surface gravity 28 times that of Earth, and a rotational

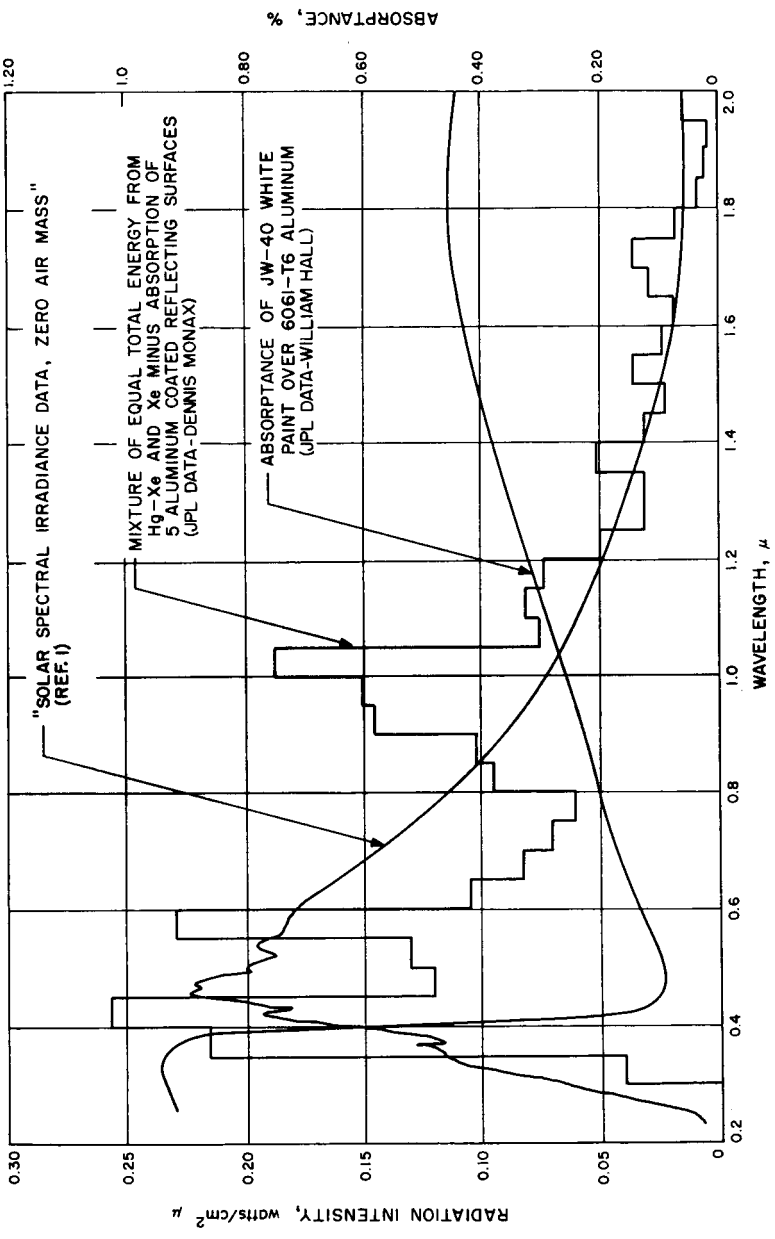

FIGURE 6.3—Effect of simulator spectrum.

period of about 25 days. The central portion of the Sun is surrounded by a layer of rarefied gas. The Sun radiates approximately as a blackbody at 10 400° R. A plot of solar intensity as a function of wavelength at the distance of the Earth from the Sun is shown in figure 6.3.

All the planets revolve in elliptical orbits roughly in the ecliptic, which is the plane of the Earth's orbit. The orbits are approximately circular, that of Earth having an eccentricity of only 0.016. The rate at which solar radiation strikes a unit area normal to the direction of the radiation is called the solar constant. The solar constant just outside the Earth's atmosphere is about 7.4 Btu/ft^2-min (442 Btu/ft^2-hr).

Since the planets have temperatures which are much lower than that of the Sun, planetary radiation has maximum wavelengths much longer than the maximum wavelength of solar emission. The maximum wavelength of Earth radiation is approximately 11.5μ, as contrasted to 0.5μ for solar radiation. The fraction of the incident radiation which is reflected or scattered to space by a planet is called the *planetary albedo*. Table 6.1 gives values of planetary albedo as well as other quantities of interest.

Spacecraft temperatures must stay within nominal values while the spacecraft is being operated on the ground, while it is being operated in the shroud before and during launch, after the shroud is separated while it is still within the regime of aerodynamic heating, within the proximity of the parent planet, and if not an orbiter, in the deep space environment. Temperatures must be controlled during in-flight maneuvers and during the periods when the spacecraft passes other planets. In the case of a planetary lander, the additional environments of atmospheric entry and possibly the planetary surface would necessarily be considered.

Because of the strict weight limitations and the extreme emphasis on reliability confronting the spacecraft engineer, it is desirable to achieve temperature control as simply, as ruggedly, and with as little additional equipment as possible. In general, if the spacecraft is able to control its temperatures in space, the ground and launch environments are not severe problems. Until launch, it is possible to cool the spacecraft by circulating a gas over the equipment. During launch, the thermal inertia of the shroud and the gas within protect the spacecraft. The shroud is usually not separated until aerodynamic heating has ceased to be a large problem. The control of temperatures during the period in which the spacecraft is in space is the major problem confronting the engineer.

Since spacecraft, like planets, are at temperatures far below the effective temperature of the Sun, the maximum wavelength of the

TABLE 6.1—Planetary data.

Object	Average diameter, miles	Average distance from Sun, miles	Albedo	Solar constant	Escape velocity, ft/sec	Surface gravity / Earth gravity	Period of rotation, days–hr	Length of year, days	Number of moons
Mercury	3100	36×10^6	0.06	48.7	14100	0.38	87–23	88	0
Venus	7500	67	.65	14.3	34100	.87	224–17	225	0
Earth	7920	93	.43	7.4	36700	1.00	1	365	1
Moon	2160	93	.08	7.4	7800	.16	27–8	------	------
Mars	4150	141	.15	3.2	16700	.39	1–1	887	2
Jupiter	87000	483	.51	.27	200000	2.65	0–10	4332	12
Saturn	71500	886	.50	.082	120000	1.17	0–10	10759	9
Uranus	32000	1790	.66	.020	73400	1.05	0–10	30686	5
Neptune	31000	2790	.62	.0082	84000	1.23	0–16	60188	2
Pluto	3560	3630	.16	.0049	17300	.5	?	90469	0

radiation from the spacecraft is much longer than that of solar radiation. For a given portion of spacecraft, average absorptance to solar radiation will therefore be different from average emittance to other portions of the spacecraft or to black space. For a better understanding of the mechanisms available to the temperature control engineer, let us examine a portion of a spacecraft in space in proximity to a planet (fig. 6.4). Performing an energy balance gives

$$q_s+q_{PE}+q_{PR}+q_i+P=q_P+q_R+q_o+C_{SC}\frac{dT}{dt}$$

where C_{SC} is the thermal capacity of the spacecraft portion. Let us examine each of these terms.

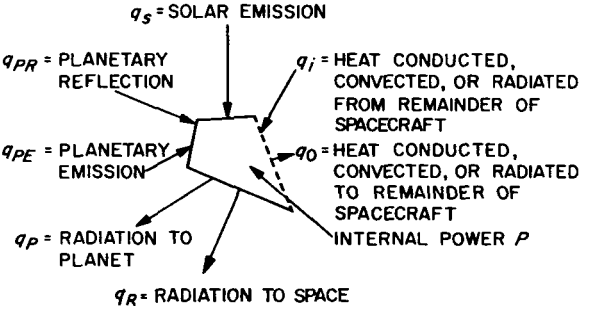

FIGURE 6.4—Portion of spacecraft.

The term q_s is the heat input from the Sun:

$$q_s=A_s\alpha_s S$$

where

A_s area normal to the solar radiation
α_s average absorptance to solar radiation over A_s
S solar constant

The quantities q_{PE} and q_P are heat rates from the planet to the spacecraft segment and from the spacecraft segment to the planet. Both depend upon the area–shape-factor product between the planet and the segment and the quantity $\sigma(T_{SC}^4-T_P^4)$, where the temperatures represent the mean effective temperatures of the segment and of the planet. The quantity q_{PE} depends also upon the absorptance of the spacecraft segment to planetary radiation and upon the emittance of the planet. The quantity q_P depends only upon the emittance of the segment.

The quantity q_{PR} is the heat input due to solar radiation reflected from the planet:

$$q_{PR}=A_R F_{P-SC}\alpha_R a S$$

where

α_R	absorptance of the segment to reflected radiation
a	planetary albedo
S	solar constant
$A_R F_{P-SC}$	area–shape-factor product which takes into account the geometry of the Sun-planet-segment system

The quantity q_R is the heat radiated from the segment to black space:

$$q_R=\sigma A_R F_R \epsilon T_{SC}^4$$

where $A_R F_R$ is an area–shape-factor product between the segment and black space.

Finally, $P+q_i-q_o$ is the power into the segment from the remainder of the spacecraft, and $C_{SC}(\mathrm{d}T/\mathrm{d}t)$ is the increase of thermal energy in the segment. For a Sun-oriented isothermal body in deep space in steady state with no internal power dissipation, the energy balance reduces to

$$A_s\alpha_s S=A_R\epsilon_R\sigma T_R^4$$

so that

$$T=\left(\frac{A_s\alpha_s S}{A_R\epsilon_R\sigma}\right)^{1/4}$$

Examination of the factors in these expressions shows that the spacecraft engineer has a number of possibilities for controlling the temperature of a portion of a spacecraft. He can control temperatures either passively (temperature control is accomplished before launch by selecting various radiation characteristics and form factors) or actively (radiation characteristics are changed by some sort of mechanism after launch). Because of its inherent simplicity, dependability, and light weight, passive temperature control is preferred if the thermal problem can be solved in this manner.

To accomplish passive control of the temperature in a portion of a spacecraft, the engineer may vary either the conduction path between the segment and the rest of the spacecraft, or the radiation characteristics between the segment, black space, the Sun, and the planet (assuming no convection exists). Conduction may be increased either by providing more material between the segment and the remainder of the spacecraft or by substituting material with higher conductivity. It may be decreased either by removing material or by placing a material of low conductivity in series.

Unfortunately, conductivity across joints in space is an unknown. Mechanical joints are microscopically rough. The actual mechanical contact depends upon a number of factors, such as pressure, surface, rigidity, and the number of previous matings. These factors are not important in atmosphere, since voids in the joints are filled with molecules of gas and the conductivity is roughly proportional to the cross-sectional area of the joint. However, in a vacuum these molecules are no longer present and the conductivity depends directly upon the mechanical contact.

Control of radiation characteristics can be achieved by applying various finishes, coatings, and platings to the surfaces of the segment. Table 6.2 gives solar absorptance and average emittance (normal spacecraft temperatures) for a number of materials.

TABLE 6.2—Surface properties.

Material	Hemispherical emittance,[a] ϵ	Solar absorptance,[b] α
Aluminum, polished	0.052	0.19
Aluminum, as-received	.053	----------
Gold plate, polished	.043	.215
Gold plate, unpolished	.041	.215
Black paints	.90	.94
White paint, JW40	.76	.23
White paint, ZW40	.87	.25
White paint, ZW60	.88	.23
Aluminum paint, UC11659	.30	.25
Dow 7 (approx.)	.44	----------
Black anodize	----------	.75
Clear anodize, sealed	.67	----------
FEP (Teflon), aluminized	.82	.24
White Mylar tape	.77	----------
Stainless steel	----------	.22
Shield, standard	.061	----------

[a] Obtained from emissometer.
[b] JPL data.

It can be seen that α/ϵ can vary between 0.23 and 4.8. Since radiation characteristics depend only upon temperature and surface, coatings of these materials will have almost the same effect as the solid material itself. The area–view-factor product can be changed during design in order to affect radiation heat transfer. Thermal shields on spacecraft are a simple and lightweight method of changing radiation characteristics. They may be used to prevent portions of the space-

craft from being directly exposed to the Sun, the planet, black space, or other portions of the spacecraft.

Passive temperature control is a surprisingly powerful technique. Passively controlled spacecraft must rely upon thermal inertia and thermal isolation to stabilize temperatures during transient conditions. However, even here it is possible to sidestep the problem with techniques such as placing a radiation shield between the Sun and the payload and thereby minimizing the effects of a changing solar constant.

If transient conditions become sufficiently severe, or if enough uncertainties exist in analysis and test, passive temperature control may be inadequate. For instance, if a unique and complex spacecraft is to be developed, it may be desirable to include active temperature control devices to take into account unknown errors in analysis and test. Passive temperature control may not be able to control temperature during intermittent operation of equipment with a high power consumption. It also may be inadequate during spacecraft maneuvers or during a large change in solar intensity. Orbiters are particularly susceptible to problems due to operation in and out of the Earth's shadow.

Active temperature control techniques include the following:

(1) Active control of spacecraft attitude to alter shape-factors between portions of the spacecraft, the Sun, black space, and the planet
(2) Provision of devices which can move thermal shields either automatically or upon command in order to alter shape-factors
(3) Active variation of α/ϵ for various surfaces by devices such as shutters, Maltese crosses, etc., which can either be actuated automatically, as by bimetal strips or servomechanisms, or by command from Earth
(4) Use of devices which vary the conduction path, such as thermal knife switches and variable-contact-area devices
(5) Use of devices which either provide or remove heat in critical areas; these may be simple resistance-heating strips, chemical heaters, nuclear heat sources, thermoelectric coolers, or mechanical-chemical refrigeration devices

The next chapter will cover some samples of actual active and passive spacecraft temperature control. As a point of interest, figure 6.5 (taken from ref. 2) shows calculated temperatures for a very simple model of an Earth orbiter.

The geometrical complexity of spacecraft, coupled with the variable nature of joint conductance in a vacuum, the difficulty of ascertaining absorptance and emittance values, and the difficulty of handling spectral reflections, necessitates a large degree of approximation in

spacecraft thermal analysis. Even though the experience of those doing the analytical work decreases the error below its possible maximum, there is always the chance that the solution will be uncomfortably far from the actual flight situation. The scarcity of data from vehicles in space prohibits making gross generalizations (such as that solar panels tend to run 15° hotter than calculated). It is therefore necessary to test actual or thermally mocked-up subsystems and spacecraft in a simulated space environment.

The simulated environment must first of all be a good enough vacuum so that convection is insignificant as a heat-transfer mechanism. A vacuum of 10^{-6} mm Hg or better is sufficient for this purpose. A vacuum of this magnitude also simulates the effect of space on joint conductance and is fairly easy to accomplish in a large volume with conventional equipment, a reasonably high pumping rate, and no impractical requirements for nonorganic seals, baking-out, cryotraps, and so on.

The simulated solar environment must also approximate black space as a radiation sink. Since the rate of heat transfer is proportional to the fourth power of absolute temperature it is not necessary to achieve absolute zero. A radiator at 100° F radiating a given amount of heat to a sink at absolute zero would increase in temperature only about 0.5° F in order to radiate the same amount of heat to a sink at 100° R. Achieving the proper geometry for the radiation sink is a bit difficult. In deep space, the Sun subtends an angle of only

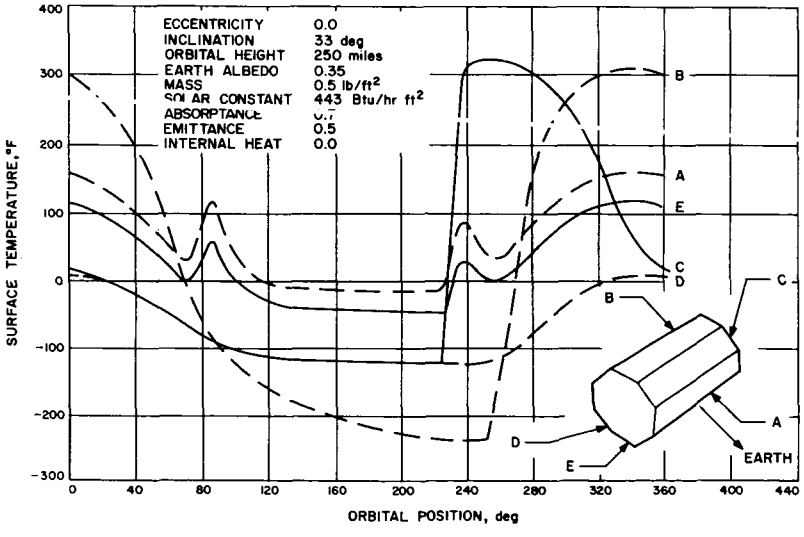

FIGURE 6.5—Cyclic temperature variation of Earth-oriented (vehicle axis on orbital path, side *A* normal to Earth's surface) eight-sided satellite model. (From ref. 2.)

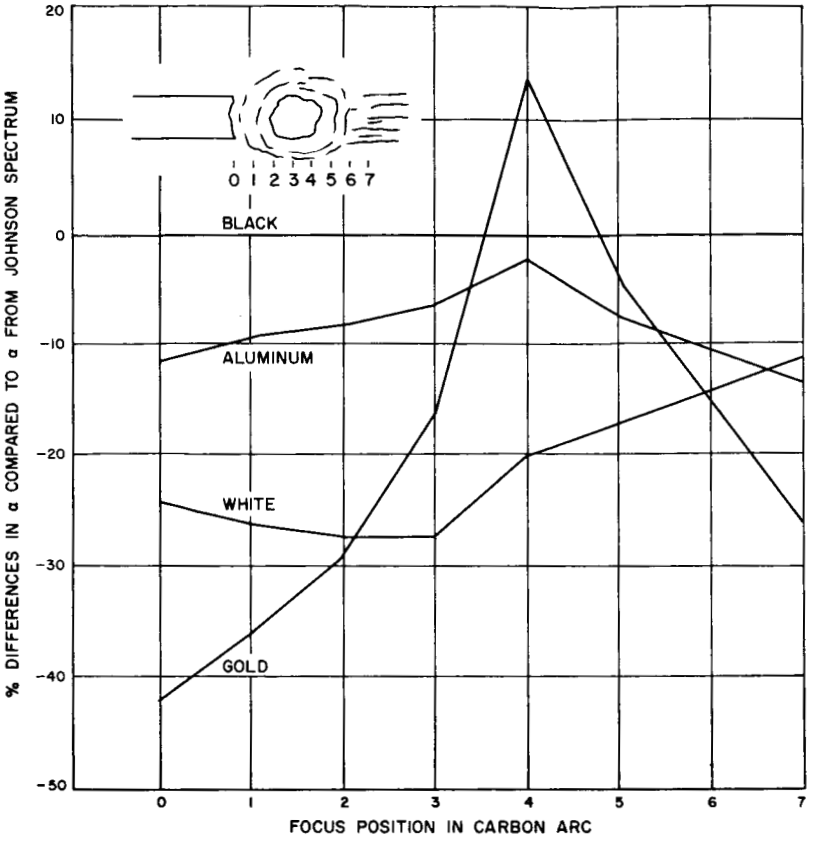

FIGURE 6.6—Effects of carbon-arc focus position on absorptance. (JPL data.)

0.5° at the distance of the Earth. This is negligible as far as the radiation form factor is concerned. To build a simulator which approximates the complete coverage of black space is sometimes tricky. An orbiter radiates to a field which may be dominated by a planet. A simulator which correctly approximates this condition causes other problems.

The third ingredient a space simulator must furnish is simulated sunlight. This is the major difficulty with presently existing simulators. As was seen in the section on basic heat transfer, the amount of energy absorbed by a material in sunlight can be found by integrating the product of an incremental portion of energy at a discrete wavelength and the absorptance of the material at that wavelength over the entire spectrum. It is obvious that if the spectrum varies, the amount of absorbed energy will vary. Figure 6.3 shows the accepted model for the solar spectrum (the Johnson spectrum),

Table 6.3—Calculated absorptance error relative to solar absorptance, percent.

[From ref. 3]

Material	(1)	(2)	(3)	(4)	(5)
Gold (polished)	+8.5	+30.9	+31	+4.5	−31.8
Aluminum (polished)	+2.1	+8.5	+7.6	+0.3	−1.4
ZW-60 white	+10	+8.8	+12.4	+4.5	−16.6
Aluminum paint	+2	+3.5	−4	−1.0	+1.7
Black paint	0	0	0	0	0

(1) Carbon arc with one aluminum reflection and transmission through 2.4 in. of quartz
(2) Westinghouse Hg-Xe (bare)
(3) Westinghouse Hg-Xe with one aluminum reflection and transmission through 1.6 in. of quartz
(4) 50% Westinghouse Hg-Xe, 50% Xe (bare)
(5) Hannovia Xe (bare)

plotted with a spectrum from one commonly used simulation source.

The carbon arc is the best approximation of the solar spectrum. However, it is also the most difficult to use. Electrodes burn up rapidly and must be replaced. The intensity is difficult to control closely because of electrode erosion. Figure 6.6 indicates another problem with a carbon arc source. The spectrum depends on which portion of the arc is at the focal point of the optics. One end of the arc is much higher in ultraviolet and the other end in infrared. Figure 6.6 shows differences in apparent absorptance of various materials as a function of focusing upon various positions between the electrodes.

Spectra are very difficult to measure accurately, as are quantities such as absorptance and emittance. Table 6.3 contains a summary of absorptance values calculated for various materials under various radiation sources. These are shown as percentage of difference from the standard spectrum and were found by integrating the curves of spectrum and spectral absorptance. These numbers show a gross difference in absorptance for various light sources. It should be realized that although the spectra used were the best available for the various sources, there is by no means exact agreement upon these spectra. Furthermore, the radiation spectrum from a given source changes drastically as it passes through optics and is reflected from various surfaces. In addition, the absorptance-wavelength curves are subject to error.

Figure 6.3 shows the spectra for sunlight and for Hg-Xe radiation plotted against wavelength. The absorptance for a white paint is superimposed. It can be seen that at the portions where the Hg-Xe spectrum is most in error, the absorptance values are large. This

causes maximum error. In fact, with the errors shown in figure 6.3, a white plate in space normal to the solar radiation at one astronomical unit from the Sun would reach a temperature approximately 100° F below that of the same plate in a simulator.

Efforts have been made to determine absorptance directly for various materials in space and in simulators. This would make direct correlation possible without the intermediate steps of absorptance and spectrum measurement.

Figure 6.7 shows a device employed to obtain absorptance in a chamber. Although a similar experiment has not been flown, one is scheduled for flight in the near future. The device functions by maintaining the surface temperature of a series of samples with alternate energy input from an electrical resistance heater and the chamber radiant source. Equating the measured amount of electrical energy to an unknown amount of absorbed radiant energy yields empirical absorptance data directly for the particular materials in the particular simulator.

Although solar simulation is far from perfect, as experience is gained with analysis-simulation-flight correlation, a much better understanding of the temperature control problem is emerging. Simulators are presently an essential tool in temperature control. Figure 6.8 is a diagram of the Jet Propulsion Laboratory (JPL) space simulator, which is rather typical of large-scale space simulators. One problem is the cost and operational clumsiness of these facilities. As spacecraft become larger, simulators become increasingly unattractive. One hoped for solution which is presently receiving some thought is thermal modeling, so that a small thermally similar model could be tested in a correspondingly smaller facility.

Modeling is a widely used tool in disciplines such as fluid mechanics. By using similar approaches it is possible to develop similitude laws for conduction-radiation heat transfer. Various dimensionless parameters which can be used to relate model temperatures to spacecraft temperatures can be defined. For instance, for a simple modeling situation in which the spacecraft is solar independent (no solar heat input), surface characteristics of the model and spacecraft are identical, and only steady-state conditions are considered, temperatures in the model will equal temperatures in the spacecraft if

$$\frac{\text{Characteristic model length}}{\text{Model thermal conductance}} = \frac{\text{Characteristic spacecraft length}}{\text{Spacecraft thermal conductance}}$$

$$\text{Model joint conductance} = \text{Spacecraft joint conductance}$$

$$\frac{\text{Model dissipated internal power}}{(\text{Characteristic model length})^2} = \frac{\text{Spacecraft dissipated internal power}}{(\text{Characteristic spacecraft length})^2}$$

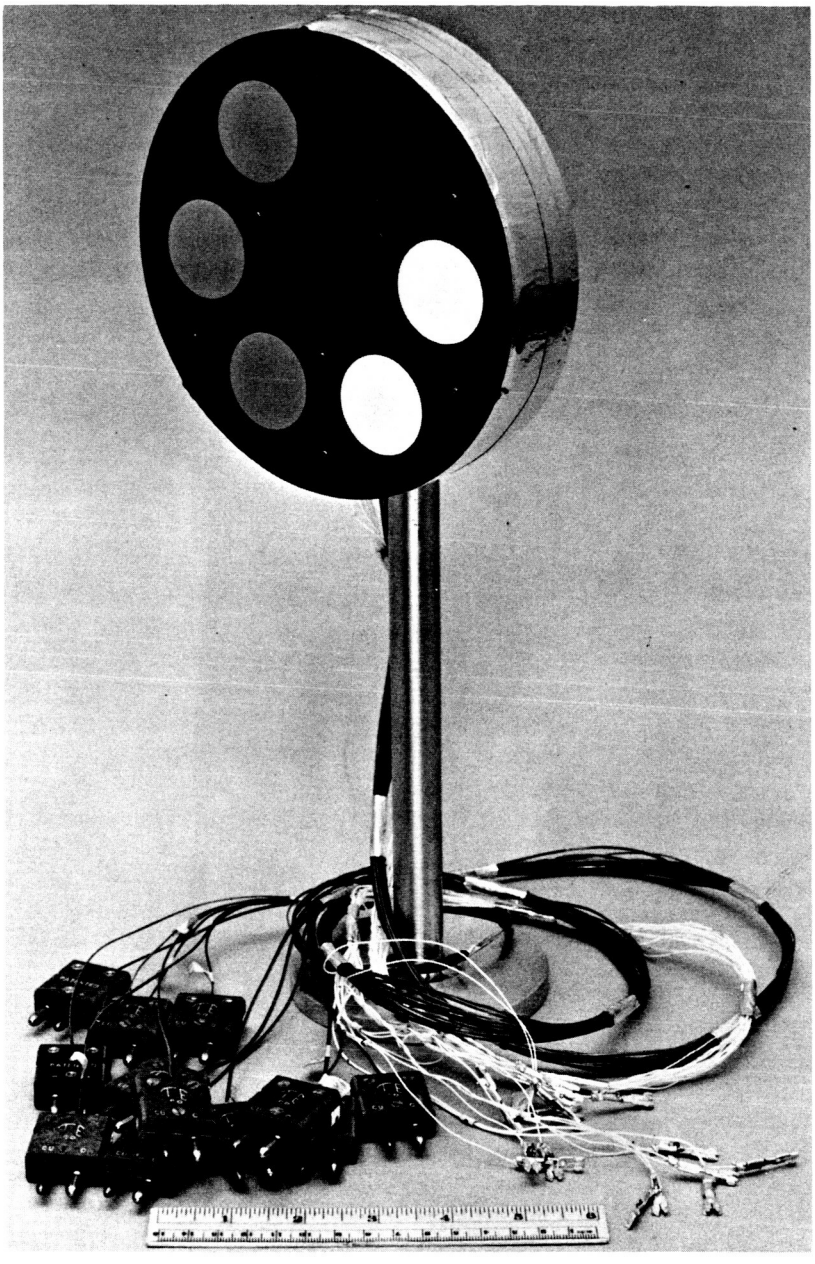

FIGURE 6.7—Absorptance experiment. (JPL photograph.)

Many other modeling relationships can be obtained, of course, depending upon choices of constant quantities and variables. The main drawback to modeling is that as absolute size decreases, losses

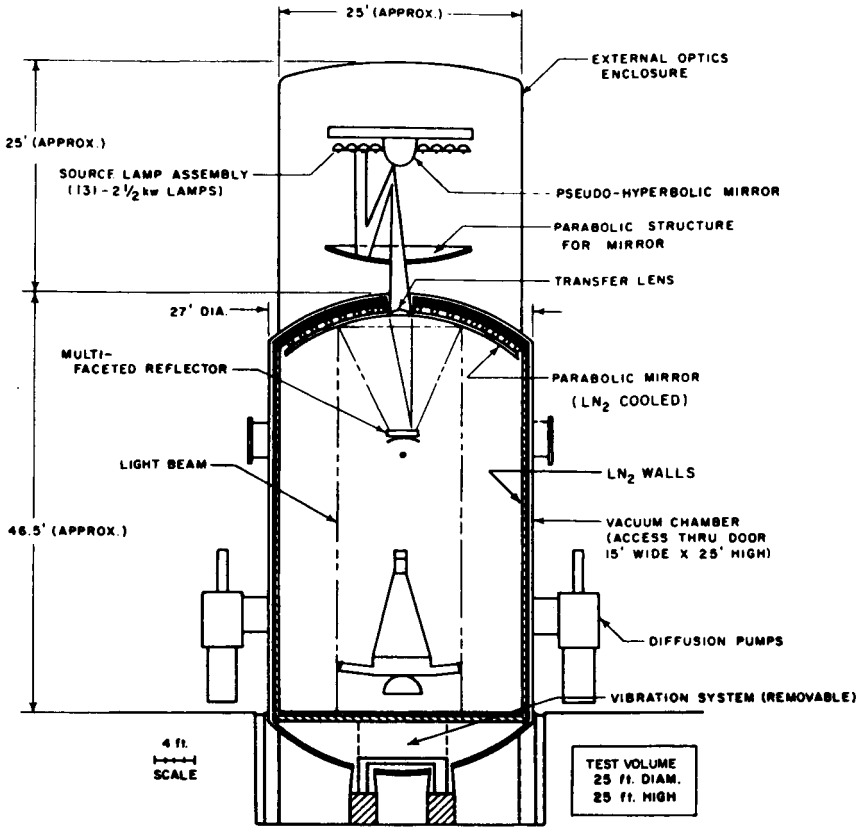

FIGURE 6.8—Cross section of JPL space simulator.

through mounting, instrumentation wires, and power leads become sizable. Economical modeling requires that the model be simpler than the original, since an exact spacecraft model would probably cost quite a bit more than the original spacecraft. This in turn tends to reduce the confidence the engineer has in the results of the model tests. However, intelligent use of very careful modeling for various portions of the system, coupled with more general modeling of the overall system, should result in useful and reliable information.

REFERENCES

1. JOHNSON, F. S.: "The Solar Constant," *J. Meteorol.*, vol. 11, no. 6, Dec. 1954, pp. 431–439.
2. STEVENSON, J. A., and GRAFTON, J. C.: "Radiation Heat Transfer Analysis for Space Vehicles," ASD Tech. Rep. 61–119, Dec. 1961.
3. KATTER, L. B., and KAHN, M. E.: "The Effect of Solar Simulator Operating Characteristics on Spacecraft Thermal Tests," JPL TM 33–175, July 15, 1964.

CHAPTER 7

Spacecraft Temperature Control

THIS CHAPTER contains illustrations pertinent to spacecraft temperature control and a discussion of a typical spacecraft temperature control problem.

Figure 7.1 is a view of one of the six mounting feet of the 1962 Mariner II Venus spacecraft. It is included merely to demonstrate the geometrical complexity which frequently plagues the spacecraft temperature control engineer. Finding pertinent radiation shape factors in a maze such as this is exceedingly difficult and can be accomplished only to a fair degree of approximation. The honeycomb

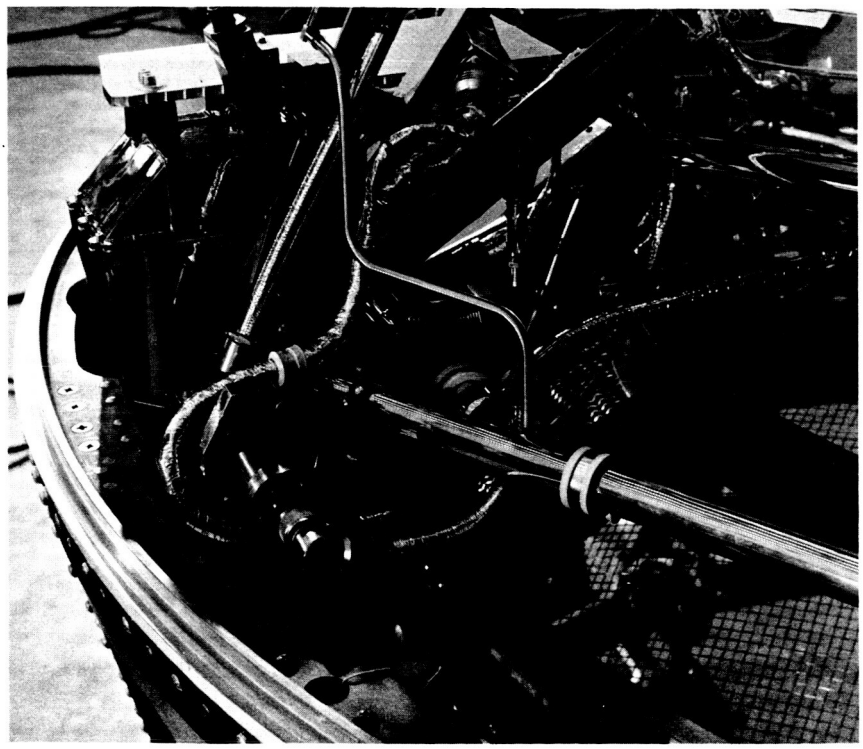

FIGURE 7.1—Foot section of Mariner II Spacecraft. (JPL photograph.)

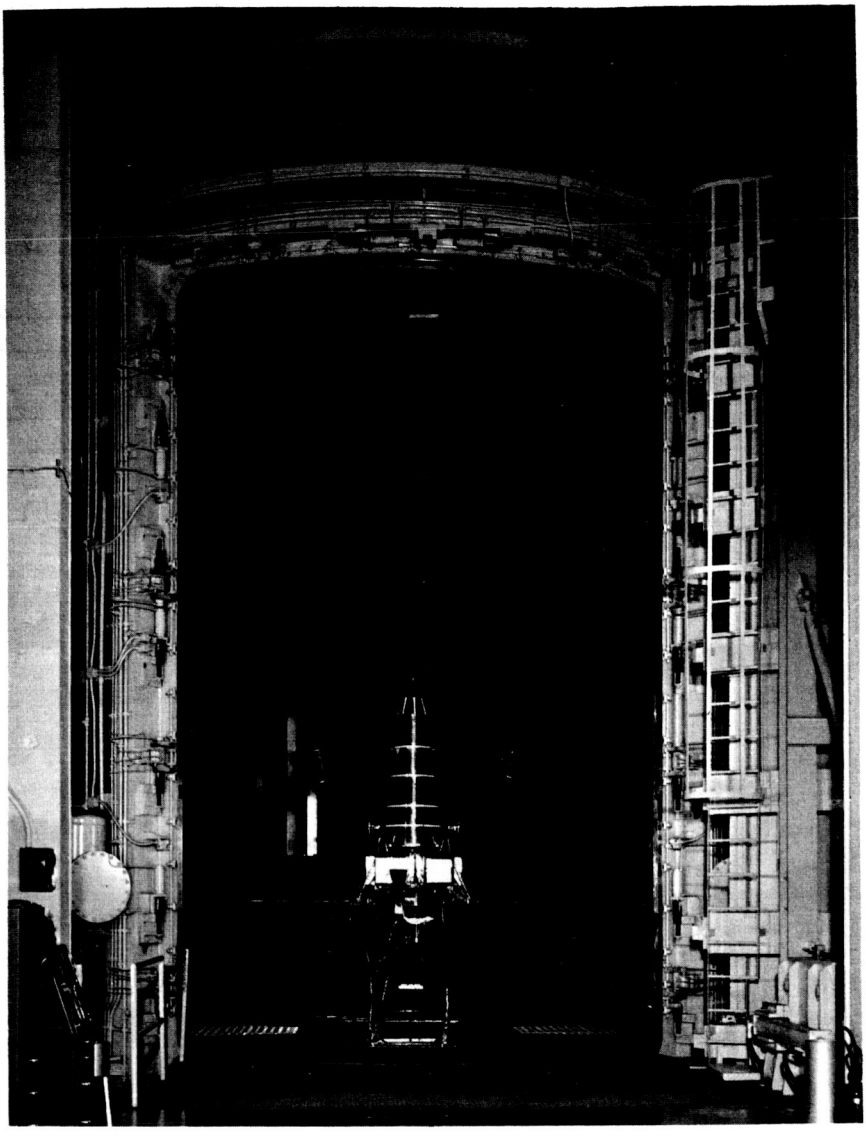

FIGURE 7.2—Ranger VII in JPL space simulator. (JPL photograph.)

plate near the top of the photograph is a thermal shield which shielded the Earth sensor from the Sun.

Figure 7.2 shows the temperature control model of the Ranger VII spacecraft in the Jet Propulsion Laboratory (JPL) space simulator. The simulated sunlight is not on in this picture. The conical structure which forms the upper portion of the spacecraft is the RCA

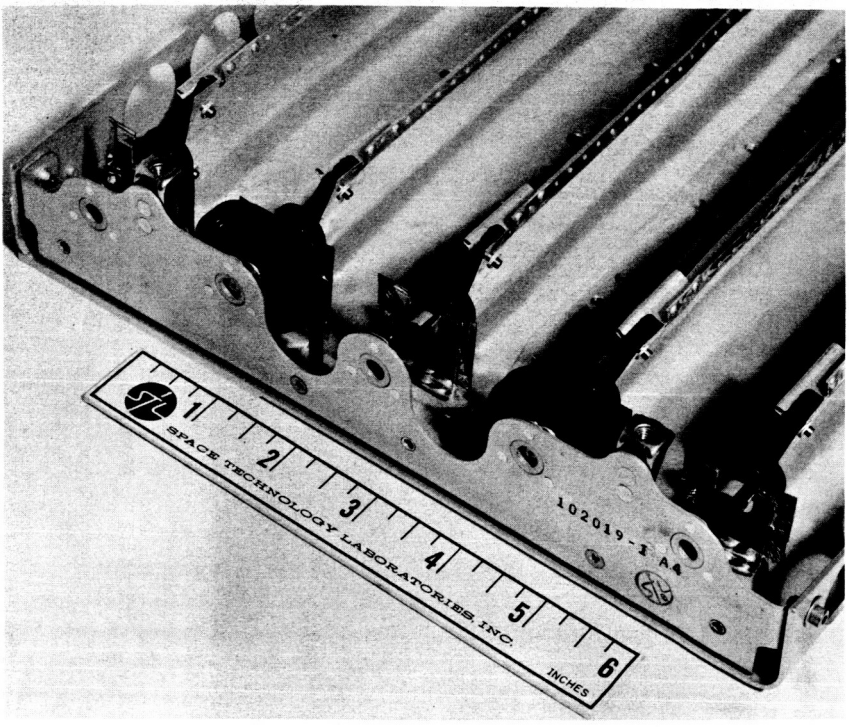

FIGURE 7.3—Bimetal-actuated louver. (STL photograph.)

television capsule. The black corrugated surface inside the simulator is the cold wall, which is filled with liquid nitrogen during chamber operation.

Figure 7.3 shows a bimetal-actuated louver. This particular version was built by Space Technology Laboratories (STL). The louvers themselves are of polished aluminum and are placed over a high-emittance background. The effective absorptance or emittance can then be varied from almost that of a polished aluminum surface to almost that of a black surface. The louver position is automatically controlled by a bimetal spring, each louver being controlled by an individual spring to obtain maximum reliability.

Figure 7.4 shows the lower thermal blanket of the 1964 Mariner Mars spacecraft. This blanket consists of 20 sheets of 0.00025-in.-thick aluminized Mylar. In a vacuum, the blanket is an excellent barrier to heat transfer. The lower thermal blanket is intended to prevent excessive heat loss to space. A similar blanket on the solar side of the spacecraft insulates the main body of the spacecraft from the Sun. The result is to decrease the thermal solar dependency of

FIGURE 7.4—Lower thermal blanket of Mariner Mars spacecraft. (JPL photograph.)

the spacecraft. The lower blanket is in two parts, the main portion and the portion which enshrouds and turns with the planet-oriented instruments.

The reasoning which resulted in the movable portion of the blanket is typical of that required to initially size spacecraft temperature control quantities. Early in the development cycle, the planetary scanning instruments in the Mariner Mars spacecraft were a television camera (operating limits $-50°$ to $+105°$ F), an ultraviolet experiment ($-22°$ to $+150°$ F), and a Mars sensor and a narrow-angle Mars gate ($-40°$ to $+130°$ F). These instruments were mounted on a structural platform which was at the lower end (away from the Sun) of a torque tube approximately 2 ft long and 3 in. in diameter. The actuator which was to perform the planetary scan was at the other end of the tube. More details of this device appear in chapter 10. The tube pivoted in Dyflon bushings mounted in an outer tube which was a portion of the octagonal structure of the spacecraft. Dyflon is similar to Teflon, and therefore a poor conductor of heat.

During the initial rough thermal analysis of the spacecraft, it was assumed that conduction through these bearings was negligible and that the heat exchange between the scan platform (and tube), space, and the remainder of the spacecraft was due to radiative interchange.

TABLE 7.1—Scan platform temperatures from early testing.

Component	Earth intensity, °F	Mars intensity, °F
Bus average temperature, T_1	52	17.5
Torque tube at octagon, T_2	13	−12
Torque tube at platform, T_3	−3	−21
Average temperature, T_4 TV camera	−23	−10
Average temperature, T_4 UV experiment	−9	−23
Average temperature, T_4 Mars sensor	−14	−30
Average temperature, T_4 Mars gate	−5	−23

Using these assumptions, analysis indicated that the planetary instruments would be cold, but within the required operating limits. Early developmental testing of a thermal mockup of the spacecraft in the space simulator resulted in the data tabulated in table 7.1.

During the Mars intensity test, 1 watt was dissipated in the television and 1 watt in the ultraviolet experiment. No power was dissipated on the platform during the Earth intensity test. As can be seen, at Mars intensity the instruments were cold, but above the minimum limits.

During the usual post-test efforts to obtain agreement between the analysis and the test, it was determined that appreciable heat was being transferred through the previously neglected Dyflon bearings. This was seen as follows.

Assume that the platform radiated at the average temperature of the platform, the ultraviolet experiment, the television camera, the Mars gate, and the Mars sensor. This was approximately −10° F at Earth and −23° F at Mars. The scan platform with instruments had an effective "black" radiating area of ϵA, q_E was the heat rate from the octagon to the platform at Earth in watts, and q_M was the heat rate at Mars. Then

$$q_E=\epsilon A\sigma(T_4)_E{}^4=0.155\epsilon A$$

$$2+q_M=\epsilon A\sigma(T_4)_M{}^4=0.140\epsilon A$$

From the two thermocouple measurements on the torque tube,

$$\Delta T_E=(T_2)_E-(T_3)_E=13+3=16^\circ\text{ F}$$

$$\Delta T_M=(T_2)_M-(T_3)_M=-12+21=9^\circ\text{ F}$$

and

$$\frac{q_E}{q_M}=\frac{\Delta T_E}{\Delta T_M}=\frac{16}{9}$$

By substitution,

$$\epsilon A = 38 \text{ in}^2$$

$$q_B = 5.9 \text{ watts}$$

$$q_M = 3.3 \text{ watts}$$

These were heat-flow rates from experimental data. Approximately the same result could have been obtained by treating the TV camera separately. The difference between the bus and the platform temperatures could also (with small error) have been taken as ΔT.

Investigation of the various heat paths between the bus and the platform showed that the radiative input from the lower thermal shield and the conductive input from cabling were negligible. The remaining paths were the radiation to the torque tube within the octagon and the conduction through the lower bearing.

For the radiation to the torque tube from within the octagon (see fig. 7.5), $\epsilon = 0.7$ for hard-anodized aluminum. The area of tube contained within the bus was

$$A = \pi d l = (\pi)(2.84)(11.3) = 101 \text{ in.}^2 = 0.7 \text{ ft}^2$$

The outer tube which radiated to the torque tube had a diameter d of 3.25 in. and was painted black inside and out, so that $\epsilon = 0.9$. For concentric cylinders,

$$A_1 \mathcal{F}_{12} = \frac{1}{\frac{\rho_1}{A_1 \epsilon_1} + \frac{1}{A_1} + \frac{\rho_2}{A_2 \epsilon_2}}$$

$$\mathcal{F}_{12} = \frac{1}{\frac{1}{\epsilon_1} + \frac{A_1(1-\epsilon_2)}{A_2 \epsilon_2}}$$

$$= \frac{1}{\frac{1}{0.7} + \frac{2.84}{3.25}\frac{0.1}{0.9}}$$

$$= 0.65$$

where ρ is the reflectivity. The radiant heat exchange between tubes was:

$$q = A_1 \mathcal{F}_{12} \sigma (T_1^4 - T_2^4)$$

or, linearizing,

$$q = \mathcal{F}_{12} A_1 h_r (T_1 - T_2)$$

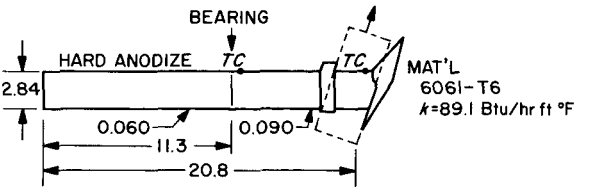

FIGURE 7.5—Torque tube.

The thermal (radiation) resistance from outer tube to torque tube was

$$R_{(\text{Earth test})}=\frac{1}{\mathcal{F}_{12}A_1h_r}=\frac{1}{(0.65)(0.7)(0.9)}=2.44\ ^\circ\text{F/Btu/hr}$$
$$=8.33\ ^\circ\text{F/watt}$$

$$R_{(\text{Mars test})}=\frac{1}{\mathcal{F}_{12}A_1h_r}=\frac{1}{(0.65)(0.7)(0.7)}=3.14\ ^\circ\text{F/Btu/hr}$$
$$=10.7\ ^\circ\text{F/watt}$$

Approximate h_r values were used since the final answer was not too sensitive to the exact h_r value.

The conduction resistance from the midpoint in the bus to the thermocouple on the torque tube at the bus was

$$R=\frac{L}{kA}=\frac{(0.5)(11.3)(12)}{(89.1)\pi(0.06)(2.81)}$$
$$=1.44\ ^\circ\text{F/Btu/hr}$$
$$=4.9\ ^\circ\text{F/watt}$$

The total thermal resistance for this path was thus

$$(R_T)_{\text{Earth}}=8.33+4.9=13.2\ ^\circ\text{F/watt}$$
$$(R_T)_{\text{Mars}}=10.7+4.9=15.6\ ^\circ\text{F/watt}$$

These values included the radiation resistance between the tubes and the conduction down the torque tube to the thermocouple.

The heat flow (from the bus to the thermocouple on the torque tube) must then have been

$$q_E=\frac{(T_1)_E-(T_2)_E}{(R_T)_{\text{Earth}}}=\frac{39}{13.2}=2.95\ \text{watts}$$

$$q_M=\frac{(T_1)_M-(T_2)_M}{(R_T)_{\text{Mars}}}=\frac{29.5}{15.6}=1.89\ \text{watts}$$

The difference between these values and the experimentally derived total heat-flow rates of $q_E=5.9$ watts and $q_M=3.3$ watts was necessarily attributed to conduction through the Dyflon bearings. Since positive radial and axial clearance was provided in these bearings, this conduction path could have vanished in the absence of 1 g loading.

To find platform temperatures in the absence of conduction through bearings, write

$$\epsilon A\sigma(T_{\text{platform}})^4=\frac{T_{\text{oct}}-T_{\text{plat}}}{R_{\text{oct-plat}}}$$

The thermal resistance of the torque tube between the bus thermocouple and the platform was

$$R_{\text{tube}}=\frac{(T_2)_E-(T_3)_E}{q}=\frac{16}{5.9}=2.7\ ^\circ\text{F/watt}$$

Using 13.2 °F/watt for remaining resistance,

$$R_{\text{total}}=13.2+2.7=15.9\ ^\circ\text{F/watt}$$

For $T_{\text{oct}}=52^\circ$ F and $\epsilon A=38$ in.^{2}, the above equation was solved by trial and error to give

$$T_{\text{plat}}=-33^\circ\text{ F}$$

Comparing this value with the experimentally obtained $T_{\text{plat}}=-3^\circ$ F showed that a potential 30° F temperature drop existed for a bus temperature of 52° F. This bus temperature was about the bus temperature desired at Mars. Since the platform temperatures were solely dependent on the bus temperatures, the TV temperature at Mars with no power might have dropped to about −50° F. This temperature was marginal for turn-on; hence some provision was needed for raising platform temperatures. Possible solutions were:

(1) Conduction coupling with bus (e.g., preloaded bearings, battery strap, sliding thermal joint)
(2) Radiation coupling with bus (e.g., modify thermal shield to place platform in a turret)
(3) Dissipate power on platform (about 6 watts required to raise temperature to 30° F)
(4) Heat input from Sun

For various reasons, the second solution was selected. After addition of the movable turret to the lower thermal shield, test temperatures were as follows:

	Earth	*Mars*
Bus average	82° F	67° F
TV camera	48° F	31° F
UV experiment	47° F	30° F

TABLE 7.2—Predicted and flight temperatures for the 1964 Mariner Mars spacecraft.

Channel		Earth cruise		Mars[a] cruise	
		Predicted, °F	Actual, °F	Predicted, °F	Extrapolated, °F
401	Bay 1	89	76	62	58
421	Bay 2	85	71	46	43
402	Bay 3	74	70	55	52
423	Bay 4	80	72	57	54
404	Bay 5	69	66	60	56
424	Crystal osc	77	72	69	65
405	Bay 6	75	71	73	69
426	Bay 7	68	63	57	54
407	Power reg	106	95	87	84
408	M/C N_2	83	70	51	48
428	Battery	85	75	64	61
409	SP 4A1	150	136	20	10
429	SP 4A5	150	136	20	10
410	Canopus Tkr	62	60	51	50
430	Lower ring	69	63	56	53
411	Scan actuator	82	71	53	50
431	Upper ring	104	87	52	48
434	Upper shield	268	223	110	82
435	Lower shield	−95	−126	−105	−136
436	Tape recorder	71	68	60	56
418	TV	46	38	26	18
438	Trapped rad. det	97	81	55	49
419	Ion chamber	100	70	10	−11
439	Magnetometer	54	34	−19	−29
217	M/C fuel	80	71	52	49
218	AC $X/-Y$ N_2	78	70	54	51
219	AC $-X/Y$ N_2	76	71	53	50

[a] Aphelion (TWT).

These temperatures were comfortably within the limits.

The point of presenting this example is to demonstrate that iterations of analysis and test are necessary to solve temperature control problems. This is because of the practical impossibility of accurately determining the constants necessary in the initial analysis without testing. Analysis is necessary for "ball-park" sizing, because of its flexibility as a design tool and because of the physical understanding which it promotes. Test is necessary to augment analysis, to determine accurate values, and to find problems which were overlooked when setting up the analytical model.

Table 7.2 shows actual and predicted temperatures for various

portions of the Mariner Mars spacecraft. The predicted temperatures resulted from data taken in solar simulator tests. The actual temperatures are from flight telemetered data.

CHAPTER 8

Mechanism Theory

SPACECRAFT GENERALLY cannot be launched in cruise configuration because of shroud envelope and structural snubbing requirements. A certain amount of articulation is necessary to "open" the spacecraft. Solar panels, antennas, and scientific instruments must be unlatched, extended, and oriented. During the lifetime of the spacecraft, various components must be oriented or scanned. In all cases, mechanisms are necessary to perform the mechanical functions. This and the following two chapters are concerned with design of these mechanisms. This chapter briefly discusses some of the mechanism elements. A good mechanism designer must be familiar with a great many elements and devices, both ingenious and standard, capable of performing various mechanism functions. He must use this knowledge of elements and devices, along with a wide variety of theoretical and experimental approaches, to evolve efficient and reliable mechanisms. Chapter 9 briefly discusses bearings and lubrication. The bearing problem is critical in any mechanism design involving rotary motion and is especially critical in the space environment. Chapter 10 discusses some actual spacecraft mechanisms used on Jet Propulsion Laboratory (JPL) and other flight spacecraft.

A mechanism is a device which transfers and/or modifies motion. In the process, it transfers and/or modifies force. Mechanisms are largely mechanical in nature, although they may contain electrical sensors, energy sources, and control loops. The design of a mechanism usually begins with a desired output motion and knowledge of the forces which must be overcome to produce this motion. The nature of the desired input is also known, as well as the desired efficiency, the desired quality of the input/output relationship, the operating environment, and the lifetime requirement. The design progresses iteratively. First, a mechanism is chosen from the designer's knowledge of various mechanical elements and movements. The elements must be sized and interconnected to obtain the desired movements, and then sized for sufficient strength. Mechanism elements are under stress both because they transmit forces as a result of the job the mechanism is doing and because they are in motion and will, therefore, be subjected to dynamic reactions.

After the mechanism design has reached the point where the desired input/output relationship can be obtained without failure, the design must be subjected to many other criteria. These may include cost, ease of maintenance, appearance, volume, noise of operation, ease of operation, safety, and so on. At any point in the design process, the original choice of a mechanism may appear to be faulty. It is then necessary to change the original concept and begin again. After several iterations (the number depending upon the clarity of the problem constraints, the importance of the design, and the experience of the designer), an acceptable design is obtained.

The mechanism designer must have a knowledge of power-producing devices, control techniques, mechanical elements, dynamics, strength of materials, materials, and processes. He must have a feeling for the physical meaning of tolerances, backlash, resonance, and other characteristics which may adversely affect the performance of a mechanism. Since the mechanism designer can seldom escape electrical considerations, he must also know about electrical devices and their capability.

Let us briefly mention several mechanisms and mechanism elements which are available to the engineer.

POWER SOURCES

Power sources may be rotary and periodic, rotary and nonperiodic, linear, or of some specialized or self-adapting nature. Examples of rotary and periodic power sources are electric motors, gas turbines, positive-displacement engines, and hydraulic or pneumatic motors. The selection of one of these devices depends upon energy availability, desired torque-speed characteristics, efficiency, required horsepower level, lifetime, reliability, weight, and so on.

Energy in the form of electricity is available aboard spacecraft because it is essential for communications, data handling, attitude control, and other functions. For this reason electric motors have been the most popular rotary power source in spacecraft. Electric motors are available in a wide variety of sizes, shapes, and types. They are simple, reliable, efficient, and have no exhaust thrust or contamination problems. They can be easily integrated into mechanisms and sealed against unknown environments. The use of an electric motor in a mechanical device requires first of all choosing the proper type (dc, induction, synchronous, split phase, etc.) and electrical size to generate the desired torque-speed characteristics. Mechanical portions, such as the shaft and bearings, must then be sized so that they will take the necessary loads.

Rotary-nonperiodic power sources include torsion springs, rotary solenoids, and specialized hydraulic and pneumatic devices. Such

devices are often built to order to provide a limited rotary mechanical input with stored or available energy sources.

Linear power sources include solenoids, pyrotechnic pinpullers and boltcutters, hydraulic actuators, pneumatic cylinders, and tension and compression springs. A large range of such devices is available for producing either limited linear motion or periodic linear motion in conjunction with a switching device. There are other power sources which do not fall into these categories. An example is the human arm, which together with a rather sophisticated control system can apply power either periodically or nonperiodically in a variety of directions. Springs, hydraulic and pneumatic devices, and devices operating from other forms of stored energy can be built to produce various specialized outputs. These will not be discussed since they are individually engineered to meet specific requirements.

CONTROLS

Control devices and techniques are extremely diversified and must be engineered into the mechanism rather than added as an afterthought. Controls are spoken of as either open-loop or closed-loop. An open-loop control is the type found on cheap electric heaters. It is merely an "on-off" switch which controls the mechanism at the whim of some logical operator. The thinking is done outside the mechanism-control combination. Expensive electric heaters containing thermostats are "closed-loop" controlled. The machine is controlled by information which is influenced by the machine's output. Some of the logic takes place within the mechanism-control combination.

Open loop control is used either when the accuracy and response of closed-loop control are not needed, when insufficient communication channels are available to conduct feedback information, or when absolute simplicity is desired in the mechanism and logic can be performed elsewhere.

No attempt will be made to cover closed-loop control theory in any detail here. However, let us look at the task of scanning a planet during the passage of an unmanned spacecraft to clarify further the difference between open-loop and closed-loop control. Two methods of performing this task are diagramed in figures 8.1 and 8.2.

The first method is open-loop control (fig. 8.1). A timer (set at Earth) or a command from Earth initiates a preprogramed scan motion prior to encounter. The planet is then scanned during passage according to this programed motion. The second method is closed-loop control of the mechanism (fig. 8.2). The desired scan is modified by subtracting the actual scan, and the result (error) is

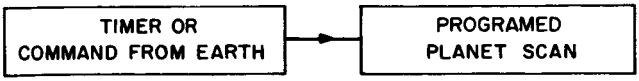

FIGURE 8.1—Open-loop control.

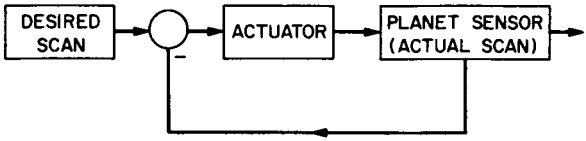

FIGURE 8.2—Closed-loop control.

fed to the actuator. The actual output is used to correct the input to more accurately achieve the desired result.

The use of feedback control in a hydraulic position servomechanism is shown in figure 8.3. Here, the output follows the input. The power source is controlled by an error signal consisting of the input minus the output.

Mechanism control devices and concepts are too numerous to be discussed in detail here. Control inputs may be put directly into a mechanism by mechanical means, such as the clutch or gearshift on a car. Rates can be controlled either by varying the relation of various mechanism elements, by introducing varying loads, or by metering the energy input to the power source. In the case of hydraulic and pneumatic systems, control is usually by means of various valves and position sensors. Mechanisms driven by electric motors are usually controlled by metering the electricity to the motor by means of mechanically operated switches, relays, rheostats, stepping switches, or other devices. If the control is closed-loop, the motor input is a function of the difference between the desired input and the actual

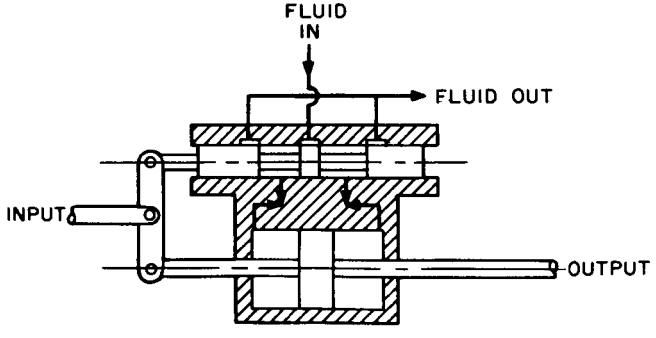

FIGURE 8.3—Feedback control in a hydraulic position servomechanism.

output, as sensed by some device such as a potentiometer, a synchro, or a tachometer.

MECHANICAL ELEMENTS

Let us now discuss various mechanical mechanism elements and combinations which produce various motions. If rotary motion is involved in the mechanism, which is frequently the case because of the popularity of rotary power sources and pivoted elements, the first mechanisms that are liable to be encountered are couplings, clutches, brakes, gears, and mechanical variable-speed mechanisms. The design of such devices requires the application of various mechanical elements and principles, the use of geometrical considerations to acquire the desired action, and the analysis of the elements and of the whole to insure that all portions are functioning efficiently and that no failures can occur.

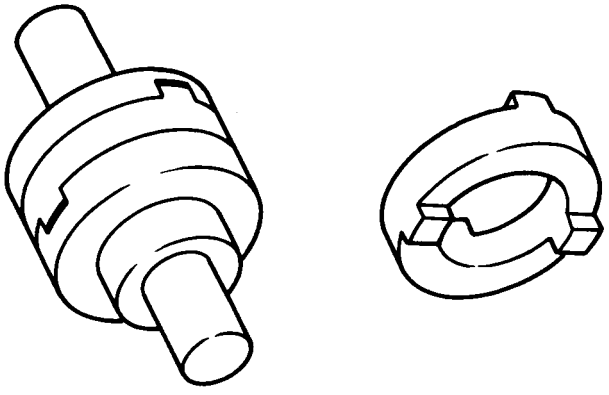

FIGURE 8.4—Oldham coupling.

Couplings transmit motion either in-line or out-of-line. They provide access to the mechanism, allow assembly and disassembly, and allow various shaft diameters to be interconnected. An example is the Oldham coupling shown in figure 8.4. It is a three-piece coupling. The loose center piece permits easy disassembly and compensates for small shaft misalinements. Another familiar example of a coupling is the universal joint on a car, which provides for power transmission at constant velocity between misalined shafts.

Clutches allow the power train to be interrupted. They may be required to operate with differential motion (automobile clutches), as override devices, or as unidirectional devices. In the one-way, or overriding, clutch shown in figure 8.5, motion in one direction causes rollers to lock between driving and driven members. Motion in the other direction unlocks members and permits free wheeling. In the

centrifugal clutch shown in figure 8.6, motion causes the shoes to expand, thereby locking the driving to the driven member. In the centrifugal clutch shown in figure 8.7, motion causes the steel shot to pack to the outside of the housing. Up to full speed there is decreased slippage. At design speed, driving and driven members are locked together.

Brakes are used to stop moving masses. Automobile brakes are a familiar example.

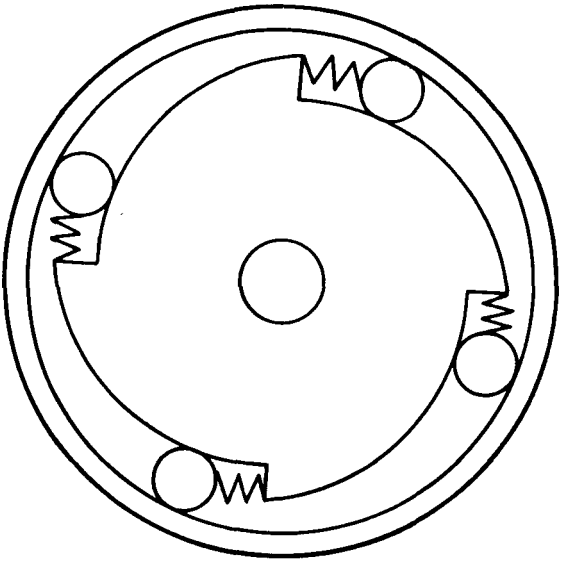

FIGURE 8.5—One-way clutch.

Variable-speed mechanisms are used to vary (usually continuously) the input-output ratio. An interesting one is the Zero-Max variable-impulse drive. The key linkage is schematically shown in figure 8.8. A large number of these linkages are used in parallel. The eccentric for each linkage is slightly rotated on the output shaft with respect to the eccentric of the preceding one. In this manner, it is possible to obtain essentially continuous movement even though the component from each linkage is discrete. By varying the position of the pivot point P, it is possible to obtain varying increments of output motion for each rotation of the input shaft.

Gears are one of the most widely used mechanical elements. They allow a tremendous variation of input-output speed and torque, are extremely efficient, and are available in many forms for various usages. Some of the commercially available types are straight-tooth spur gears (for parallel shafts), straight-tooth bevel and tapered gears (for

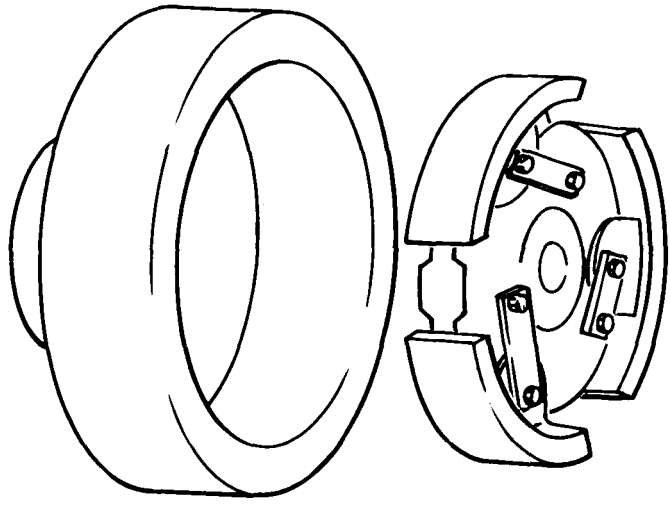

FIGURE 8.6—Centrifugal clutch.

misalined shafts), helical-tooth spur gears (for more continuous tooth action), herringbone gears (for continuous tooth action and minimum end load), worms and wheels, racks and pinions, crossed helical gears, and hypoid gears (used in automobile differentials).

Gears are usually, though not always, required to transmit motion at a constant angular-velocity ratio. This means that the values of the radii from the gear centers to the point of contact of the teeth must remain constant during operation. Gear teeth profiles that allow the transmission of uniform rotary motion are called "conjugate." There is a "law" of conjugate gear teeth which states that if gear

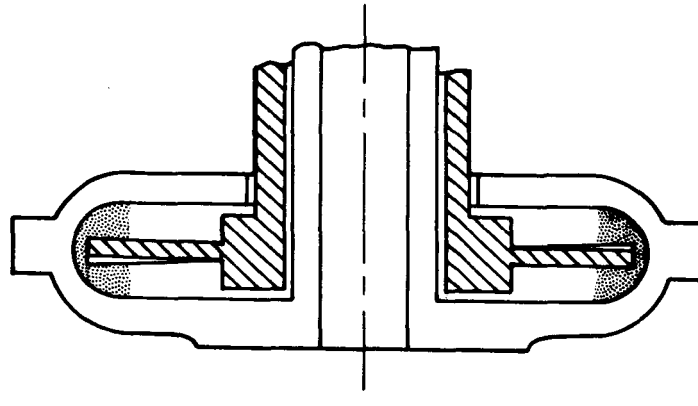

FIGURE 8.7—Centrifugal clutch.

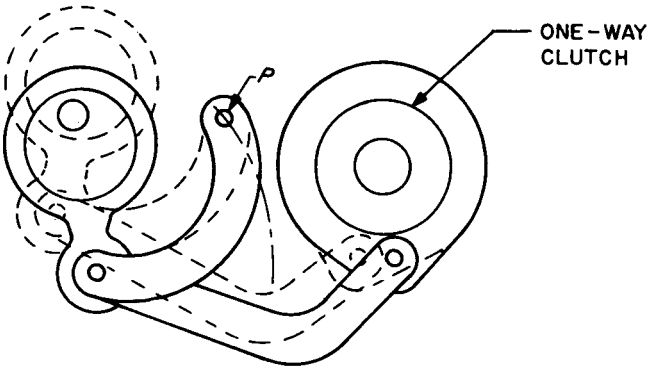

FIGURE 8.8—Zero-Max variable-impulse drive.

teeth are to transmit uniform rotary motion, the normals to the profiles of the teeth at all points of contact must pass through a fixed point in the common center line of the two shafts (the pitch point).

The most common gear tooth profile is the involute curve. This is the curve generated by a string as it is unwrapped from a cylinder. The adequacy of the involute as a gear tooth profile can be qualitatively seen as follows. If a belt runs between two cylinders, as shown in figure 8.9, the cylinders will turn together without slipping. If plates are fastened to the cylinders and a scriber fastened to the belt, the curves shown will be scribed on the plates. If the plates are then cut to this profile, they will roll and slide on each other without separating. These curves are involute curves, and if the belt is removed, one "tooth" will clearly drive the other "tooth" with continuous uniform action.

Gear train design requires, first of all, selection of gear types to obtain the desired action between the given shaft alinements within

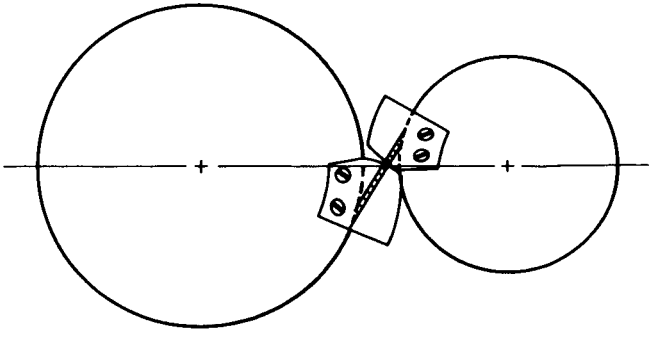

FIGURE 8.9—Involute gear tooth profile.

such constraints as desired lifetime, cost, quietness, and so on. Secondly, the various gear ratios (number of teeth on driven gear to number of teeth on driving gear) must be determined for the desired torque or speed multiplication. The various gears, shafts, and bearings must then be sized to take the loads safely.

Gear failures may be due to heat generated during operation(teeth both roll and slide on each other; sliding causes heat to be generated), failure of teeth by breakage, failure of the tooth surface by fatigue, or excessive abrasive wear of the tooth surface. The loads which cause these failures are due to the quasi-static transmitted loads and to dynamic loads which arise because of imperfections and elastic behavior in gear trains.

There are many semiempirical equations for the strength of gear teeth. The most popular is probably the Lewis equation. A modified form of the Lewis equation, which can be used for both steady and dynamic loads, is

$$W_{max}=\frac{fK_2YC_vS_e}{K_fK_1P}$$

where

W_{max}	maximum tangential load, lb
f	face width, in.
K_2	form factor to correct Lewis form factor to worst-load case (−1.70 for full-depth teeth)
Y	Lewis form factor
C_v	velocity factor
S_e	endurance limit
K_f	fatigue stress-concentration factor
K_1	service factor (1.25 for steady loads, 1.50 for shock loads)
P	diametral pitch

A full development of the use of this equation can be found in reference 1, along with tabulations of the form and stress-concentration factors.

The Buckingham equation is widely used to determine the load (dynamic and static) on gear teeth. It can be expressed as follows:

$$W_d=W+\sqrt{F_a(2F_2-F_a)}$$

where

W_d	total load, lb
W	tangential load, lb
F_a	acceleration load, lb
F_2	force required to deform teeth through effective error, lb

$$F_2=\frac{fe}{C_2\left(\frac{1}{E_1}+\frac{1}{E_2}\right)}+W$$

where

f face width, in.
e error in action, in. (tabulated in ref. 1)
C_2 9.345 for 14.5° gears
E_1 modulus of elasticity of pinion, lb/in²
E_2 modulus of elasticity of gear, lb/in²

$$F_a=\frac{F_1F_2}{F_1+F_2}$$

where

$$F_1=HmV^2$$

in which V is pitch line velocity and

$$H=C_1\left(\frac{1}{R_1}+\frac{1}{R_2}\right)$$

where

C_1 0.00086 for 14.5° gears
R_1 pitch radius of pinion, in.
R_2 pitch radius of gear, in.

$$m=\frac{m_1m_2}{m_1+m_2}$$

where

m_1 mass of pinion, slugs
m_2 mass of gear, slugs

A more thorough treatment of the Buckingham equation and tabulations of various values for the constants can be found in reference 1.

Similar semiempirical relationships are available for finding the heat generated by gear operation and tooth surface wear. These relationships are also covered in reference 1 and will not be discussed here. The use of expressions for gear strength and gear loading enables the designer to select gears which will offer the desired safety margin. If the reader is seeking more detail on the analytical design of gears, he is encouraged to become familiar with reference 2, which is an extremely detailed and authoritative treatise on gearing.

Uniform rotary motion can be transformed into nonuniform motion through noncircular gearing. Intermittent motion can be obtained with intermittent gears. Another method of obtaining intermittent

motion is the Geneva movement (fig. 8.10). This is the mechanism element commonly used in indexing heads on turret lathes.

Rotary motion can be transformed into straight-line motion by using cams. Cams are of so many types (disk, face, translational, cylindrical, conical, spherical, helical, three dimensional), utilize so many followers (roller, flat, curved, shoe), and are used for so many purposes (power transmission, information transmission, timing) that they cannot be covered here. A good brief discussion of cams can be found in reference 3. In the design of a cam, the shape of the cam and follower must first be determined in order to obtain the proper

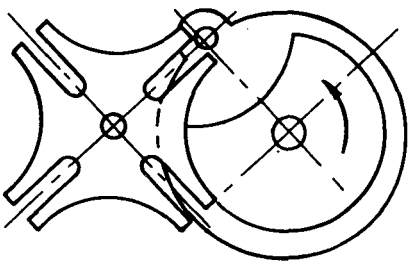

FIGURE 8.10—Geneva movement.

motion transmission. The cam and follower must then be sized so that stresses are not exceeded at contact or bearing points. Surface stresses in cams are often critical since contact is usually along a line or at a point.

If reasonable rates of speed are involved, cams cannot be designed merely by considering the desired input-output displacement relationship. It is apparent that followers should not be required to jump displacement steps because infinite velocities would be required. Similarly, velocity steps (infinite acceleration), acceleration steps (infinite jerk), and so on, should be avoided. The higher the derivative, the more subtle the problem. However, if rates are high, at least the third derivative must be considered.

With high-speed cams, the system containing the cam must be dynamically analyzed both to determine loads and to insure that the desired input-output relationship is being obtained. Such familiar phenomena as automobile valve float at high speeds are examples of dynamic behavior in which the driven quantity no longer follows the cam. If the desired output is to be obtained, the characteristics of the system (including such phenomena as compression and expansion waves and their rates of propagation) must be taken into account in cam design. In a high-speed system, the cam outline may necessarily deviate markedly from the desired motion of the driven quantity.

Many mechanisms which perform a wide variety of motion transformation can be analyzed as linkages. Linkages can be represented as members joined end to end with pivots. Figure 8.11 represents a four-bar plane linkage. A three-bar plane linkage (fig. 8.12) is a structure. No movement of one bar is possible relative to the others. A five-bar (or more) plane linkage (fig. 8.13) does not have a defined input-output relationship and is, therefore, not a bona fide mechanism element. Many mechanisms can be analyzed as four-bar linkages or combinations of four-bar linkages (fig. 8.14). Linkages may, of

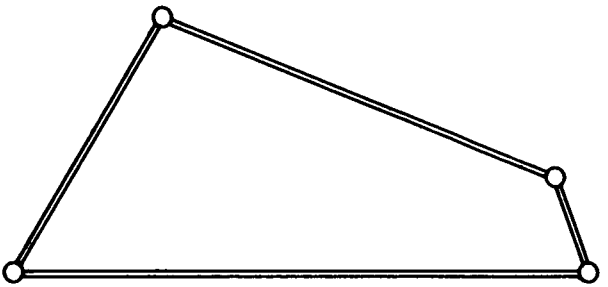

FIGURE 8.11—Four-bar plane linkage.

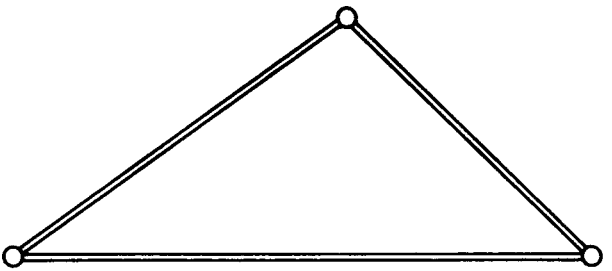

FIGURE 8.12—Three-bar plane linkage.

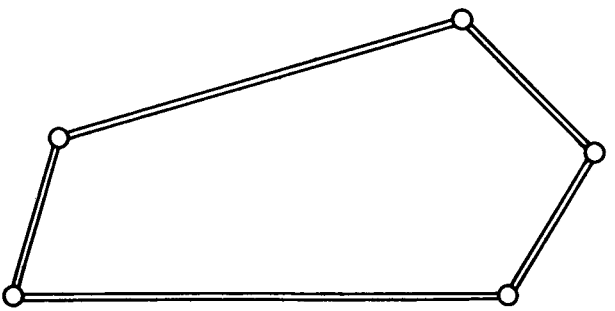

FIGURE 8.13—Five-bar plane linkage.

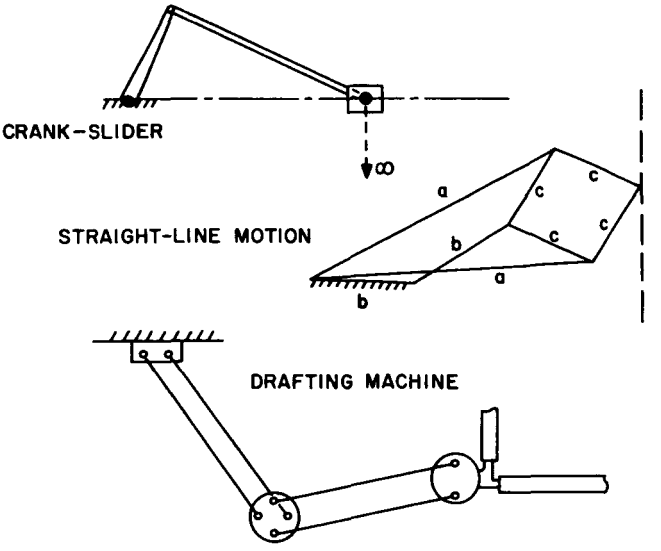

FIGURE 8.14—Linkage mechanisms.

course, be three dimensional as well as plane. A more thorough discussion of linkages is found in reference 3.

In order to size the members of linkages in mechanisms, it is necessary to find the loads on them. These are both static, due to the force being transmitted, and dynamic, because of the motion of the members. Static loads can be found by using known input conditions, linkage geometries, and static considerations. Linkage motions for defining dynamic loads can be found either graphically or analytically by using considerations similar to the following.

(1) *Graphical solution of a crank-and-slider mechanism.*

(a) To find velocities, use is made of the fact that relative motion of one end of a member to another (no shrinkage or stretching) can be only normal to the member. Knowing V_A and V_B, V_{BA} can be found as shown in figure 8.15. Velocities for the crank-and-slider mechanism with rotary input ω_A at point A can therefore be

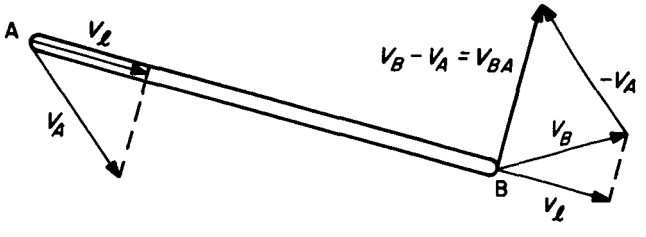

FIGURE 8.15—Crank and slider mechanism.

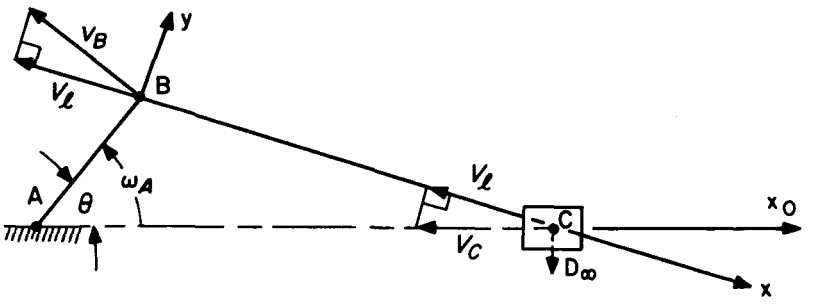

FIGURE 8.16—Graphical velocity solution.

graphically found as shown in figure 8.16. In this figure V_B is merely the magnitude of ω times the crank length AB.

(b) To find accelerations, use is made of the vector expression for the absolute acceleration of a point in a moving coordinate system. The moving coordinate system is xy and the fixed one is x_oy_o.

$$\boldsymbol{a}_o=\boldsymbol{a}_m+\dot{\boldsymbol{\omega}}\times\boldsymbol{r}+\boldsymbol{\omega}\times(\boldsymbol{\omega}\times\boldsymbol{r})+2\boldsymbol{\omega}\times\boldsymbol{V}+\boldsymbol{a}$$

where

- $\boldsymbol{a}_m$ acceleration of origin of moving coordinate system
- $\dot{\boldsymbol{\omega}}$ angular acceleration of moving coordinate system (positive counterclockwise in fig. 8.16)
- $\boldsymbol{\omega}$ angular velocity of moving coordinate system (positive clockwise in fig. 8.16)
- $\boldsymbol{r}$ distance from origin of moving system to point
- $\boldsymbol{V}$ velocity of point in moving system
- $\boldsymbol{a}$ acceleration of point in moving system

The acceleration a_o must act along the x_o axis. Since $\dot{\omega}=0$, $\boldsymbol{a}_m$ is equal to $|\omega|^2$ times the length of crank AB and acts toward A. Also, $\dot{\omega}\times\boldsymbol{r}$ ($\boldsymbol{r}$ is the length BC) acts perpendicular to link BC, $\omega\times(\omega\times\boldsymbol{r})$ acts

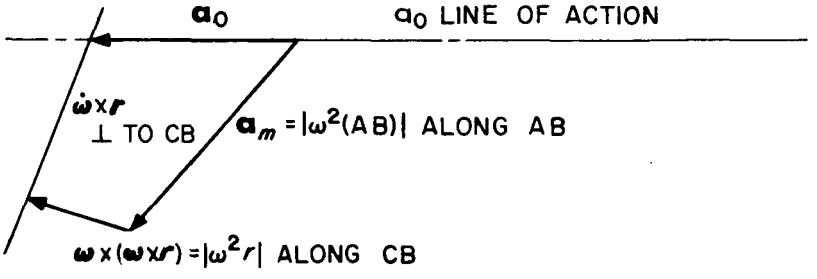

FIGURE 8.17—Graphical acceleration solution.

along BC in the direction of B, and $V=0$. A vector diagram showing the acceleration of the slider can therefore be drawn (fig. 8.17).

(2) *Analytical solution of a three-dimensional linkage:* Shafts are at right angles to each other; coordinate systems are parallel (fig. 8.18).

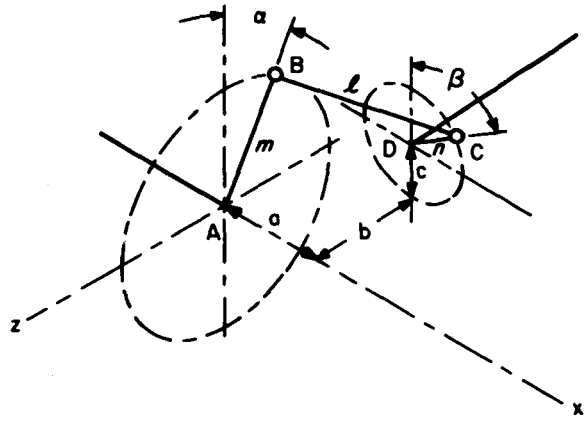

FIGURE 8.18—Three-dimensional linkage.

$$l_x=a+n\sin\beta$$

$$l_y=c+n\cos\beta-m\cos\alpha$$

$$l_z=-b+m\sin\alpha$$

$$l^2=l_x^2+l_y^2+l_z^2$$

$$=a^2+n^2\sin^2\beta+2an\sin\beta+c^2+2cn\cos\beta-2cn\cos\alpha+n^2\cos^2\beta$$

$$-2mn\cos\alpha\cos\beta+m^2\cos^2\alpha+b^2-2nb\sin\alpha+m^2\sin^2\alpha$$

or

$$l^2=a^2+b^2+c^2+m^2+n^2-2mc\cos\alpha-2mb\sin\alpha$$

$$+2cn\cos\beta+2an\sin\beta-2mn\cos\alpha\cos\beta$$

By differentiating this expression twice with respect to time, expressions containing the quantities $\dot{\alpha}$, $\dot{\beta}$, $\ddot{\alpha}$, and $\ddot{\beta}$ can be obtained.

Knowing any three of the quantities α, β, $\dot{\alpha}$, $\dot{\beta}$, $\ddot{\alpha}$, and $\ddot{\beta}$, the three equations can be used to find the other three quantities.

REFERENCES

1. SHIGLEY, J. E.: *Machine Design,* McGraw-Hill Book Co., Inc., 1956.
2. BUCKINGHAM, E.: *Analytical Mechanics of Gears.* McGraw-Hill Book Co., Inc., 1949.
3. BEGGS, J. S.: *Mechanism.* McGraw-Hill Book Co., Inc., 1955.

CHAPTER 9

Bearings and Lubrication

BEARINGS AND LUBRICATION are extremely important in spacecraft mechanisms. As in any mechanism, good bearing and lubrication practices lead to high efficiency and low wear. The bearing and lubrication problem in space is somewhat severe because of weight limitations, reliability requirements, and the space environment. However, the problem may be satisfactorily solved in most cases by proper application of basic bearing theory and use of the proper materials and lubricants.

Lubrication can be divided into thick-film, or fluid, lubrication and thin-film, or boundary-layer, lubrication. Metal surfaces are microscopically rough, with peaks, or asperities, which project above the mean surface level. In thick-film lubrication, the two bearing surfaces are completely separated by a layer of lubricant during steady-state operation. In this mode of lubrication, the characteristics of the bearing surfaces are of secondary importance and the behavior of the bearing depends on the properties of the fluid.

The behavior by which the fluid supports the load is interesting but too complex to study at great length here. A good discussion of the mechanisms involved can be found in reference 1. In brief, there are two types of thick-film bearings, hydrodynamic and hydrostatic. In hydrodynamic bearings, the relative motion of the surfaces, in conjunction with the viscosity of the fluid, causes a load-bearing "wedge" of high pressure to build up within the fluid layer. This "wedge" does not exist unless the relative motion is present. If the load-carrying capability of the film is desired with no relative motion, or if the viscosity is insufficient to build up a wedge which will support the load, a hydrostatic bearing must be used. In hydrostatic bearings, the pressure in the fluid layer is obtained partially or completely from outside the bearing. Many gas bearings are designed to be hydrostatic, since viscosities are low and no lubrication exists at all unless the load-supporting fluid layer is present. Some bearings are a combination of hydrostatic and hydrodynamic, in that the fluid layer is pressurized for start-up (hydrostatic), and then the bearing is operated with pure hydrodynamic action once relative motion is obtained.

At present, very few thick-film-lubricated bearings are used in spacecraft. For such applications as bearings in the turbopumps used to pump fuel to booster engines or gimbal mounts for rocket engines, thick-film lubrication may be required. However, thick-film lubrication is best suited for applications where loads are high and lifetimes are long. Fluid lubrication systems are frequently heavy and complex, as a large quantity of fluid must be supplied at all times to the bearing. In the future, when spacecraft may contain turbines for production of secondary-power and other high-load, long-life machines, fluid lubrication may be more widely used. However, at present the more spartan nature of thin-film-lubricated bearings make them more compatible with spacecraft design philosophies.

It is worthwhile to examine the nature of boundary lubrication in some detail. An understanding of boundary lubrication is necessary for any bearing design. Even thick-film bearings usually fail because of wear resulting from stopping and starting or faulty operation when boundary lubrication is the only means of lubrication present. It is foolish not to use boundary lubrication fundamentals when designing a thick-film bearing, since if the bearing has poor boundary lubrication inherent in its design, even a brief loss of the pressure "wedge" can result in failure. Rolling-element bearings usually fail because of excessive cage or rolling-element wear which could be minimized by better boundary lubrication. In fact, practically all bearing failures occur in the regime of thin-film lubrication.

In boundary lubrication, the small asperities of the two surfaces make contact. The properties of the materials of the two surfaces are therefore extremely important. The properties of the lubricant are also very important, as they influence the interaction of the two surfaces. There are many theories of friction, but the presently accepted one is the adhesion theory which was independently hypothesized by Merchant in the United States and Bowden and Tabor (ref. 2) in England.

The reasoning of this theory is as follows. As a load is applied to a bearing, the asperities of the two bearing surfaces make contact with extremely high local loads at the point of contact. These high loads force the lubricant from between the asperities. Since the local stresses are in excess of the yield strength of the materials, the materials are subject to plastic flow. This flow breaks through the surface layer of the materials and welding occurs at the junction. Further motion requires either breaking this weld or tearing one of the bearing materials.

The Merchant-Bowden-Tabor theory contains another friction mechanism besides the "cold welding." This is the plowing of the asperities through the softer bearing surface, a roughness phenomenon

that is usually much less important than the "welding" mechanism. The theory states that, in general, the friction coefficient can be reduced by using bearing materials which have very low shear strengths and very high yield strengths. Such materials are difficult to find. However, materials with high yield strengths can be coated with very thin films of a material with very low shear stress. The hard base material can then support the load while shear takes place within the soft film.

Boundary lubrication is actually the provision of a contaminant between the bearing surfaces. This contaminant allows the bearing of a load by the bearing materials while it prevents effective welding of the surface asperities. Boundary lubrication is offered by many contaminants other than the familiar oils and solid lubricants. Oxide layers, metal films, chemical-reaction films, and other thin films improve the bearing qualities of surfaces.

Coefficient of friction and wear are not necessarily related. Severe wear can take place at a relatively low coefficient of friction, or conversely, two surfaces can run together with a very high coefficient of friction and little or no wear. However, one type of wear, referred to as adhesive wear, is due to the welding and tearing of the asperities of the material. This type of wear is minimized by the "contaminant," just as the coefficient of friction is reduced. Burwell (ref. 3) breaks down wear into adhesive or galling wear, abrasive and cutting wear (due either to asperities on harder material abrading softer material or to the presence of a third party, such as grit or sand), corrosive wear (chemical), surface fatigue, and others.

Within the region of usual engineering practice, adhesive wear is directly proportional to load and distance traveled and is completely independent of apparent area of contact. Figure 9.1 shows the results of a NASA wear experiment in which nominal contact stresses varied from 41 to 273 lb/in^2. As can be seen, the wear-time curve is independent of this apparent contact stress. Abrasive or cutting wear depends to a certain extent upon hardness and also upon the elastic limit of the material. Harder materials tend to wear less by cutting and abrasion. With some materials (for instance, water-lubricated rubber bearings for use in the presence of sand) elastic yielding prevents damage. In general, it appears that the larger the ratio of indentation hardness to elastic modulus, the better the resistance to abrasive and cutting wear.

Figure 9.2 shows the effect of three commonly used film lubricants on the coefficient of friction. The coefficient of friction of the unlubricated configuration decreases because the increasing heat causes the formation of beneficial oxides which act as a lubricating film. Lubricating films may be formed by the presence of a liquid or a solid

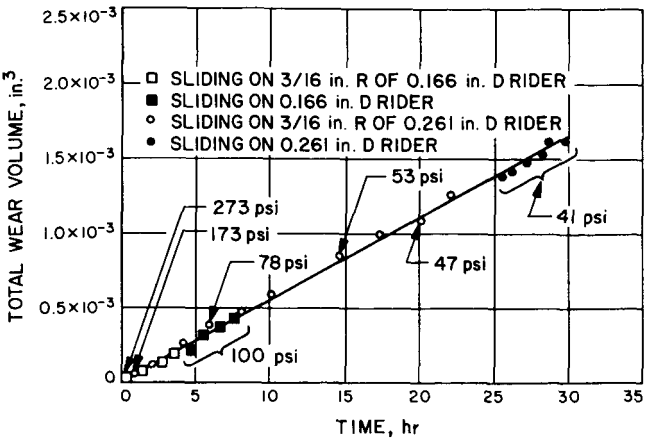

FIGURE 9.1—Wear of carbon against chromium plate. Velocity, 10 000 ft/min; load, 1000 gm; temperature, 360° F. (From ref. 4.)

(such as molybdenum disulfide or Teflon) which coats the bearing surfaces, or by plating, chemisorption, chemical reaction, or physical absorption. Films may be either preformed or self-repairing. Plated coatings are preformed. In chemisorption, chemical bonding occurs but a reaction does not take place. The materials are not changed and no new structure is formed. On the other hand, chemical reaction is the formation of a new compound with a new structure. Physical absorption is the least stable of all film-forming processes and amounts to an impregnation type of coating.

Above and beyond careful selection of the lubricant, it is essential to

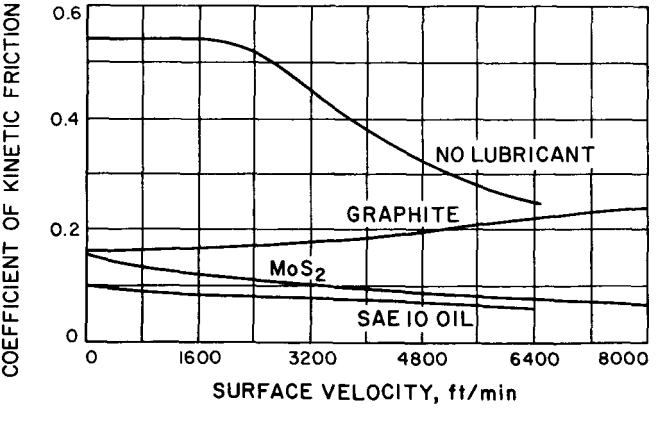

FIGURE 9.2—Effect of film lubricants on coefficient of friction for steel against steel, 1/8-in.-radius spherical rider. (From ref. 5.)

carefully consider the solid solubility of the metal combination. If metals which are poorly soluble in each other can be picked, a very poor weld will occur at the contact of the surfaces. Friction and wear will then be low, as the shear strength of the weld will be low, and adhesive wear will be minimized.

A great number of the bearings used in spacecraft are rolling-element bearings. Ball, roller, and needle bearings are the common forms of rolling-element bearings. The advantages of the rolling-element bearings are

(1) Low starting friction
(2) Low operating friction (increase in operating friction with speed is less than in a hydrodynamic bearing)
(3) The capability of supporting both axial and radial load in one bearing
(4) No elaborate lubrication system
(5) No tendency toward instability (fluid bearings can attain a resonant oscillation during which they cannot carry a load)
(6) Maintenance of accurate alinement because of the capability of having zero clearance

Considerable sliding takes place in a rolling-element bearing. The primary occurrence of sliding is between the rolling element itself and the separator or guide. The other source, which is very small in comparison, is between the rolling element and both the inner and outer races. In a ball bearing, for example, rolling actually takes place in only two lines of the contact ellipse, and the remainder of the area of the ellipse represents sliding. Because of this sliding, lubrication is extremely important even for a rolling-element bearing. The theory of friction and friction losses, stress, and fatigue in rolling-element bearings is very long and involved. Fortunately, the bearing industry has converted the critical parameters into bearing selection charts, which are provided for the design engineer.

Some of the important parameters of rolling-element bearing selection are inner-race contour, outer-race contour, separator design and material, race and ball material, the temperature range of the shaft and the housing in which the bearing is to be used, initial bearing clearance, preload, operating speed, operating load, and lubricant characteristics.

One of the problems in the high-speed application of a ball bearing is the generation and dissipation of heat. All of the factors which have just been listed influence the heat balance of the bearing. In addition to the friction between the ball and the separator, a great source of heat in high-speed bearings is the friction caused by ball spin. Ball spin is controlled by the race contour. A bearing can be selected for either inner-race control or outer-race control. This means that the

771-733 O-65-9

ball will roll on the controlling race and will spin on the other race at a speed which is a function of the contour of the races. In normal applications, inner-race ball control is used because it is usually easier to remove heat from the outer race than the inner, and because the velocity of the retainer is higher with respect to the inner race than with respect to the outer race. The significance of the latter point is that since the inner race will fail from fatigue before the outer anyway, it is desirable not to complicate the problem by adding ball spin heat.

At high speeds, centrifugal force will shift ball control to the outer race because of the high normal force. The transfer of control from race to race is undesirable, and the attitude usually taken in designing high-speed bearings is to join rather than fight; that is, put ball control at the outer race to begin with. Also, at high speeds, the gyroscopic forces on the balls will add to the moment, creating spin in very lightly loaded bearings. High-speed ball slippage is also a possibility. Thus, for certain high-speed light-load applications, a light bearing may be a better selection than a heavier bearing.

The load capacity of a bearing is dependent on the material. A Rockwell rating of 58 is usually considered the minimum hardness for the races and balls of a bearing. Both the operating load and the static load are directly affected by the material. The life of a bearing decreases by the cube of the load. Static load can also destroy a bearing, particularly in a vibration environment where the stress can go high enough to cause the race to yield, creating dents and ruining the bearing. The design of the separator and the selection of its materials is the most critical part of the bearing in terms of operating life up to the point of race fatigue. As mentioned previously, the separator will always fail first in a situation of inadequate lubrication of a bearing because a sliding interface with boundary lubrication exists. It has been found that bearings can be operated with no external lubrication if the separator is used as a reservoir of lubricant. This can be done by impregnation of plastics with solid lubricants or plating of metal separators with solid lubricants. The lubricant is transferred from the separator to the balls and then to the races.

Problems with bearings and lubricants in space arise from the following factors:

(1) The vacuum of space causes rapid evaporation of lubricants and prevents the formation of various beneficial films
(2) Radiation in space affects the stability of many common lubricants
(3) Zero gravity makes it difficult to control fluids
(4) Missions are long, and extreme reliability is required
(5) Weight is limited

The first factor is by far the most bothersome. The Langmuir equation which governs evaporation of materials is

$$G=\frac{P}{17.4}\sqrt{\frac{M}{T}}$$

where

G vaporization rate, gm/cm²-sec
P vapor pressure, $Ce^{-L/RT}$ where C, L, and R are constants
M molecular weight
T temperature, °K

If the ambient pressure is not zero, some of the vaporized particles return to the surface because of collisions with particles in the surrounding gas. As an approximation to this effect, it is sometimes considered that deviations from the Langmuir equation are appreciable at pressures above which the mean free path of the vaporized particles is of the order of the dimension of the evaporating surface or smaller. Since mean free paths are of the order of 10^{12} cm for pressures of 10^{-14} mm Hg, the Langmuir equation is quite accurate for the vacuum of space.

Table 9.1 shows evaporation rates in vacuum for various lubricants at 200 °F. The solid-film lubricants such as molybdenum disulfide and Teflon are less likely to evaporate in vacuum and are therefore preferred for use in space. Silicone oils and greases are less likely to evaporate than mineral oils and are adequate for most space uses. However, they have certain disadvantages, which will be discussed below.

The problems due to evaporation of coatings and lubricants are twofold. First, the evaporating material may condense upon other portions of the spacecraft such as optical equipment, switching contacts, solar panels, and temperature-control surfaces. Second, the surfaces may be left clean. Once the surfaces become clean or are wiped clean by abrasion, no oxides or other commonly found atmosphere-dependent contaminants will form. Figure 9.3 shows

TABLE 9.1—Evaporation rates in vacuum

Material	Evaporation rate, gm/cm²-sec
Mineral oil	10^{-6} to 10^{-7}
Mineral-oil-based grease	10^{-7}
Molybdenum disulfide	10^{-10}
Teflon	10^{-9}

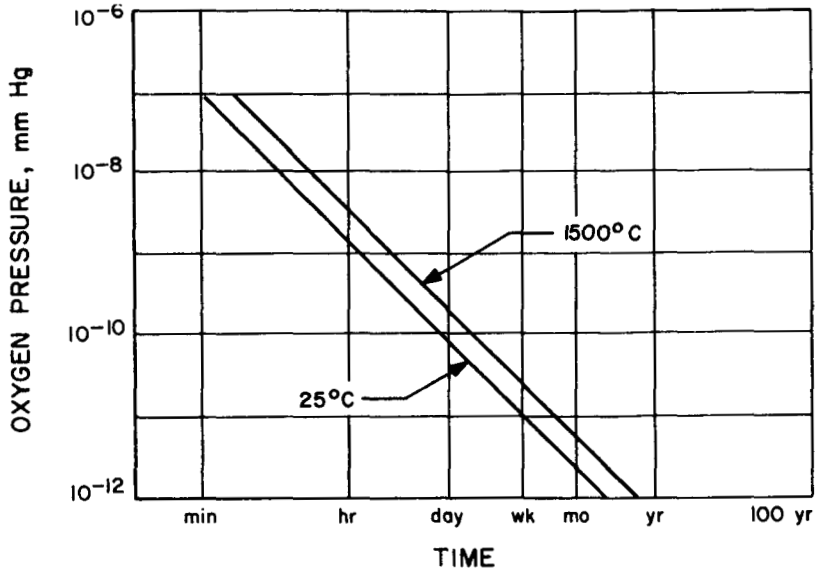

FIGURE 9.3—Time to form film of FeO one angstrom thick. (From ref. 6.)

the rate of formation of an oxide layer as a function of the oxygen pressure.

As bearing surfaces become clean, friction and wear increase markedly. Reference 3 discusses experiments which show that with thorough outgassing of specimens in vacuum at relatively high temperatures, friction coefficients increase by a factor of 10 or so. Figure 9.4 shows the results of an experiment with an iron-based alloy sliding on another piece of the same material in vacuum. As can be seen, after about 30 minutes the materials welded together so firmly that the drive motor was stalled.

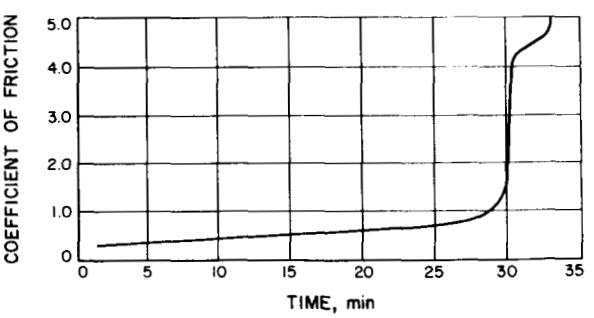

FIGURE 9.4—Coefficient of friction for 52100 steel sliding on 52100 steel in a 2×10^{-7} mm Hg vacuum. Sliding velocity, 390 ft/min; load, 1000 gm. (From ref. 7.)

TABLE 9.2—Properties of various spacecraft lubricants.

Name	Properties
General Electric Versilube F–50 oil.	A methyl chlorophenyl silicone lubricant Viscosity: 2500 centistokes at −65° F 52 centistokes at 100° F 16 centistokes at 210° F 2. 3 centistokes at 600° F Pour point: −100° F maximum Flash point: 500° F minimum Weight loss in vacuum: 0.34 percent Lubricity (4 ball): 0.53 mm wear scar at 77° F, 600 rpm, 1 hr, 50-kg load
General Electric Versilube G–300 grease.	Versilube F–50 oil with a lithium soap thickener. Designed for operation over −100° F to 450° F. Weight loss in vacuum is 3.0 percent.
Electrofilm 4306	A molybdenum disulfide solid-film lubricant. Good between −300° F and 600° F. Excellent vacuum storage characteristics. Used either alone or in conjunction with oils and greases; coefficient of friction as low as 0.05 with 0.26-ft minimum speed; steel shaft rotating against steel block. Good for 100 to 200 hr before failure. Usual coefficients of friction are 0.09 to 0.12.
Teflon	A soft and tough thermoplastic melting at 620° F. Stable and inert. Coefficients of friction of about 0.04 obtainable; coefficients as low as 0.016 observed. Good resistance to wear.

Success of bearings in space depends upon proper design of the bearing for the load and application, and a lubricant-sealing combination which will guarantee adequate lubrication of the bearing. Rolling-element bearings, and even sleeve bearings, can be run dry in a vacuum for a short time. However, bearing performance is so markedly increased by applying film lubrication that it is foolish not to lubricate.

If the bearing is to operate only during or shortly after launch and evaporating lubricant is not a contamination problem, conventional oils and greases can be utilized in conjunction with an unsealed system, since the oils will not evaporate completely during a few minutes or even hours in space. A rolling-element bearing containing seals will confine lubricants for some time, as leakage through an orifice is quite slow at very low pressures. If the bearing is expected to operate for long periods of time (months or years) after launch, it is necessary to use extremely stable lubricants or sealed systems,

or both. Spacecraft mechanisms make use of sealed and sometimes pressurized areas whenever practical. Silicone oils and greases and vacuum-refined hydrocarbon oils and greases are frequently used even though they are not as good lubricants as hydrocarbon oils and greases. Teflon is used quite widely, as well as such dry lubricants as molybdenum disulfide and plated soft metals. Mechanism designers frequently use a belt-and-suspenders approach, such as dry-lubing parts and then lubricating them with a low-vapor-pressure oil in a sealed case. Table 9.2 shows properties for a few lubricants which are typical of those used in spacecraft application.

REFERENCES

1. Bisson, E. E., and Anderson, W. J.: *Advanced Bearing Technology.* NASA SP–38, 1964.
2. Bowden, F. P., and Tabor, D.: *The Friction and Lubrication of Solids.* Oxford Univ. Press (London), 1954.
3. Burwell, J. T.: "Survey of Possible Wear Mechanisms." *Wear,* vol. 1, no. 2, Oct. 1957, pp. 119–141.
4. Johnson, R. L.; Swikert, M. A.; and Bailey, J. M.: *Wear of Typical Carbon-Base Sliding Seal Materials at Temperatures to 700° F.* NACA TN 3595, 1956.
5. Johnson, R. L.; Godfrey, D.; and Bisson, E. E.: *Friction of Solid Films on Steel at High Sliding Velocities.* NACA TN 1578, 1948.
6. Atkins, J. H.; Bisplinghoff, R. L.; Ham, J. L.; Jackson, E. G.; and Simons, J. C.: *Effects of Space Environment on Materials.* Research Project 40–1–041, National Research Corp., Aug. 15, 1960.
7. Buckley, O. H.; Swikert, M. A.; and Johnson, R. L.: "Friction, Wear, and Evaporation Rates of Various Materials in Vacuum to 10^{-7} mm Hg. *Trans. Am. Soc. Lubrication Eng.,* vol. 5, no. 1, Apr. 1962, pp. 8–23.

CHAPTER 10

Spacecraft Mechanisms

THIS CHAPTER contains illustrations of a few typical spacecraft mechanisms, with brief descriptions included where pertinent.

Pyrotechnic devices are an excellent method of obtaining strong, easily timed, and reliable one-time actuations. Figure 10.1 shows a pyrotechnic pinpuller, perhaps the most widely used of all space mechanisms. It weighs 0.21 lb complete with squibs and is the type used on the Mariner class spacecraft. It is a piston in a cylinder, which is actuated by gas from the ignition of small explosive squibs (two squibs are used to insure actuation). The squibs are ignited by a current pulse which is fed through either a hot bridge wire or an exploding bridge wire. This bridge wire then ignites the squib charge. The pinpuller contains a motion sensor which signals the end of the piston stroke.

Figure 10.2 is a sealed-drive mechanism developed by Space Technology Laboratories (STL). All rolling and sliding surfaces of the motor, gearhead, gears, and bearings (except the final output gear and bearing) are hermetically sealed in a pressurized volume. The output gears are specially cut wobble gears. The driving gear contains 100 teeth and the driven gear 99 teeth. One rotation of the driving gear will therefore result in a 1/100th rotation of the driven gear. The driving gear wobbles instead of rotating and is attached permanently to the sealing bellows. It is driven by a motor, a gear reducer, and a tilted bearing inside the bellows. The unit was designed for driving the OGO panels and has an output rate of 1 deg/sec with a torque capability of 100 in.-lb. The gear reduction from the motor is 23 760 to 1. The unit is 7.25 in. long, 5.25 in. in diameter, weighs 5 lb, and is made of stainless steel, aluminum, and sintered bronze. The motor is a size 11, two-phase, 115-V, 400-cycle sealed servomotor.

Figure 10.3 is an exploded view of the solar-panel deployment mechanism of the Ranger spacecraft. This actuator contains a compression spring to provide the deployment force and a dashpot to limit the deployment rate. It weighs 1.15 lb and provides a force ranging from 160 to 30 lb over a travel of 3⅜ in. It requires about 45 sec to complete its stroke at 77° F. The actuator is 9¼ in. from pin to pin when closed. At the top of figure 10.3, the actuator is shown

completely assembled. It consists of two concentric cylinders which load the spring when placed together. One output bearing is attached to one tube, and the other tube is attached to the damping piston shown in the lower right-hand corner which is attached to the other output bearing. This piston contains a differential valve that provides a large orifice for cocking the actuator and a small orifice for damping the action stroke. The other piston shown in figure 10.3 merely compensates for the change in effective cylinder volume as the actuator extends. Sealing is done with O-rings. The actuator is

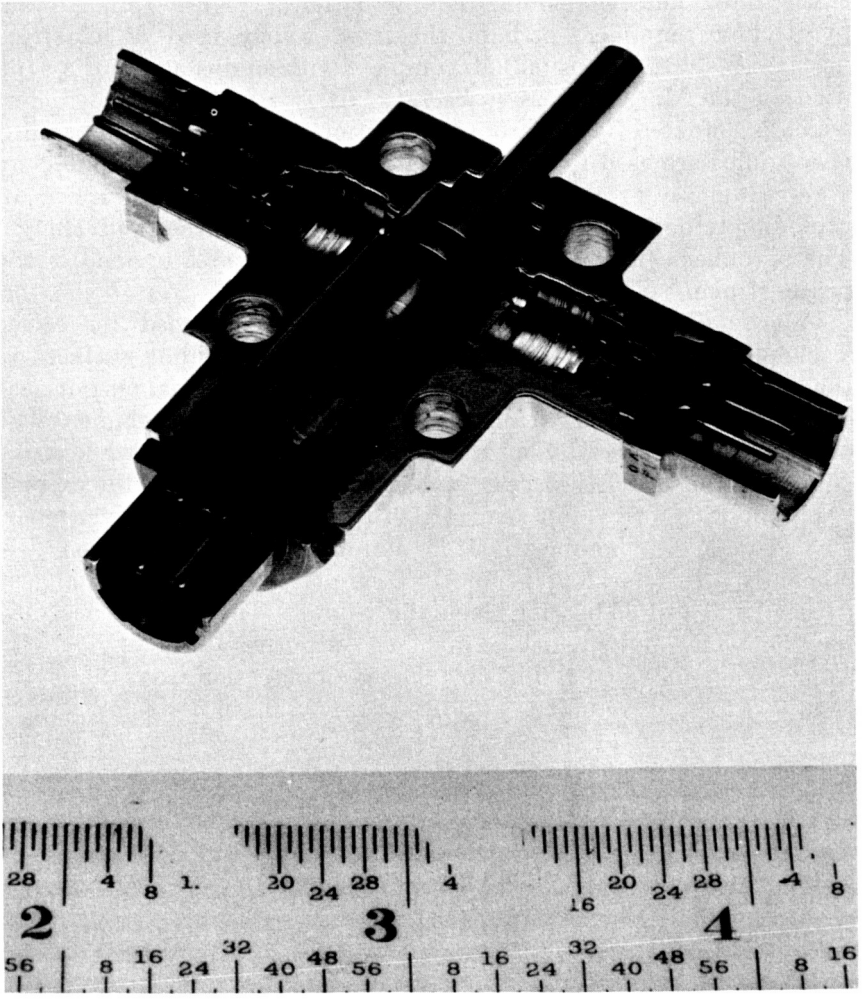

FIGURE 10.1—Pyrotechnic pinpuller. (JPL photograph.)

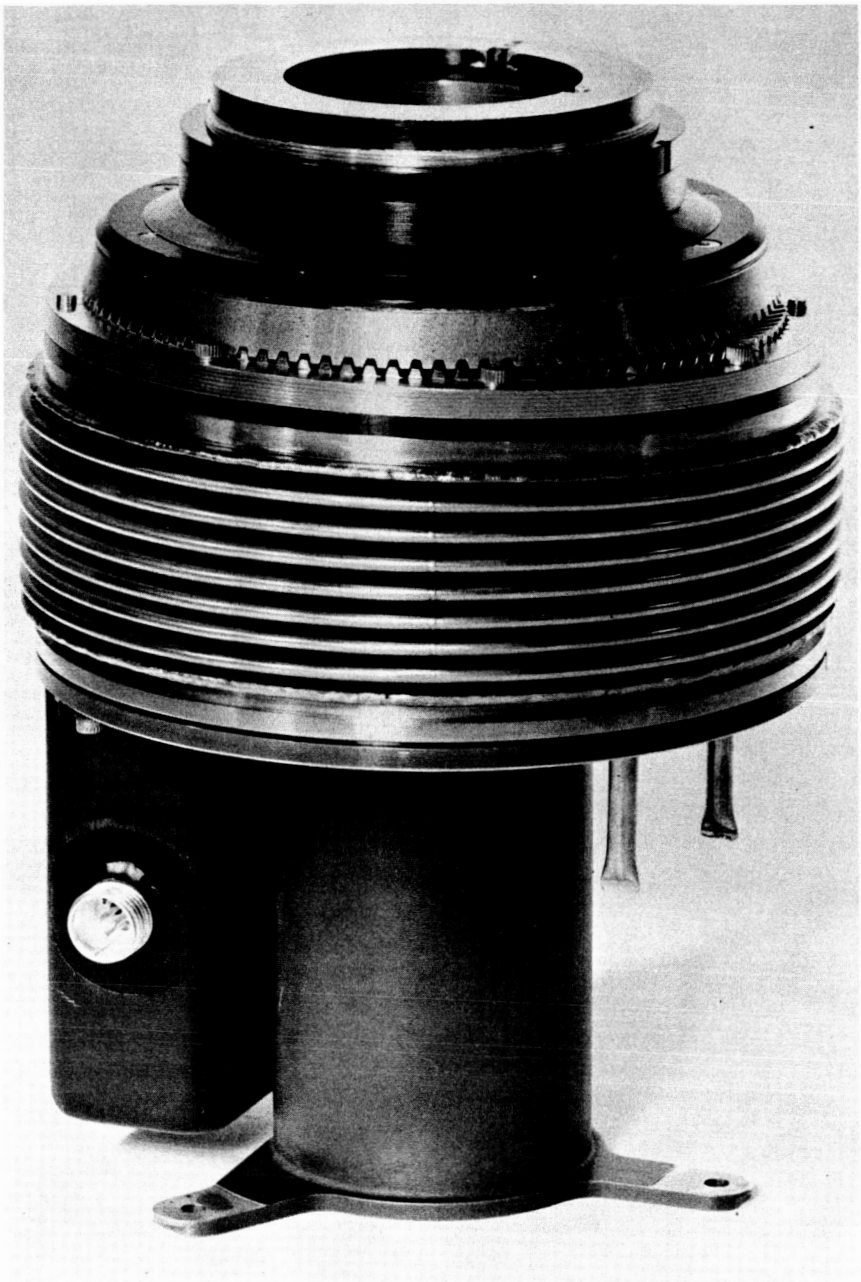

FIGURE 10.2—STL wobble-gear drive mechanism. (STL photograph.)

filled with silicone oil. The actuator parts are fabricated mainly from either 7075–T6 or 2024–T4 aluminum. The springs are of 17–7PH stainless steel and the piston rod is of 4130 steel.

Figures 10.4 and 10.5 show the hydraulic timer on the Ranger and Mariner Mars spacecraft. This timer is essentially a spring-loaded dashpot and is used to actuate various mechanical switches. The device is used both as a backup timer for the electronic sequencing unit and as a primary timer for certain less critical events. Figure 10.4 shows the parts of the piston. The purpose of the bellows is to compensate for the effective change in cylinder volume as the piston travels through its stroke. The object nearest the ruler in the figure is a capillary tube (0.050-in. diameter by 0.006-in. wall thickness typical) which is wrapped around the spool shown directly above it. The sleeve is then placed over the spool and the tube to form the piston. One end of the capillary opens within the sleeve, the other at the end of the piston. The semirectangular parts are the spring and washer of a flapper valve, which opens a large orifice to permit

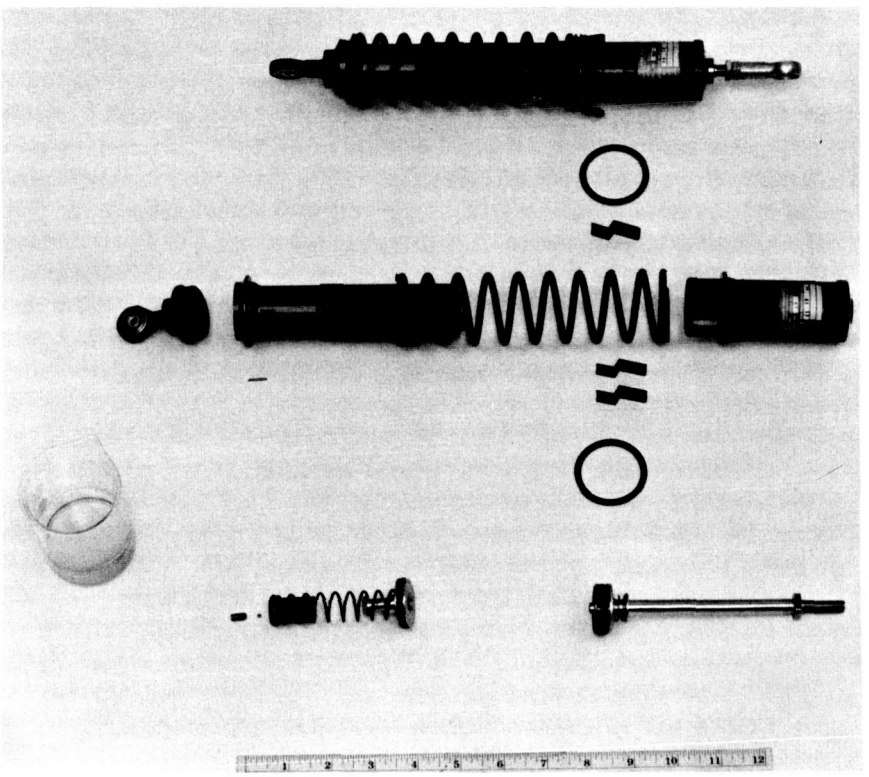

FIGURE 10.3—*Ranger solar-panel actuator.* (JPL photograph.)

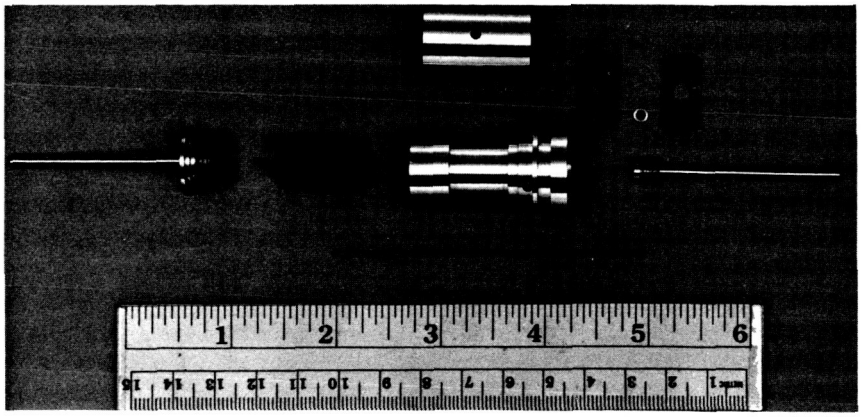

FIGURE 10.4—Hydraulic-timer piston. (JPL photograph.)

easy cocking of the timer. The two rods attach to the opposite ends of the piston.

Figure 10.5 shows the assembled piston and spring and the cylinder and end plates into which they fit. The timer operates because the spring forces silicone oil at a controlled rate through the orifice tube. By changing the spring constant, the orifice dimensions, and the oil

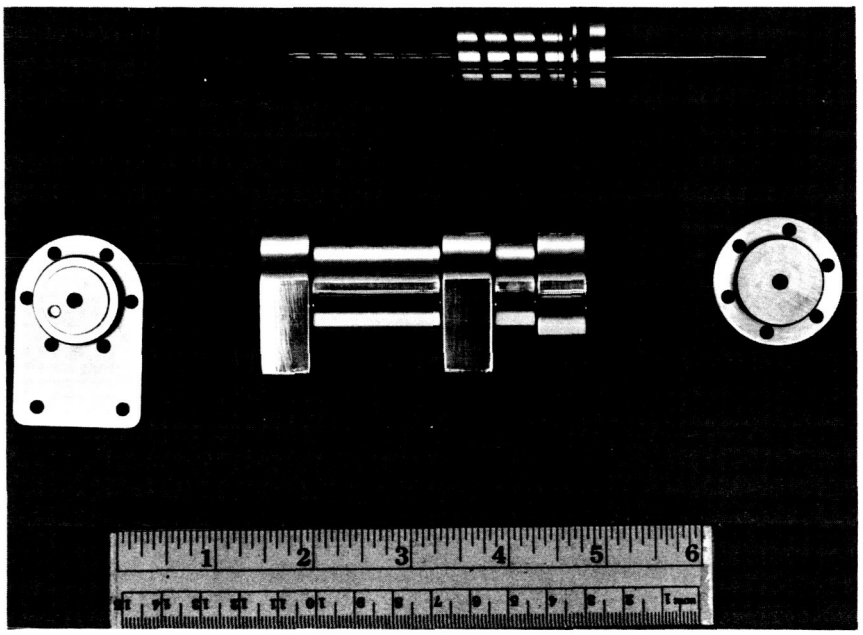

FIGURE 10.5—Hydraulic timer. (JPL photograph.)

viscosity, the timer rate can be changed to suit the application. The version used in the Ranger spacecraft travels 1.17 in. in an hour at 70° F. It weighs 0.5 lb loaded with oil. The majority of the timer parts are fabricated from 2024 aluminum. The springs are of beryllium copper.

Figure 10.6 shows an extending boom which was developed for positioning a magnetometer and a radiation experiment at a distance from an early Mariner spacecraft. The boom in the telescoped configuration was constrained to fit in a given small volume and survive the launch environment. In its extended configuration it was to position the experiments in a known orientation and be sufficiently rigid to avoid degrading the autopilot stability. The initial boom design incorporated six stages and was 4 ft long closed and 26 ft long extended. The outside diameter of the outside tube was 3¼ in. and the inside diameter of the inside tube was 1$\frac{1}{16}$ in. The wall thickness of the tubing was 0.30 in. The completed boom weighed 7 lb, and the instruments supported weighed approximately 1½ lb. A flat, reel-wound cable weighing 2 lb provided electrical connections with the instruments.

The boom sections were keyed to prevent rotation with respect to each other. The tubing sections, including the external key, were longitudinally milled to shape. The keyway was contained in the threaded tubing end fittings. Each section of tubing was guided by nylon inserts in the end fitting of the next larger section. Teflon lip seals were provided on the outside of the opposite tubing ends to provide sealing between sections. The telescoped boom was held together by a sear, which engaged the inner tube. The inner tube was in tension and the outer in compression. The intermediate tubes were loaded against their seals. The tube was extended by a single

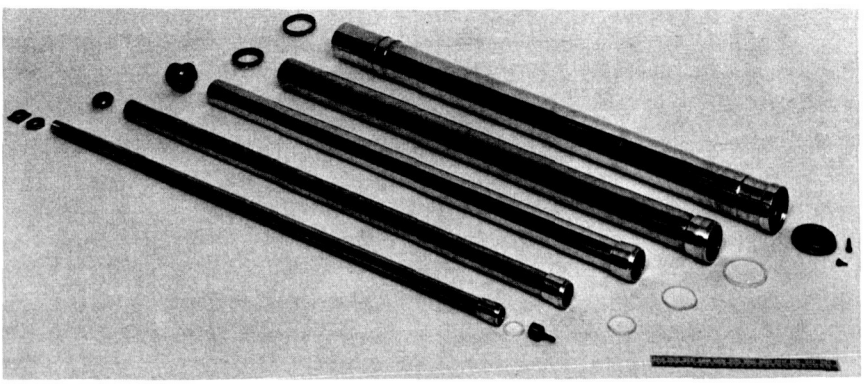

FIGURE 10.6—Extending instrument boom. (JPL photograph.)

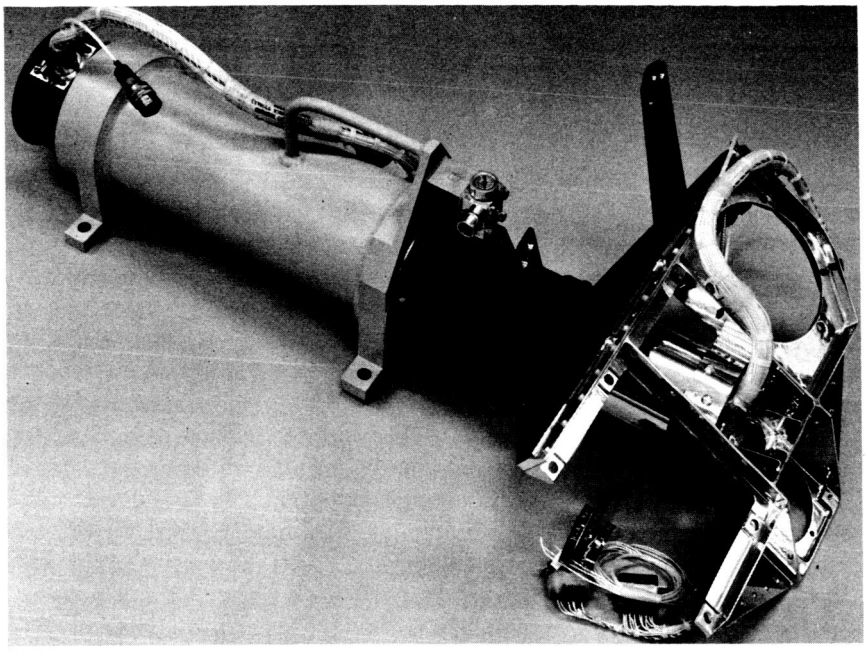

FIGURE 10.7—Mariner Mars planetary scan platform. (JPL photograph.)

command, which released the latch and opened a 1-in^3, 2000-lb/in^2 nitrogen storage chamber. The nitrogen was throttled through a 0.010-in. orifice. The final pressure inside the boom when extended was about 2 lb/in^2. The boom extended in about 5 sec and was locked in the extended position by locking tapers.

The boom shown in figure 10.6 is a later modification. Because of an increase in autopilot sensitivity and a spacecraft center-of-gravity problem, it was necessary to shorten and stiffen the boom. The tubing wall thickness was doubled, the extended length was shortened to 18 ft, and the boom weight was increased to 10 lb. The resulting resonant frequency of the boom was 2.2 cps.

Figure 10.7 shows the Mariner Mars planetary scan platform. The structure weighs 3.04 lb and is roughly 3 ft long. The light-colored painted cylinder in the photograph is a holding fixture and is not included in the structure weight. The platform rotates and holds a television experiment, a wide-angle Mars sensor (for planet acquisition), and a narrow-angle Mars sensor (for planetary scan). The structure is made of 6061–T6 aluminum. A 75-conductor cable runs from the platform up the inside of the tube to the upper end. The tube rotates on Dyflon bushings which are at the two ends of the holding fixture in figure 10.7.

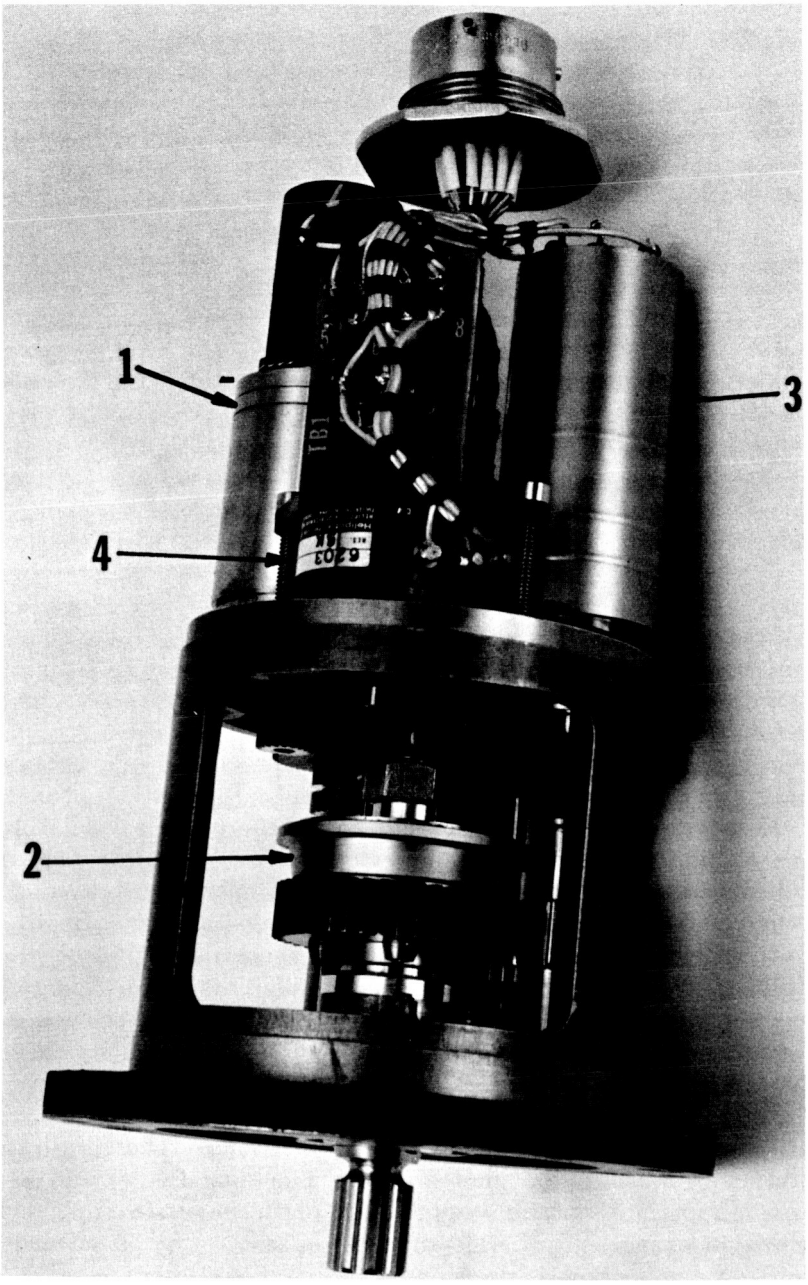

FIGURE 10.8—Mariner Mars planetary scan drive. (JPL photograph.)

Figure 10.8 shows the drive which turns the scan platform shown in figure 10.7. This device (fig. 10.8) weighs 2 lb and uses a 26-V, 400-cps, 8000-rpm synchronous servomotor to produce an output of ½ deg/sec. Limit switches control the rotation of the output to 180°. The gearhead (1) attached to the motor provides a 1000:1 reduction. The remaining gear train provides an additional 100:1 reduction. An overload clutch (2) prevents damage due to unexpected overloads or binding. This clutch uses small balls which act as cams to exert force against the spring-loaded pressure plate. If torque exceeds a preset amount, the cams force the pressure plate away from the driven plate. A pressure transducer (3) modifies a 6-V input by means of a sliding potentiometer in order that the pressure inside the sealed and pressurized case may be monitored. A potentiometer (4), geared directly to the output, transmits a signal proportional to output position. The gears in the output gear train are alternately made from electrofilmed 303 stainless steel and anodized 2024 nickel-plated aluminum. They are lubricated with small amounts of F–50 silicone oil. Maximum use is therefore made of dissimilar metals, film lubrication, and fluid lubrication. Phenolic separators are used in the rolling-element bearings and are impregnated with F–50 silicone oil. The body of the drive is machined from AZ–60 magnesium. Dyflon bear-

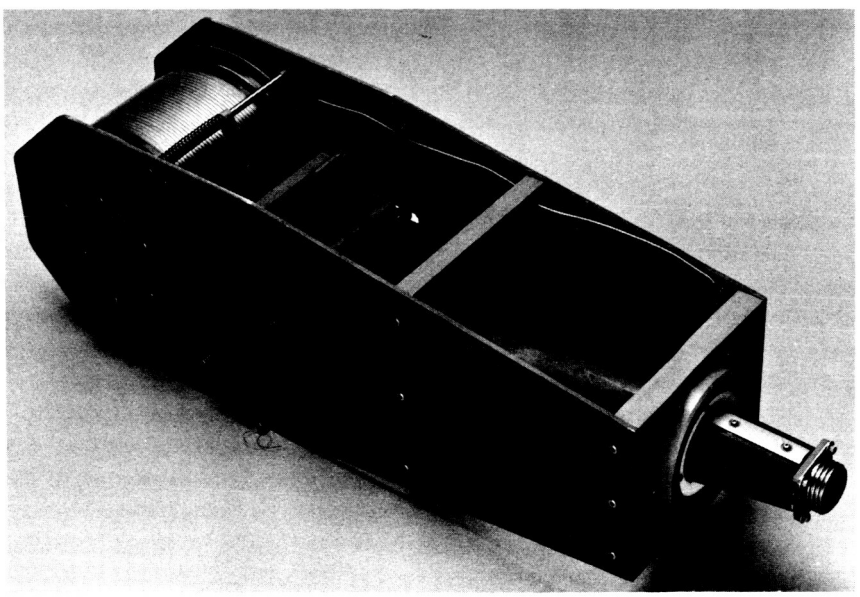

FIGURE 10.9—Erectable de Havilland boom. (JPL photograph.)

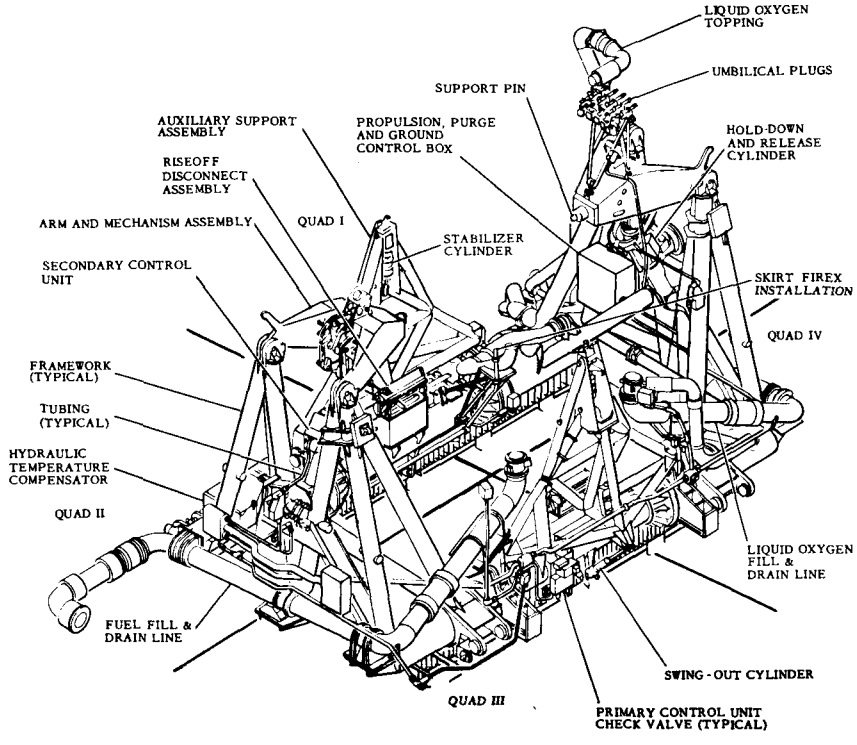

FIGURE 10.10—Overall view of missile launcher. (Courtesy of General Dynamics Astronautics.)

ings are used in the output and in the clutch. A can fits over the completed unit and is pressurized with dry nitrogen.

Figure 10.9 shows an erectable de Havilland boom. This boom is made from a strip of beryllium copper which is first heat treated in a tubular shape. The strip is then flattened and rolled up in the orthogonal direction. This is done with no plastic deformation. The roll of copper strip, including a printed flat cable harness, is shown in a deployment fixture in figure 10.9. It is allowed to unroll through a flat-to-round section. The boom, which assumes a tubular shape naturally due to its initial forming, emerges from the round opening at the end of the fixture. It has good stiffness because of its tubular shape. However, it is not torsionally stiff unless the tube section is closed by some mechanical means. It has a very large ratio of extended length to stored volume. The device shown extends a boom 20 ft long and 1½ in. in diameter. The boom itself weighs 1½ lb and the deployment device weighs 7 lb (no effort was made to minimize the deployment weight). The boom was rolled around a 5-in.-diameter

spool. It is apparent that an extremely long boom which would be stiff enough to position instruments under the low accelerations encountered in space could be placed in a very small volume for launch.

Figure 10.10 shows the launching mechanism for the Atlas booster. This launcher is made of heavy-walled welded tubing. It is approximately 22 ft long, 16 ft high, and 16 ft wide, and weighs about 30 tons. The Atlas booster rests upon the support pins on the pivoted wishbones at each end. It is stabilized by the support assemblies at either side. By pressurizing the two release cylinders with air, it is possible to restrain the Atlas from rising with the engines at full thrust. For launching, the pressure in the release cylinders is vented at a controlled rate and the booster is allowed to rise. After approximately 6 in. of rise, the launcher no longer restrains the booster and the support pins begin to retract. In an additional 2 in., the pins are retracted and the booster is free. The launcher contains hydraulic, pneumatic, and mechanical elements. It supports the booster during erection and pad checkout and static tests. It restrains the missile until an optimum thrust value is achieved and then releases it in a controlled manner.

771-733 O-65-10

CHAPTER 11

Electronic Packaging

A SPACECRAFT is an electromechanical system. By many yardsticks, it is more electrical than mechanical. In a sense, the nonelectrical portions of the spacecraft form an extremely sophisticated chassis. The 1964 Mariner Mars spacecraft contains 37 700 electrical components, as opposed to a few hundred components in the average television set. The components are listed by type in table 11.1. Of the total spacecraft weight of 585 lb approximately 210 lb is electrical equipment.

The electrical system of a spacecraft may typically perform the following functions:

(1) Regulate and distribute the output from the solar cells, battery, or whatever the source of raw electrical power may be
(2) Collect and process the signals from sensors in the instruments and throughout the spacecraft
(3) Feed the converted, commutated, and encoded data into the communication system, which impresses it upon an RF signal and transmits it to Earth
(4) Receive and decode command signals from the Earth and route them to the proper users
(5) Store data for predetermined periods of time
(6) Sequence events and initiate the actuators which perform the events
(7) Stabilize the spacecraft during rocket burning and sense spacecraft attitude
(8) Provide power for electromechanical devices which perform various spacecraft functions

The integration of the electrical system with the mechanical portion of the spacecraft is called electronic packaging. This is sometimes referred to as product engineering. It may be performed by officially recognized packaging engineers, smuggled by mechanical design groups, or done by mechanical engineers working in electrical design groups. Electronic packaging is the process of converting circuit designs into hardware.

The reason for the existence of packaging engineers is that electrical failures can usually be traced to a mechanical failure mode. A part

TABLE 11.1—Mariner-Mars electrical components.

Component	Total no.	Types
Resistors	13 567	28
Capacitors	4 619	49
Inductors	56	31
Transformers	333	71
Chokes	48	15
Connectors	386	8
Cores	2 712	2
Relays	95	13
Crystals	10	4
Cells	1	1
Controlled switch	1	1
Magnetic amp	2	2
Fuses	12	2
Tubes	3	2
Thermistors	7	5
Transducers	18	6
Switches	47	5
Filters	2	2
Coils	136	5
Amplifier	1	1
Sensistor	3	2
Delay line	1	1
Lamp	4	1
Photocell	4	1
Diodes	8 809	120
Transistors	3 711	105

burns out because it generates more heat than can be dissipated; a dielectric breaks down because of a mechanical flaw; or a component, insulator, or joint breaks during mechanical vibration or shock. In order for electrical equipment to be rugged, reliable, and predictable, the hardware must be engineered mechanically as well as electrically. There is presently a shortage of electrical engineers who understand mechanical problems and of mechanical engineers with a good feel for electrical problems. Packaging engineers fill the gap.

Packaging engineers are usually mechanically trained. They realize the limitations of mechanical design, the need for simple and efficient structure, the need for understanding the thermal environment, and the unpredictable nature of materials, processes, and hardware. However, they also realize the complexity of electrical equipment, the need for flexibility, and the problems of circuit development and component reliability.

Because of the nature and number of the variables, the many interests represented, and the necessary emphasis upon such factors as producibility and electrical testability, packaging is as much an art as it is a science. However, it is an extremely technical art which requires a good understanding of many phases of engineering, experience with a variety of electrical and mechanical hardware, and enough overall perspective to be able to define the proper balance between electrical, mechanical, and operational considerations.

Packaging problems invariably result in compromises. Some of the characteristics of packaging which may or may not be competing are

(1) Weight
(2) Volume
(3) Usable electric area or volume
(4) Compatibility with spacecraft configuration
(5) Static structural load capability
(6) Dynamic characteristics (resonant frequency and amplitude)
(7) Ease and speed of fabrication (cost)
(8) Thermal conductivity
(9) Compatibility with spacecraft thermal system
(10) Standardization
(11) Ease of modification
(12) Ease of repair
(13) Ease of replacement
(14) Ease of test (bench and systems)
(15) Compatibility with electrical components
(16) Technical sophistication
(17) Reliability

It is obviously not possible to achieve any single simple solution which will optimize all characteristics. The existence of numerous solutions to the problem can be seen by looking at packaging schemes used by different organizations in the spacecraft and missile business. This will be done in the next chapter. The remainder of this chapter will consist of a brief discussion of packaging details. The discussion will begin with the smaller details and proceed to the larger.

THE COMPONENT

The electrical component has traditionally been the smallest building block used by the packaging engineer. For use in spacecraft, great care must be taken to insure that the components are properly designed, are properly used, and are inherently extremely reliable. Schedule, cost, and reliability considerations usually favor the use of an available, familiar component if possible. However, the usual commercial component is far from adequate for spacecraft use.

Spacecraft components are built to high reliability specifications which insure the best in materials and assembly techniques. Rigid inspection criteria are imposed. The end products are then carefully tested. Any component deviating from the norm to a significant degree is rejected. To minimize "infant mortalities" (early failures due to invisible flaws) many components are "burned in" for several hundred hours. Frequently components are assigned serial numbers and a case history is kept on each component. Extreme precautions are taken to avoid physical damage to the component during handling.

Since the development of the transistor, it has become increasingly difficult for the packaging engineer to define components and thus cleanly define where his responsibility begins. Before the "solid-state age," circuit designers used resistors, capacitors, inductors, transformers, relays, rectifiers, tubes, and other familiar elements. With the advent of transistors and solid-state diodes, circuit design was altered both electrically and physically. The small size of solid-state components plus the technology which evolved from the fabrication of these components led to what is generally called "microminiature circuitry." The parallel emphasis on digital circuitry led to the use and fabrication of functional blocks which could be purchased like components but which perform much more complex tasks.

Microcircuitry began as dense packaging of solid-state active (amplifying) and passive (nonamplifying) components. Concepts such as "tinker-toy" and "micromodule" combined small discrete transistors, diodes, inductors, and capacitors, with "printed" resistors and interconnect paths. The "printing" was done with conductive inks and epoxies either by plating and etching, evaporative deposition, or silk-screening. Present day "micromin" concepts can be broken into three categories: integrated circuits, deposited (thin film) circuits, and hybrid circuits.

Integrated circuits are functional circuit elements (flip-flops, amplifiers, gates, etc.) which are formed from a single chip of active base material. Transistors (including solid-state diodes) are formed from a small chip of a semiconductor such as silicon or germanium by successive processes of masking, etching, and diffusing. By slightly complicating the processes and the masks, it is possible to fabricate several transistors on the same semiconductor chip. Resistances may be obtained either by using the inherent resistance of the semiconductor or by depositing resistive material on the chip. Capacitance may be obtained either by using the capacitance of the chip or by plating on successive layers of conductor and dielectric.

The values of resistance and capacitance available with this technique are naturally limited. However, they are sufficient for most digital functional elements. With the present rate of progress in

integrated circuits, many analog devices should soon become available. These circuits offer an intuitive (not yet proven by usage) increase in reliability since several transistors created in the same series of processes should be more reliable than several discrete transistors created in separate series of processes. The Minuteman project has for some time set the pace in component reliability and is now investing heavily in integrated circuits. Within a few years, the use of integrated circuits in space should be quite common.

The transistors, diodes, resistors, and capacitors in integrated circuits are interconnected by circuit paths which are deposited during the process of building the circuit. The chip is then placed in a package and leads are attached and brought through the case. Figure 11.1 is an enlarged photograph of a chip inside a package. The package actually measures ¼ in. by ⅛ in. by 1/32 in. without the leads. Although these packages contain many components in the traditional sense of the word, they can be considered a single component in that they are made by specialty fabrication house and delivered sealed in cases.

The task of defining the component is even more difficult in the case of deposited circuitry. Figure 11.2 shows a deposited circuit from a Bell Telephone Laboratories commercial digital arithmetic unit. The circuit is placed upon a glass substrate which is 1.7 in. by 3 in. by 0.060 in. thick. Conductors, resistors, and layered capacitors are fabricated upon the surface of the glass by successive vacuum depositions through masks and photoetching processes. Active devices are added as discrete components. This approach to microcircuitry offers much more flexibility to the circuit designer than integrated circuits since the circuit designer has more latitude to select circuit parameters. Since physical dimensions are larger, fabrication of the passive elements is not as critical. However, no one has yet succeeded in depositing a satisfactory, stable, solid-state active device. Many companies have come close, and those in the field are sure that deposited active devices will be developed within a few years. However, until that time, deposited circuits must be used in conjunction with discrete active devices.

Hybrid microcircuits are very popular as they permit the designer to take advantage of the good features of the various forms of micromin. The circuit shown in figure 11.2 is properly a hybrid circuit since it combines discrete components with deposited circuitry. Similarly, integrated circuits may be used in conjunction with discrete components to provide larger parameter values than those obtainable within the integrated circuit. Microminiature discrete components, such as microdiodes or uncased transistors, may be used in conjunction with deposited resistor-capacitor networks. Microcircuits

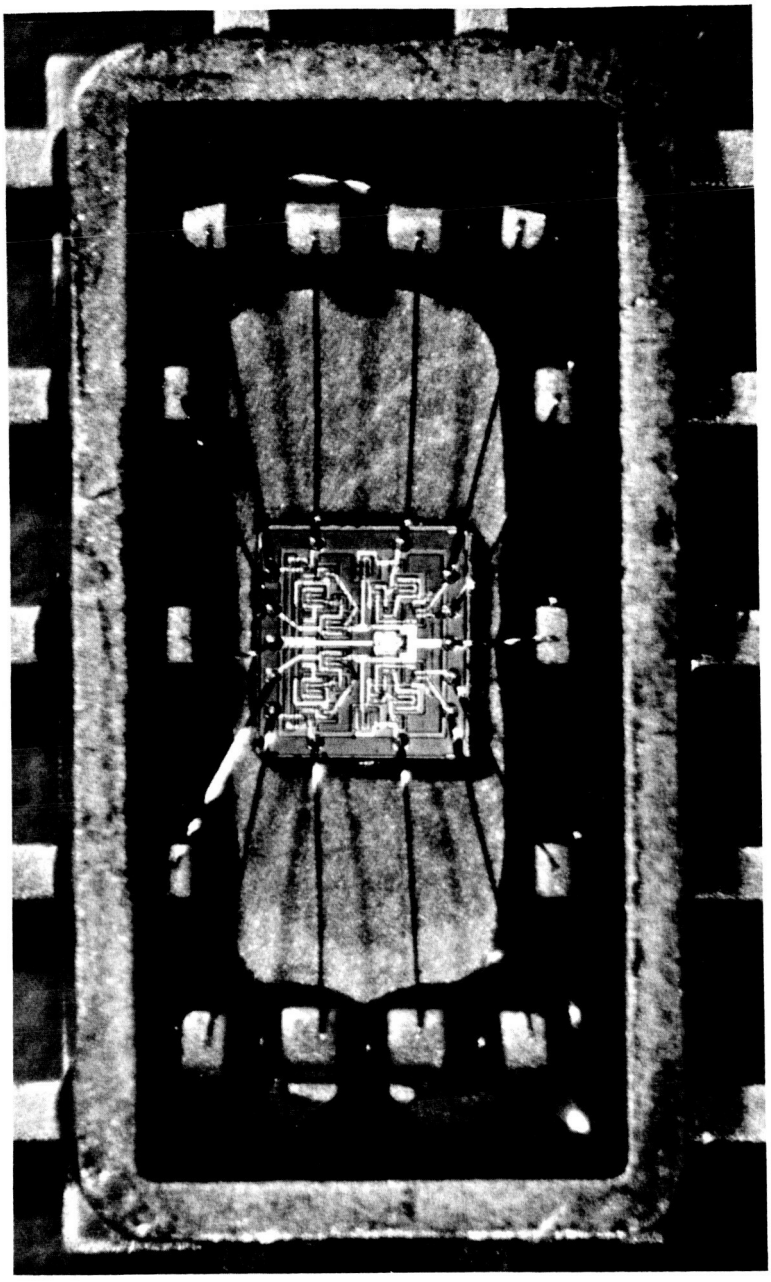

FIGURE 11.1—Integrated circuit. Replaces seven transitors, seven diodes, three resistors, two capacitors, and six resistor-capacitor combinations. Manufactured by Texas Instruments. (Texas Instruments photograph.)

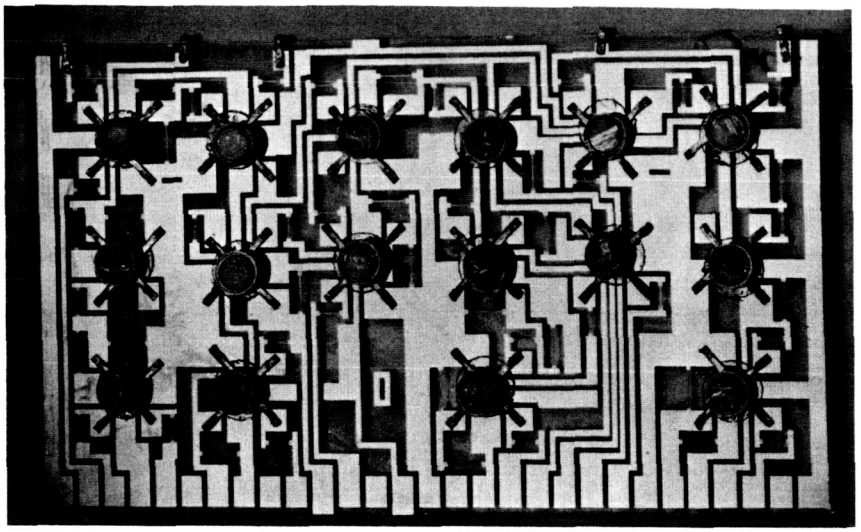

FIGURE 11.2—Thin film deposited circuit. Contains approximately 50 resistors. Manufactured by Bell Telephone Laboratories. (BTL photograph, from ref. 1.)

may also be included in conventional soldered or welded circuitry. In hybrid microcircuits, the packaging engineer sometimes considers a functional element as a component, sometimes as a group of components.

INTERCONNECTS AND COMPONENT MOUNTING

Components are selected for electrical function, ruggedness, and reliability. The packaging engineer must interconnect the components so that they perform the circuit function. He must also mount the components so that they operate as comfortably as possible in the spacecraft environment. The components must be protected against harmful vibration and shock inputs. In certain cases, they must be shielded or insulated for electrical reasons. They must be protected against stray chips, handling damage, and test and repair operations. They must be provided with sufficient heat path so that dissipated heat can be rejected.

Figures 11.3, 11.4, 11.5, 11.6, and 11.7 show a few methods of interconnecting and mounting components. Depending upon such factors as weight, fragility, heat dissipation, and lead geometry, components may be either supported by their leads, bonded or clamped to a metal chassis or heat sink, bonded or clamped to an interconnect board, or potted into modules. The method shown in figure 11.3 is the "classical" one used in older hand-wired radios. It is well

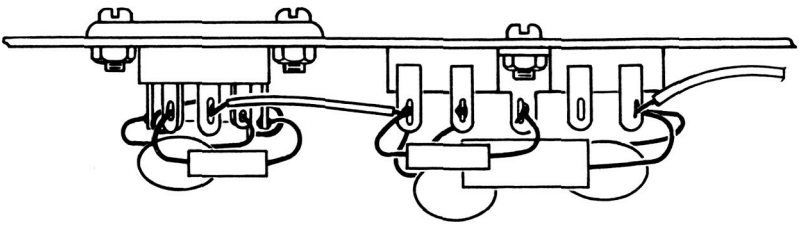

FIGURE 11.3—Terminal strip interconnection.

suited for large components, tubes with large heat dissipation, simple modification and repair, and cheap, conscientious labor. However, as components and assemblies become subject to more severe volume and weight restrictions, this form of interconnection becomes less attractive. It is also rather difficult to control in a dynamic environment such as that encountered in a spacecraft launch.

Figure 11.4 shows the technique used by the Jet Propulsion Laboratory (JPL) in the Ranger and Mariner II Venus spacecraft. Interconnection is by means of etched circuit boards made from copper-clad epoxy-fiber-glass laminated boards by photoetching. Terminals are swaged and soldered into holes through the boards and the conductor and the components are soldered to the terminals. The assembly is then coated for additional protection. The interconnect board is bonded to a metal chassis which provides the necessary structure and heat sink.

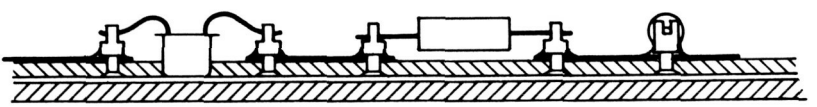

FIGURE 11.4—Printed circuit board with terminals.

The printed circuit board is much more controllable and consistent than hand-wired interconnections. It also provides component mountings which are controlled and easily accessible. Circuits can be easily inspected after assembly and tested, modified, and repaired if necessary. However, a single-layer circuit board is limited to one or two layers of interconnect paths, which effectively restrict the possible component density.

Figure 11.5 illustrates a very common technique used both in spacecraft and in commercial high-production manufacturing. Instead of providing terminals to connect to components, a hole is drilled and copper is plated onto the sides of the hole so as to intimately contact the copper conducting surface. The leads of the component are then bent down through the holes, and the bottom of

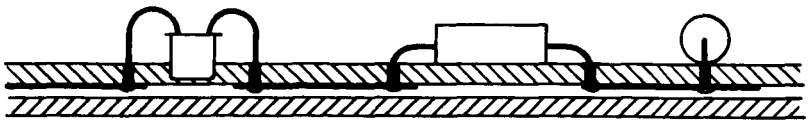

FIGURE 11.5—Mass-soldered interconnection.

the board is either dipped in a vat of molten solder or passed through a wave of molten solder formed by a fountain in a soldering pot. The advantage is that a great number of solder joints can be made simultaneously in one operation. The question of whether a large number of handmade solder joints is more or less reliable than a large number of solder joints made in one dip is a classic packaging debate.

Figure 11.6 shows a method of interconnecting and mounting components that is being used in present spacecraft. The components are assembled in functional blocks as follows:

(1) Functional elements are laid out on paper with the components stacked like cordwood so that the leads can be interconnected in one or more planes at the ends of the components
(2) The drawings are photoreduced to actual size and printed on Mylar
(3) Holes are punched in the Mylar for component leads and the components are placed between two layers of Mylar
(4) Interconnections are made according to the lines on the Mylar by resistance welding a conductor (usually nickel ribbon) to the various leads
(5) All leads except those for inputs and outputs to the module are trimmed and the module is encapsulated in plastic

The functional blocks may be interconnected as components. In the method shown in figure 11.6, a matrix is welded from wire and ribbon. The matrix is made up in several layers using printed Mylar. It is then encapsulated to form a protected structural interconnect. In this manner it is possible to incorporate a large amount of inter-

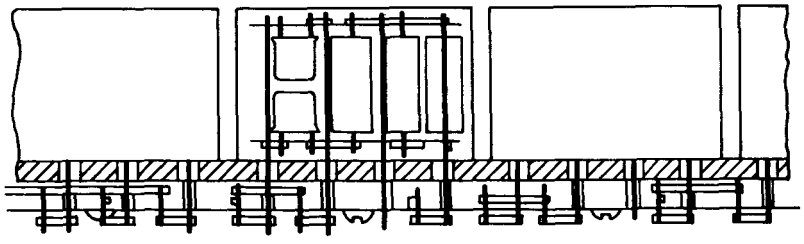

FIGURE 11.6—Welded cordwood interconnection.

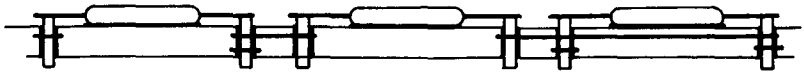

FIGURE 11.7—Multilayer interconnection.

connection with a known and controllable process. However, it is not possible to avoid a relatively large number of joints in series.

Figure 11.7 shows integrated circuits in so-called flat-packs interconnected by means of a multilayer interconnect board. These boards are made by laminating single-layer circuit boards before final curing, successive depositions, or other techniques. They are advantageous as they are theoretically a one-piece interconnect fabricated with a minimum of hand operations. However, as yet they are not truly tried-and-proven, since they have accumulated only a limited amount of spacecraft usage.

Another type of interconnection which creates many problems, but which is difficult to avoid in a complex system, is the friction connector. Most spacecraft electrical systems are modular and can be disconnected at various points for test, modification, and repair. Friction connectors are ordinarily used at these points. These connectors are heavy because they are mechanical in nature and mechanical parts such as spring clips are difficult to miniaturize reliably. They are also inherently unreliable in that they suffer from breakage and plastic deformation, and are subject to abrasion and wear. The ultimate solution to the problem is to eliminate connections by providing joints which are dematable until shortly before launch, at which point they can be permanently fused. Unfortunately, this "fusing time" is not practically attainable because of unpredictable last-minute emergency repairs. There are several connectors on the market which can be fused and opened a limited number ot times. However, none of these are sufficiently reliable or operationally convenient. The friction connector seems to be a necessary evil at this point. It will be used until feelings against it rise to the point where operational inconvenience will be chosen over the presence of the connector, or until a breakthrough is made in matable-dematable electric joints.

MATERIALS AND PROCESSES

Electronic equipment usually contains most of the plastic in a spacecraft. Polymeric materials are less consistent, less stable, and less trustworthy than metals. The properties of plastics depend upon such factors as mixing, storage, curing, and past history. They tend to outgas unwanted products in a vacuum. It is obviously impossible at this point to examine plastics in detail. However, table 11.2 shows some of the types of plastic used in spacecraft electrical systems.

Some of these materials are extremely nonhomogeneous and nonlinear. An example is the syntactic foam used to encapsulate welded cordwood modules. A typical material is Stycast 1090, which is an epoxy resin filled (approximately equal parts by volume) with small (30–300 μin. diameter) hollow glass balloons. These balloons decrease the shrinkage rate, decrease the coefficient of expansion, and decrease the density. However, properties of the resulting material depend partly

TABLE 11.2—Plastics used in electronic packaging.

Plastic	Usage	Comments
Epoxies	Bonding, potting.	High peel and shear strength, relatively easy to control, consistent, good adhesion, low shrinkage, expensive, hard to remove, upper temperature limit about 300° F. Epoxies are usually filled with an inert material for potting to improve electrical properties, decrease density, and decrease shrinkage and coefficient of expansion.
Epoxy polyamide.	Coating	Approximately same as above. Chief advantage is strength and adhesion. Main disadvantage is difficulty of removing and possible tendency to lose resiliency with time.
Silicones	Bonding, potting, coating.	Poor adhesive qualities and tricky curing requirements (for instance, humidity dependence). Resilient and easy to strip mechanically. Good temperature stability (adhesives good from −50° F to 600° F). Usually filled with an inert material for potting. Higher density than epoxies. Good stability and electrical qualities.
Urethanes	Coating, potting.	Resilient, easy to strip either mechanically, chemically, or thermally. Retain resiliency, moderate to good adhesion, good filleting properties, cheap.
Phenolics	Bonding, coating.	Not resistant to solvents, moderate adhesion, not as strong as epoxies. Ability to char extremely valuable for usage where short-term high temperatures are experienced (as in entry vehicles).
Polyesters	Potting	Cheap, easy to use, and well understood (transformer potting).
Acrylics	Coating	Not used widely. Low temperature resistance, poor wetting, poor peel strength.

upon the relatively stable nature of the glass, partly upon the nonlinear nature of the plastic, partly upon such factors as shattering the balloons, and so on.

Apart from plastic processes and metal forming, packaging engineers must work with a large variety of circuit interconnection processes. Besides soldering, these may include opposed-electrode resistance welding, parallel-gap welding, series welding, percussion welding, ultrasonic welding, electron beam welding, laser welding, crimping, wire wrapping, thermocompression bonding, vacuum deposition, chemical plating, and silk-screening of conductive inks and epoxies. Each of these processes presents different problems. Since destructive testing is useful only to create confidence in a joint, and not to test flight joints, it is necessary to understand the interconnection processes thoroughly in order to guarantee a low probability of failure among hundreds of thousands of joints in a spacecraft electrical system.

THE SUBASSEMBLY

The electrical system of a spacecraft is composed of various elements, usually designed by different groups and connected together to form the system. These are commonly called subsystems (attitude control, data processing, transmitter, power, etc.). To the packaging engineer they are subassemblies. They consist of a number of electrical functions interconnected to form a piece of spacecraft electrical equipment. The subassemblies may or may not consist of easily disconnectable modules.

The components and the interconnections must be adequately supported structurally in the subassemblies, which will in turn become a portion of the completed spacecraft structure. Proper thermal conduction and radiation paths must be provided to allow heat to be dissipated in a manner consistent with the spacecraft thermal control system. The subassembly must be sufficiently intact to be removed and installed as a unit. It must also be capable of interconnection with other subassemblies.

In a complex electrical system, some degree of modularization is necessary to enable design, development, test, and modification to proceed in parallel. One-piece approaches to complex systems tend to be more expensive, risky, and inflexible. The degree of modularization and the resulting module size depend upon the nature of the system, the nature of the project, the amount of manpower and money available, and the number of technical advances in the system. They also depend upon the philosophy of the agency creating the spacecraft. Examples of different philosophies will be evident in the next chapter. Some agencies prefer the black-box approach, wherein each subassembly is a unique unit, delivered and modified only by the

responsible group. Others prefer to standardize modules and integrate the various portions of various subassemblies without as sharp a distinction between units. An extreme of this approach would be a "one-piece" electrical system. A compromise approach is to attempt to retain individual identity of subassemblies, yet provide a maximum of integration of the subassemblies into the spacecraft.

THE SPACECRAFT

Electronic packaging plays an important part in the overall spacecraft configuration and operational procedures. Packaging must be considered from the beginning of the design phase in order to ensure the proper mixture of structural and thermal efficiency; ease of fabrication and assembly; ease of test, modification, and repair; and technical advancement. For instance an attempt to maximize structural efficiency (use the packaging structure at full capability as a portion of the overall spacecraft structure) is frequently impractical because of the difficulty of working with the system while portions of the electronics are removed.

A small amount of thought should result in a large variety of examples of spacecraft-packaging interdependence. For instance, since most spacecraft depend upon conduction and radiation to transfer heat, the high-power portions of deep-space electrical systems are ordinarily placed near or in the external skin of the spacecraft. In the case of orbiters, the packages may be placed within, and isolated from, the skin to maximize thermal inertia. Such subassemblies as communication and science electronics are frequently placed so as to minimize cable runs to antennas, instruments, and sensors. Large objects such as batteries and cavity amplifiers tend to dictate special envelopes. If access is to be provided to the electrical system while it is operating in test, the packages must open to the outside of the spacecraft or there must be room on the inside for whatever operations are necessary.

Interconnecting conductors between subassemblies and between points such as the umbilical connector, guidance sensors, actuators, solar panels, attitude-control jets, and correction motors must be accessible and simple to fabricate and install. Heat dissipated from the electrical system must be channeled from heat-sensitive items and used to warm cold-sensitive items. The shape of the subassemblies, which may in part be dictated by electrical and interconnect considerations, will have a strong effect upon spacecraft appearance. The Ranger, Mariner Venus, and Mariner Mars spacecraft have a distinct similarity due to the concept of packaging in "boxes" which are arranged around the periphery of the body of the spacecraft. In spin-stabilized spacecraft, the dense electronics are placed around the

periphery to achieve a stable spin axis. The importance of packaging to the overall spacecraft configuration should become even more obvious in the next chapter.

REFERENCE

1. BERRY, R. W.; MAYER, E. H.; MULLER, E. E.; SCAGNELLI, H. J.; and STIEFEL, K. E.: *Thin Film Logic Units.* Paper given at 1963 EIA Packaging Conference at University of Colorado.

CHAPTER 12

Spacecraft Electronic Packaging

THIS CHAPTER contains illustrations of a few typical approaches to spacecraft electronic packaging, with brief descriptions where pertinent.

Figure 12.1 shows the Bell Telephone Laboratories (BTL) Telstar electronic container before foaming and sealing. All electronic assemblies were prepared by using terminal boards, conventional components, and hard-wired soldered joints. The boards were then assembled in subassemblies and encapsulated in foam. The foamed subassemblies together with the waveguide equipment were then wired together and placed in the aluminum can shown in figure 12.1. This can was then filled with foam and a lid was seam-welded on it. BTL decided to use this packaging approach in order to avoid the materials problems associated with the space environment and because it gave them the rigid support they required. The container, when filled and sealed, weighed 85 lb. Thermal problems were solved by placing the hotter components next to the wall of the can, which conducted heat around the package. The can was wrapped in a superinsulating blanket and equipped with a bimetal-controlled shutter on each end. The can was supported within the satellite by nylon lacing, which thermally isolated the can from the satellite skin. The transient thermal conditions due to operation in and out of the Earth's shadow were minimized by this isolation, the shutters, and the thermal mass of the electronics assembly.

Figure 12.2 shows the electronic assemblies in the Space Technology Laboratories (STL) Pioneer V spacecraft. Pioneer V was launched into a solar orbit on March 11, 1960, and transmitted successfully until it reached a distance of 22.5 million miles from Earth. This spacecraft was about 26 in. in diameter and weighed 95 lb. It is an excellent example of the "black-box" approach to packaging. Each subsystem (transmitter, command receiver, decoder, battery, data conditioner, etc.) is packaged as an individual unit. These units are designed and built independently by individual groups and assembled at spacecraft assembly. This system is extremely convenient operationally, but can be structurally and thermally inefficient, as the structural and thermal capacities of the packages are difficult to integrate into the spacecraft.

771-733 O-65-11

Figure 12.3 shows the electronic assemblies of the Tiros satellite, built by RCA. These assemblies are also "black-box" in nature and are mounted upon the base-plate structure of Tiros. This plate is reinforced with ribs and is the basic structure of the satellite. The Tiros program has been extremely successful. Eight satellites have been successfully launched and have taken more than 300 000 pictures of the atmosphere. The satellite is spin stabilized and incorporates

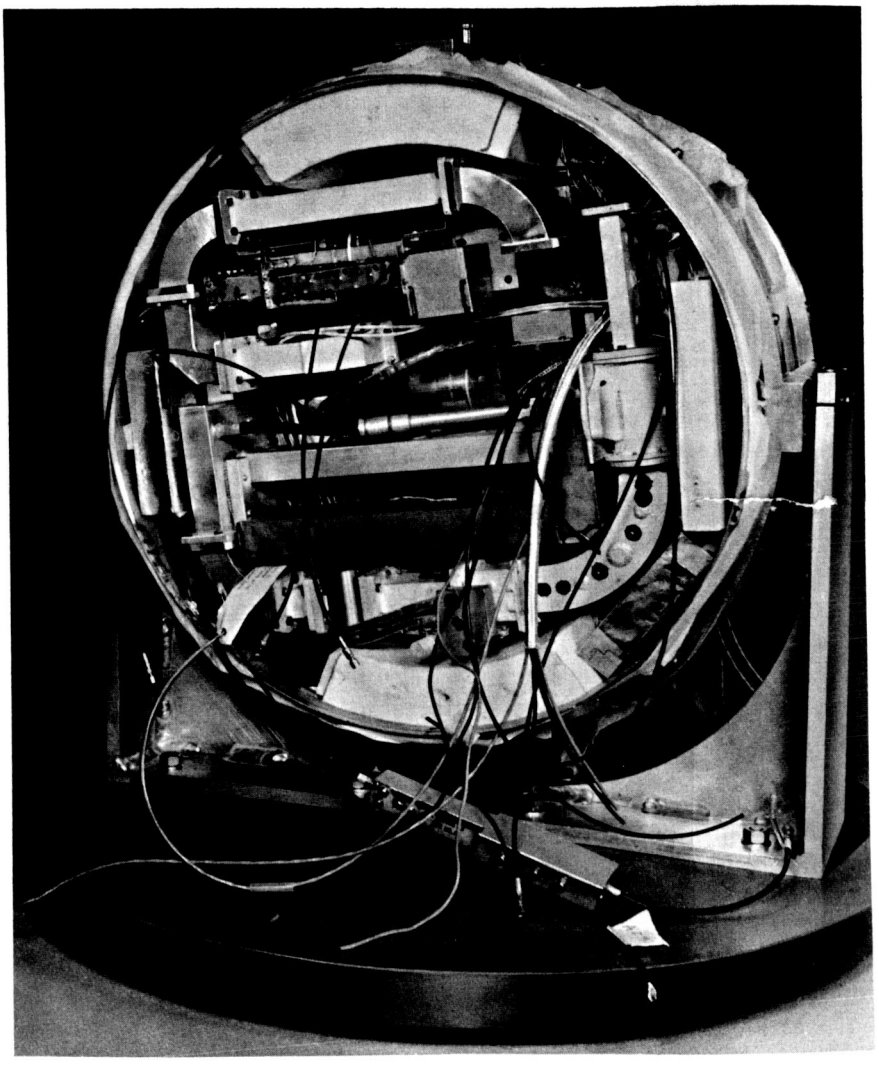

FIGURE 12.1—Telstar electronics assembly. (BTL photograph.)

spin-up motors, a despin device, and magnetic torquing for adjusting the spin axis in flight. The electronics in this satellite consist of conventional components mounted either on terminal boards or printed circuit boards and mounted in the various boxes.

A more integrated approach to packaging is taken in the Mariner class of space vehicles. This approach makes better structural and thermal use of the packaging in the system, but is operationally more difficult to control than the black-box approach. Figure 12.4 shows the packaging layout for the Mariner II Venus spacecraft. The electrical equipment was mounted in 6-in. by 6-in. modules, which were in turn mounted in the six boxes that were mounted on the periphery of the spacecraft. The boxes served as shear panels for the structure, as conduction paths, and as radiating surfaces. The boxes hinged open for access during assembly and testing. Each box contained one or two subassemblies.

Figure 12.5 shows a typical Mariner Mars module containing conventional electronic components soldered to terminals on a printed circuit board. This particular module weighs 1.6 lb, of which 0.3 lb is module magnesium weight. Figure 12.6 shows a module which contains welded functional digital units. These units are soldered to terminals in this particular application.

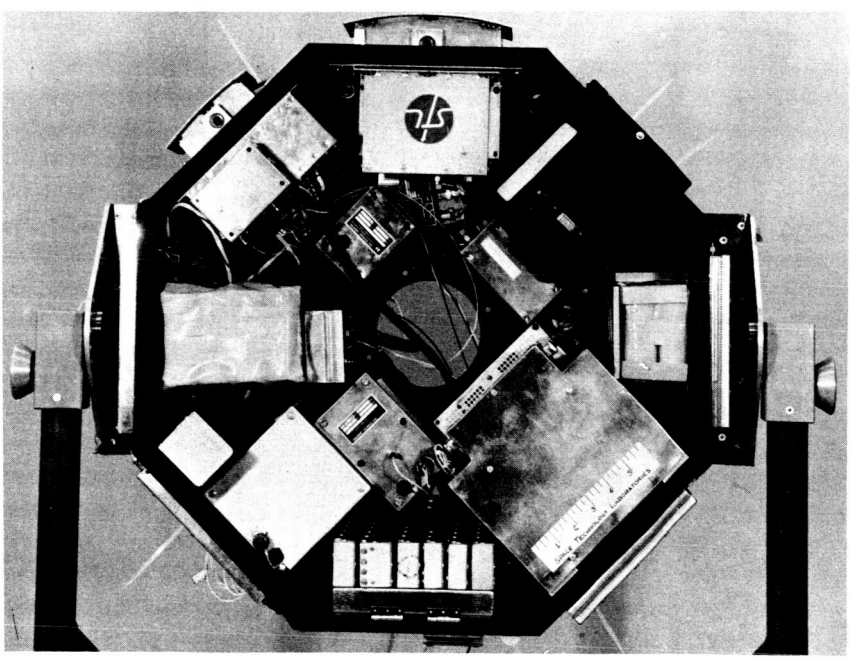

FIGURE 12.2—Pioneer V electronic assemblies. (STL photograph.)

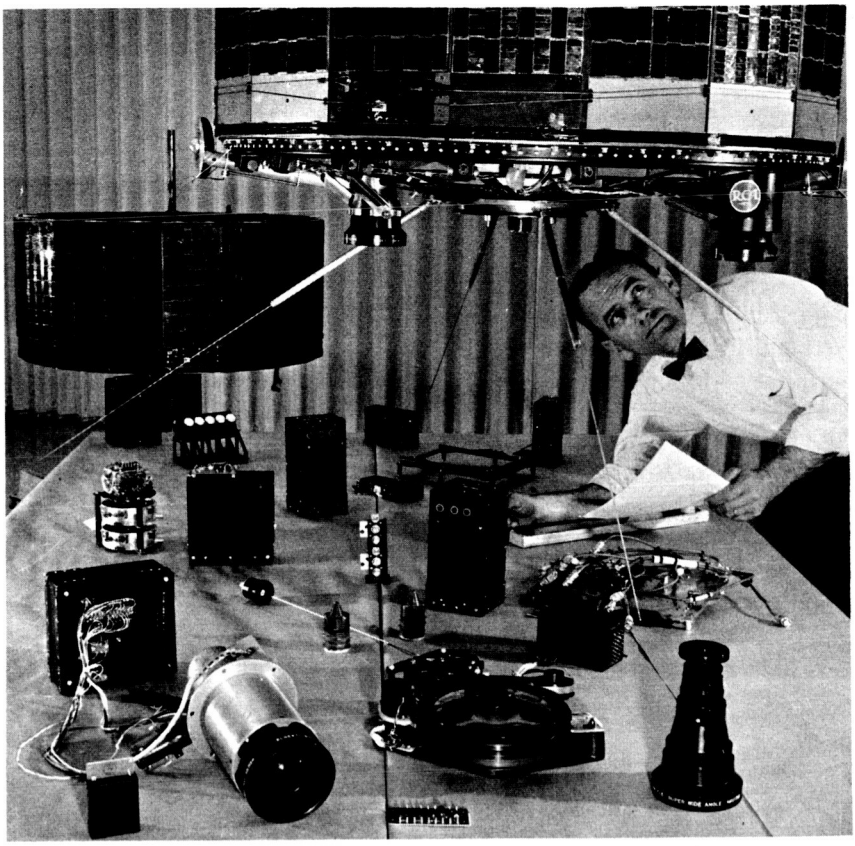

FIGURE 12.3—Tiros electronic assemblies. (RCA photograph.)

Figure 12.7 shows the box of science equipment from the Mariner II Venus spacecraft. This box contained the power switching for the spacecraft (on the outside of the box), the science data conditioning system, the magnetometer electronics, and the solar plasma experiment and electronics. The box, complete with electronics and instruments, weighed 25 lb.

Figure 12.8 shows the manner in which the modules are assembled with the chassis in the Mariner Mars spacecraft. This is a structural mockup used to test the dynamic response of the modules. The chassis plates act as the shear panels for the faces of the octagonal primary spacecraft structure and as thermal radiation surfaces. The Mariner Mars spacecraft depends upon the electronic units for primary structure to a greater degree than the Mariner II Venus spacecraft. This results in greater structural efficiency, even though some operational convenience is sacrificed. The modules used in the Mariner

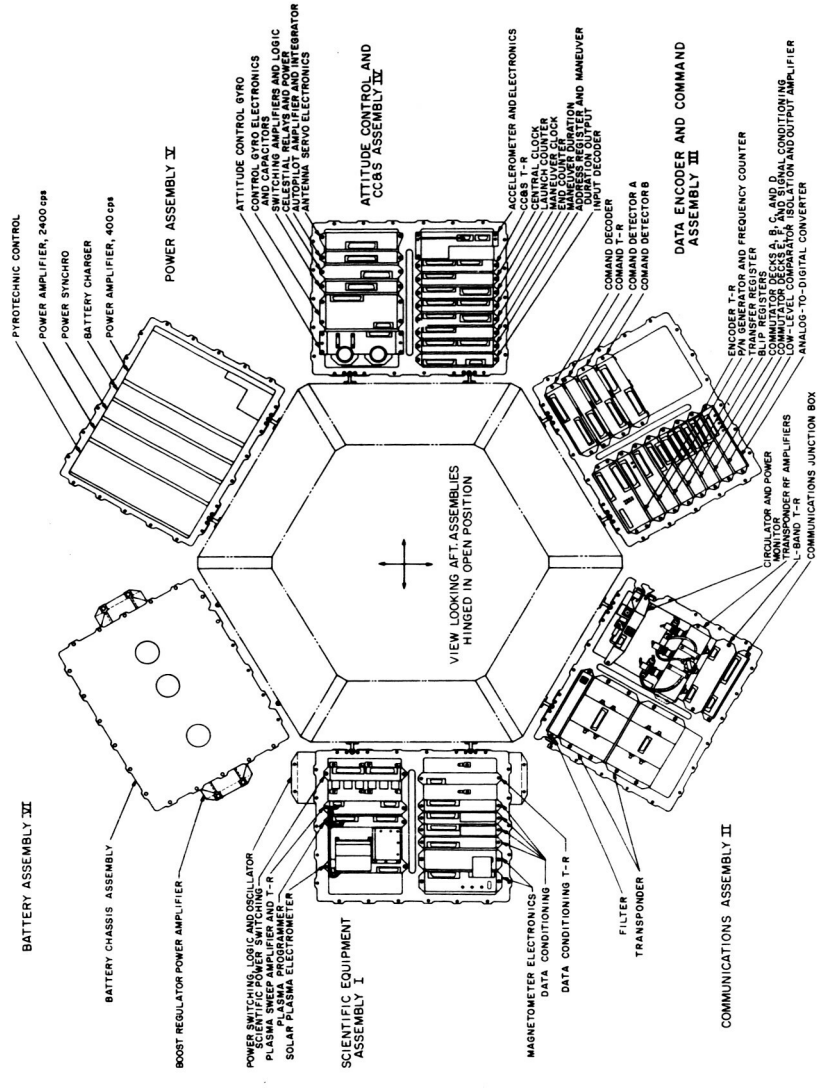

FIGURE 12.4—Mariner II spacecraft electronic equipment arrangement. (From ref. 1.)

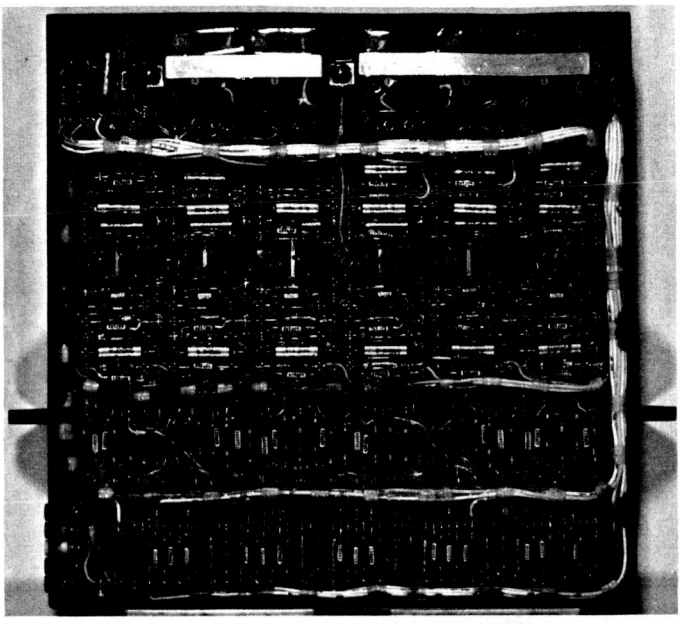

FIGURE 12.5—Address register and maneuver duration output. (JPL photograph.)

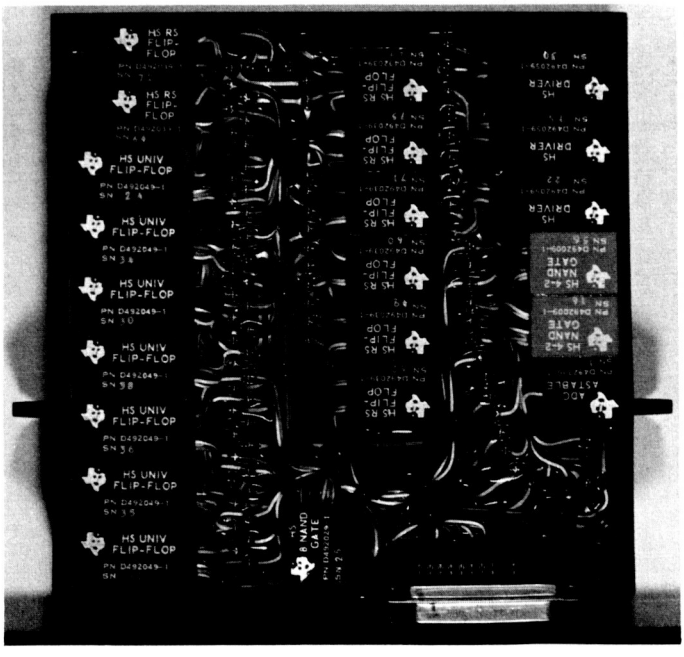

FIGURE 12.6—Analog-to-digital converter. (JPL photograph.)

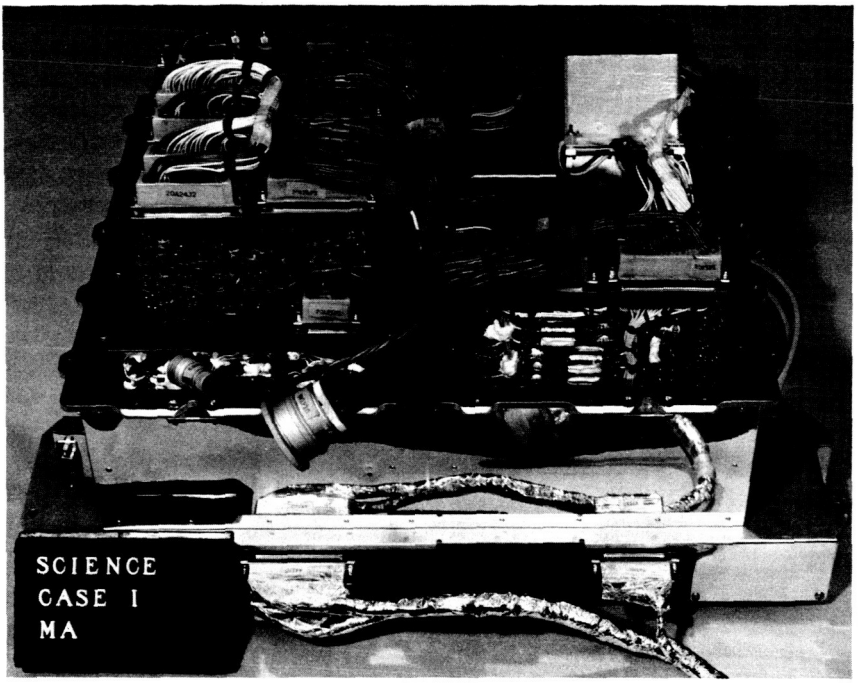

FIGURE 12.7—Mariner II science box. (JPL photograph.)

spacecraft are machined from magnesium and have a thickness in both web and flange of 0.090 in. When loaded with bonded-on circuit and backing boards and conventional components, they are extremely stiff, having a first vibration resonance above 500 cps.

Figure 12.9 shows a welded cordwood functional module before it is encapsulated. This module is an emitter-follower from a data conditioning unit. The Mylar assembling and positioning sheets and the welded nickel ribbon interconnects discussed in chapter 11 are apparent. This module will be encapsulated in a potting compound such as glass-bubble-filled epoxy resin.

Figure 12.10 shows a module filled with potted welded cordwood functional units. The plate of the module is drilled in a grid pattern. The cordwood units are secured to the plate as was shown in chapter 11. The leads are interconnected on the other side of the plate by welded matrix. A typical encapsulated welded matrix is shown in figure 12.11.

Figure 12.12 shows an experimental digital data-handling assembly developed by STL. One of the problems in the design of data-handling equipment is that the circuitry must respond to changes in most of the other subsystems. It is therefore extremely difficult to

"freeze" the circuitry early enough to design and develop sophisticated and specialized hardware. The unit shown in figure 12.11 is completely modular. Welded and encapsulated cordwood modules are mounted in trays which will hold up to 10 modules and which provide hole grids for the leads of the cordwood modules. The module leads are then interconnected by wire. STL developed a process of deriving wire diagrams by use of a computer and then automatically welding the proper wires to the proper leads without removing the wire insulation. The resulting joint is very strong because of the inherent strength of the weld and the presence of the insulation which is not burned off during the welding operation.

The trays of interconnected modules can, in turn, be fastened into larger assemblies which are interconnected by means of the same wiring technique. These assemblies can then be stacked into the final assembly, which is interconnected in a similar manner. Figure 12.12 shows an assembly, in open form, containing 250 cordwood modules and weighing approximately 17 lb. After checkout, the assembly is closed and secured with tiebolts through the covers.

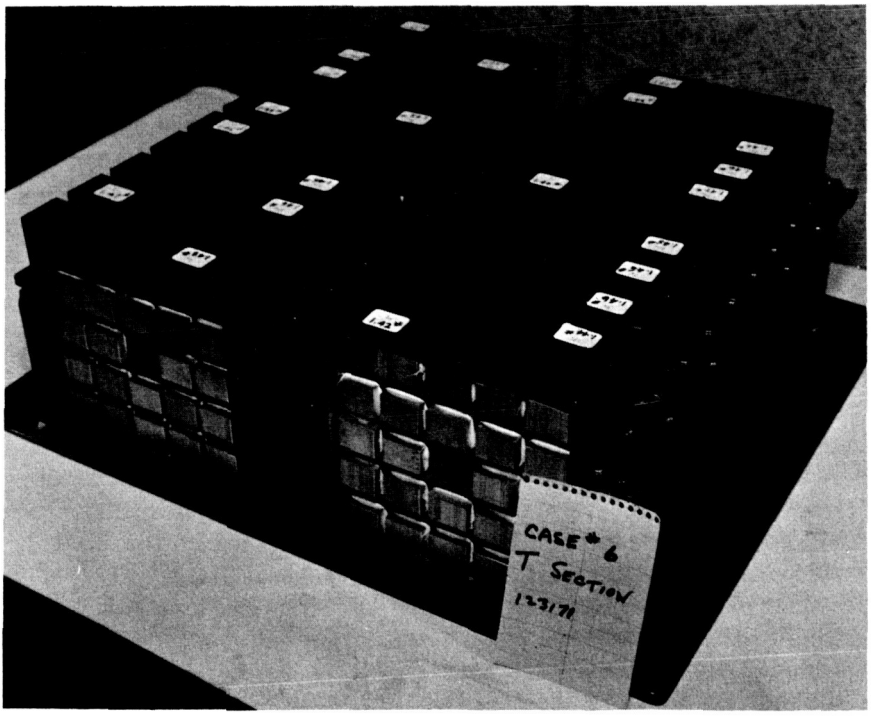

FIGURE 12.8—Mariner Mars electronic structural mockup. (JPL photograph.)

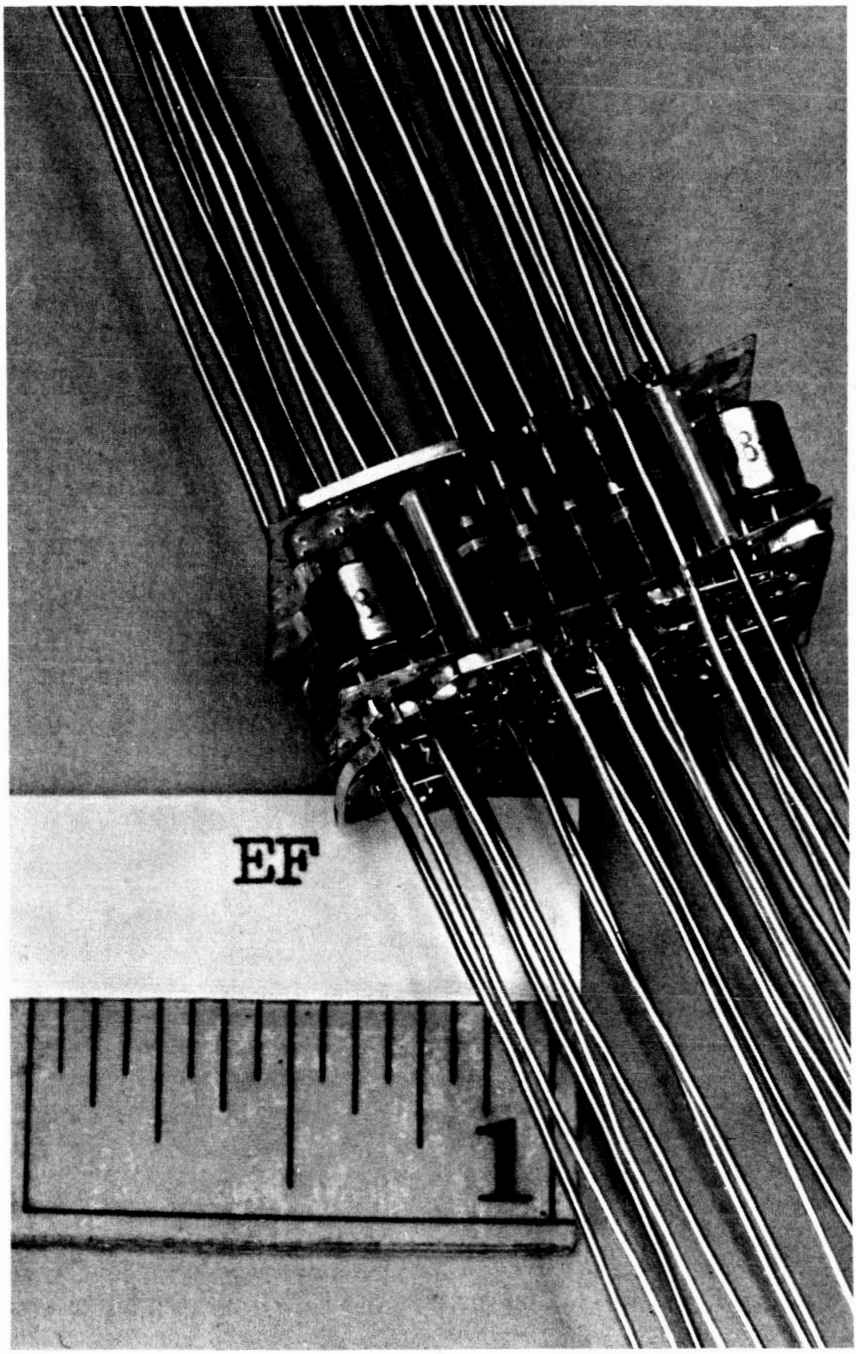

FIGURE 12.9—Welded cordwood emitter-follower assembly. (JPL photograph.)

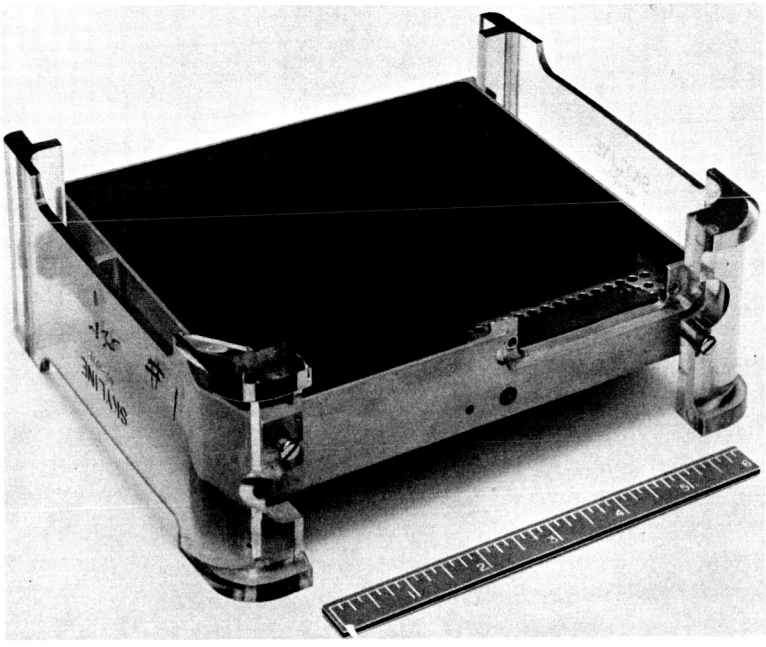

FIGURE 12.10—Welded cordwood assembly. (JPL photograph.)

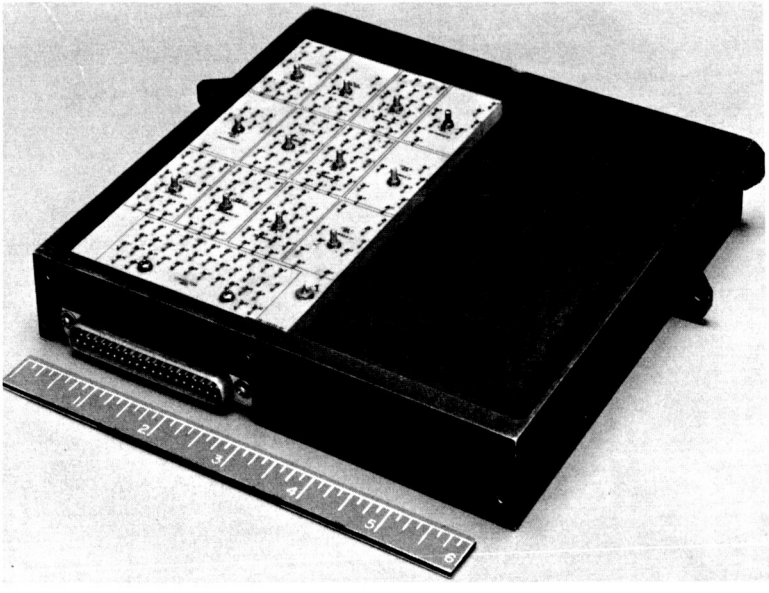

FIGURE 12.11—Welded interconnect matrix. (JPL photograph.)

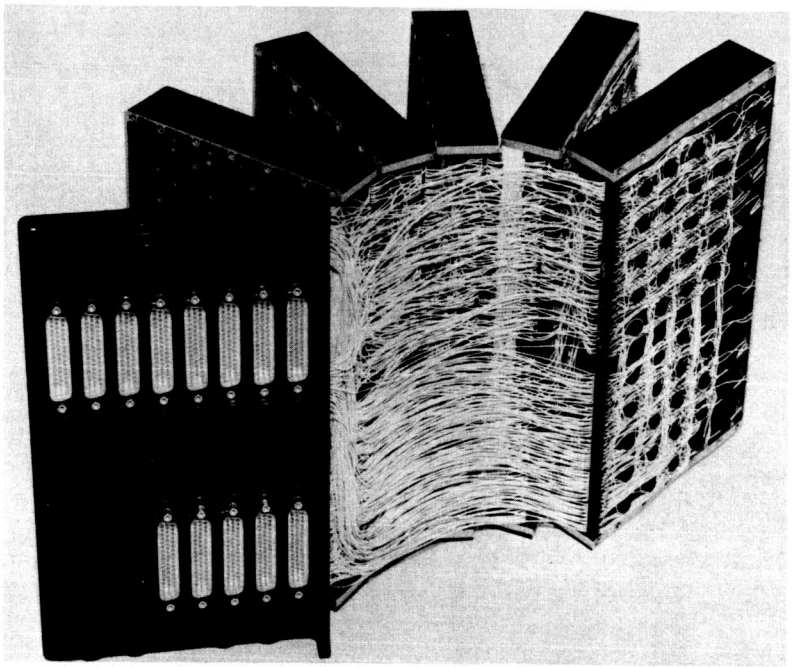

FIGURE 12.12—STL digital data-handling assembly (open). (STL photograph.)

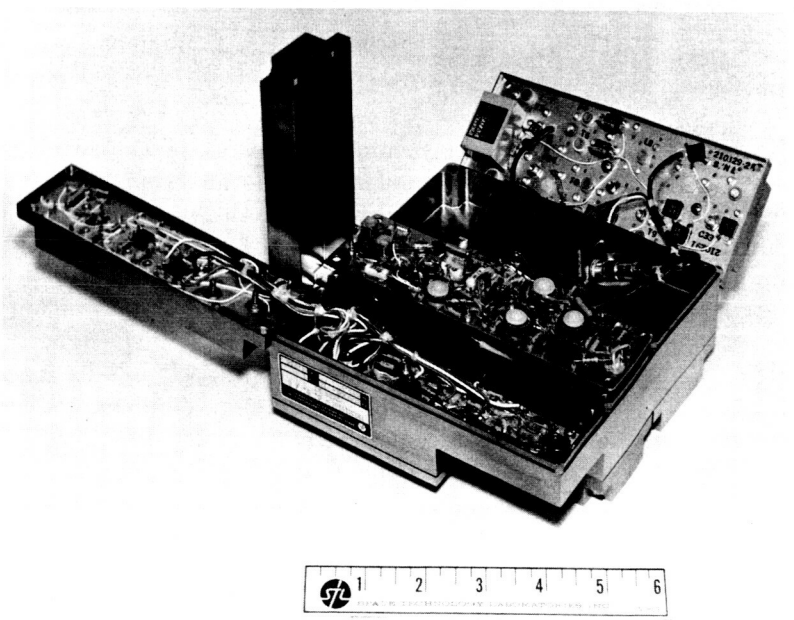

FIGURE 12.13—STL phase-lock command receiver. (STL photograph.)

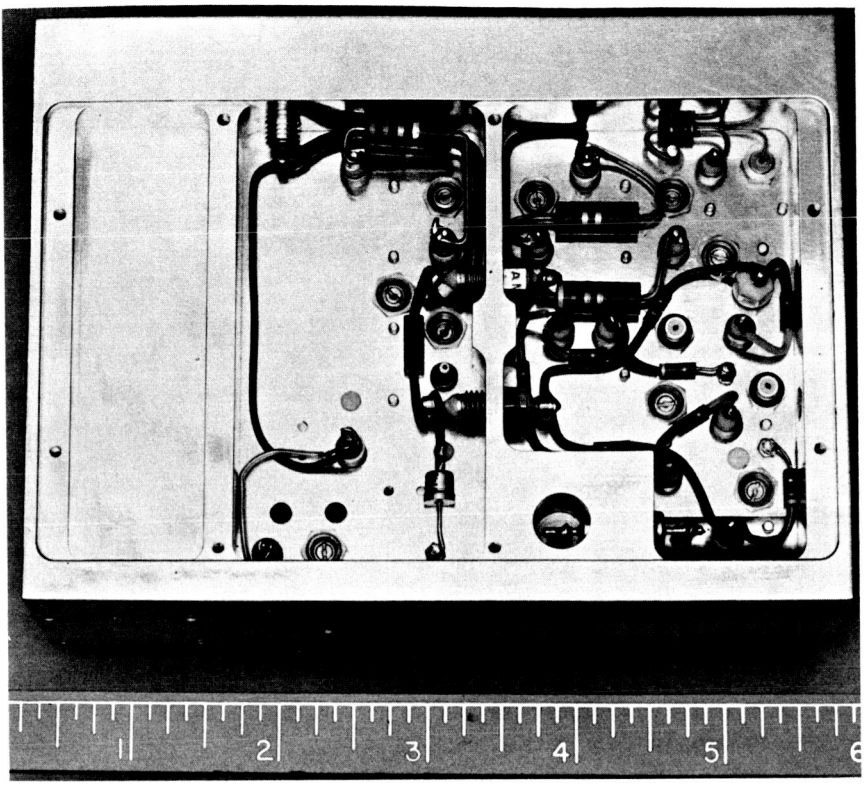

FIGURE 12.14—JPL high-impact-resistant beacon. (JPL photograph.)

Figure 12.13 is a phase-lock command receiver developed by STL. It is a portion of a satellite Doppler tracking and command system and is packaged in a machined chassis with machined covers. This configuration provides the shielding necessary in a unit which must handle high (radio) frequencies.

Figure 12.14 is an experimental high-impact-resistant transmitting beacon developed by Jet Propulsion Laboratories (JPL). The transmitter operates at 960 Mc with a 2-watt output. It is 2 in. by 4 in. by 5.5 in. and weighs about 2.25 lb. The design emphasizes rigidity and all components are hard-mounted whenever practical. This transmitter is very similar to the one used in the Ranger seismometer capsule. With the development of a high-impact-resistant crystal, which is presently underway, this transmitter will be able to survive a 10 000g shock with a velocity change of 200 ft/sec. A schematic of the transmitter is shown in figure 12.15.

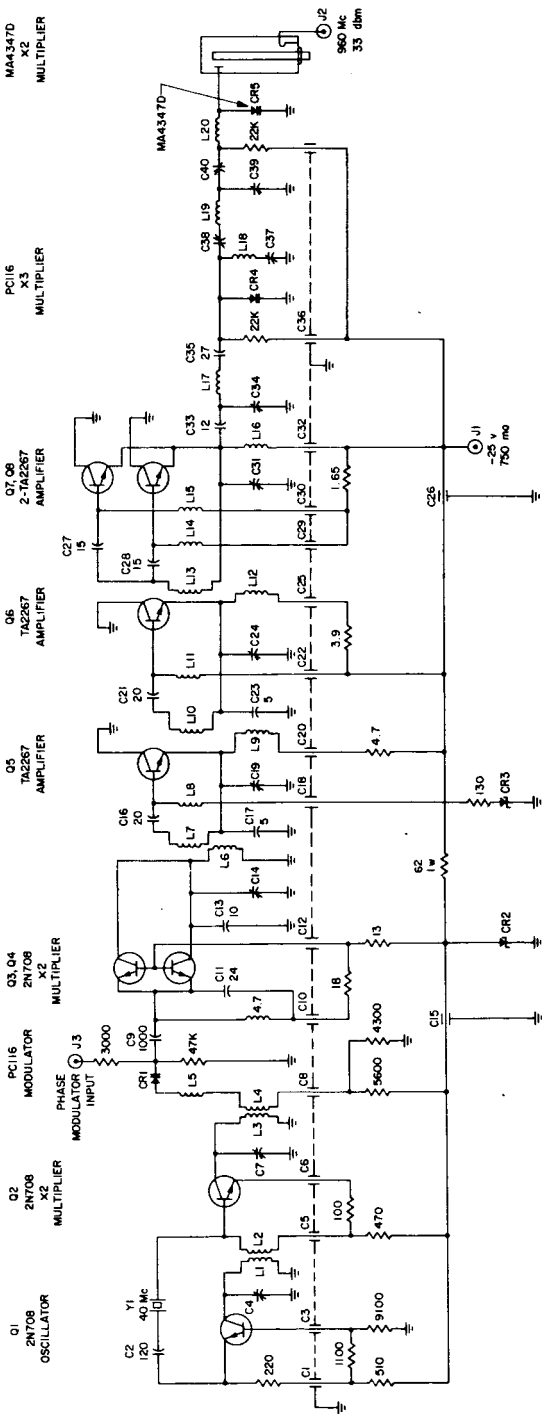

FIGURE 12.15—Circuit diagram of high-impact-resistant transmitter.

REFERENCE

1. JODELE, J.: *Mariner Spacecraft Packaging.* TR 32-451, Jet Propulsion Lab., 1963.

U.S. GOVERNMENT PRINTING OFFICE: 1965 O—771-733